

University of Naples “Federico II”



Ph.D in Aerospace, Naval and of Quality Engineering

Analysis of Flow Fields in a Deposition Chamber
by a Molecular Approach

Candidate: Francesco Romano

Tutor: Prof. Gennaro Zuppardi
Co-ordinator: Prof. Antonio Moccia

a.y. 2009/2010

Index

INTRODUCTION.....	4
Chapter 1 PROBLEMS OF DEPOSITION CHAMBERS.....	7
1.1 Introduction.....	8
1.2 Types of Deposition Chambers.....	10
1.3 Thin film Deposition Process.....	10
1.4 Expanding Thermal Plasma.....	12
Chapter 2 PLASMA CHEMISTRY.....	13
2.1 Introduction.....	14
2.2 Chemical Models.....	16
Chapter 3 RAREFIED FLOW FIELDS.....	25
3.1 Introduction.....	26
3.2 Rarefaction Parameters.....	27
Chapter 4 PRE-PROCESSOR.....	32
4.1 Introduction.....	33
4.2 Basic Equations.....	35
4.3 Torch.....	51
4.4 Nozzle.....	55
Chapter 5 DIRECT SIMULATION MONTE CARLO METHOD.....	69
5.1 Introduction.....	70
5.2 Basic DSMC method.....	71
5.3 “Sophisticated” DSMC method.....	73
5.4 DS2V Code.....	75
Chapter 6 POST-PROCESSORS.....	78
6.1 Introduction.....	79
6.2 Rarefaction parameters.....	80
6.3 Film.....	83

Chapter 7 ANALYSIS OF THE RESULTS.....	85
7.1 Introduction.....	86
7.2 Heater.....	89
7.3 Nozzle.....	100
7.4 Chamber.....	110
7.4.1 Shock Wave.....	118
7.4.2 Fluidics.....	122
7.4.3 Film.....	129
CONCLUSIONS.....	134
REFERENCES.....	137
Publications linked to this thesis.....	139

Introduction

Nowadays the thin film deposition process is very important and useful because it is involved in a lot of industrial applications, such as chemical, electronic, mechanical, optic fields and so on. In fact, thanks to its particular characteristics, the thin film is widely used for the coating purposes, magnetic recording media, semiconductor quantum dots, solar cells, displays, sensors, electrodes and so on. Due to this high importance the research and the science community are extremely interested to analyze in more detail this technique and in the last decade many researchers made a lot of studies both by experiments and by numerical computations.

Different types of deposition processes were born in order to discover the best and the most efficient technique. Obviously, a unique method for all types of film can not exist. Many researchers from several universities around the world are working to understand the physical-chemical processes correlated to the thin film deposition and to develop new methods for optimising the deposition process. All these processes are illustrated in more detail later.

Among the numerous types of deposition processes, the Expanding Thermal Plasma (ETP) technique will be analyzed and simulated in this Ph.D thesis. This method was developed by Prof. van de Sanden and co-workers at the University of Eindhoven (Netherlands). In this deposition process, Argon is ionized in an electrical torch. The thermal plasma mixture (Ar , Ar^+ and electrons) expands supersonically in the nozzle and after into a low pressure vessel where is compressed by a barrel shock wave. A precursor gas like Acetylene or Methane or Sylane is injected in the nozzle or directly in the chamber near the position of the shock wave. The chemical composition of gas mixture changes because the precursor reacts with Argon ion generating a lot of different species. All these species flow (sub-sonically) towards a surface called substrate and some of them deposit forming new types of materials like for instance Diamond Like Carbon films.

The simulation of the flow field in a deposition chamber has been already studied and many codes were also born for the simulation of the flow fields in the deposition apparatus. Different codes based on Navier-Stokes equations, thus on continuum approach and/or molecular approaches have been taken into account. As shown later and as already verified by other researchers, the flow field in a deposition chamber is usually rarefied. Several researchers studied the flow field in the deposition chamber by Computational Fluid Dynamic (CFD) approach, by molecular or Direct

Simulation Monte Carlo (DSMC) procedure and also by hybrid codes involving both CFD and DSMC techniques.

In this thesis an exclusively molecular approach by means of the commercial DS2V code by Bird is proper. In fact, as shown in the next section, this code is sophisticated and thus can simulate in accurate way also the flow field characterized by a Knudsen number not very high without the necessity to consider hybrid codes.

The aim of this thesis is to examine closely the flow field in a deposition chamber and to understand the influence in the evolution of the gases of the following test parameters:

- 1) electrical power supplied to the torch,
- 2) precursor mass flow rate, the precursor considered is Acetylene.
- 3) thermo-fluid-dynamic parameters at chamber inlet section by using supersonic conical nozzles characterized by different geometry, i.e. different lengths and ratios of exit area to throat area.

Furthermore a simple method to estimate in a first evaluation the thin film distribution on substrate has been developed. For this reason it is possible to write that the ultimate purpose of this thesis is to provide a research of the ETP deposition chamber with a computing tool for optimising the deposition process.

In order to obtain these results a pre-processor code considering the flow field in the torch and in part of the nozzle (from throat until to 90% of divergent part) has been elaborated. The output from this code is the input for the DS2V code which simulates the flow field in the last part of the nozzle and in the van de Sanden deposition chamber by a DSMC approach. A post-processor code is written to analyze the output by DS2V.

The thesis develops in 7 chapters and more specifically:

Chapter 1: Summary of the problems related to deposition chambers. A short overview of various and most popular types of deposition technique is considered and the ETP method is explained in more detail.

Chapter 2: Analysis of Plasma Chemistry. Different types of chemical processes are studied and the most excellent estimation of numerous parameters to implement in the molecular code for the gas reactions is computed.

Chapter 3: Study of rarefaction and classification of rarefaction parameters. An accurate examination of local Bird parameter and of local Knudsen number based on some parameters such as density, velocity, temperature, pressure is carried out.

Chapter 4: Examination of the various fluid-dynamic equations used in the preprocessor. More specifically the Saha's equation for the first ionization and the balance equation of the thermo-fluid-dynamic parameters for the whole flow field are explained.

Chapter 5: Illustration of the Direct Simulation Monte Carlo method. Furthermore the commercial DS2V code developed by Bird based on the DSMC approach is shown.

Chapter 6: Explanation of the post-processor used to evaluate the post-run rarefaction analysis in the chamber deposition and to compute the thin film distribution along the substrate surface.

Chapter 7: Analysis of flow field in a Deposition Apparatus. The results linked to the various thermo-fluid-dynamic quantities are shown and a numeric quantification is carried out. The most useful quantities linked to the deposition process, such as for example the ionization degree, the intensity and the position of the shock wave are evaluated. More over a preliminary and simple evaluation of film thickness distribution on the substrate is carried out. As said before, the flow field simulations involve Argon with Acetylene as precursor gas.

Conclusions

Chapter 1

PROBLEMS OF DEPOSITION CHAMBERS

1.1 Introduction

Thin film deposition procedure consists essentially in the formation of thin film on a surface called substrate. This method is of great interest in many and different applications, such as for example in the coatings, magnetic recording media, solar cells, displays, sensors and so on. The importance is due to the fact that starting from simple gases (for instance Argon, Acetylene, Methane, Silane, etc) this process generates diverse films characterized by small thickness (order of nano/micrometers) but high properties, such as hardness, conductivity, elasticity, adhesion, chemical stability and so on. An example of thin film is the Diamond Like Carbon (DLC) film, which is a metastable amorphous material usually composed by Hydrogen and Carbon. It is used as protective coatings on magnetic storage disks, razor blades and in other applications thanks to its characteristics of high mechanical, chemical, electronic and optic properties. In the last years DLC are becoming more and more important and there is a great interest also for the future. In fact DLC film is biocompatible, presents low friction coefficient, does not produce metallic wear debris and thus can be used as compatible coating on parts such as for example hip joints and heart valves.

For this reason many researchers from several universities around the world are working hard to analyze in more detail (both by experiments and by numerical computations) the thin film deposition process and understand the very complex physical-chemical aspects in order to develop new techniques for optimizing and improving the film properties and also generating varied thin films. In the present section a short overview of various and most popular types of deposition technique such as the Ion Beam Deposition, Mass Selected Ion Beam Deposition is carried out and the Expanding Thermal Plasma method is explained in more details.

1.2 Thin Film Deposition Process

The thin film deposition methods can be classified in two main categories:

- 1) Chemical Vapor Deposition (CVD) technique,
- 2) Physical Vapor Deposition (PVD) technique.

In the first method a precursor fluid is used and the film is formed thanks to the various chemical reactions occurring in the gas mixture and/or at the substrate. The film obtained is made up of “new” chemical species generated thanks to the chemical reactions.

In the PVD process the film is achieved by the condensation of vaporized material onto the substrate. In this way the film is made up of the same chemical species injected in the deposition apparatus. The processes of vaporization and of condensation are purely physical and “new” chemical species are not generated (there are no chemical reactions).

It is clear that in each deposition method the fluidics assumes always a crucial role. In particular the characterization of Mach number is very important. In fact the Mach number provides useful information about intensity, position and extension of shock wave and these information are useful because influence strongly the fluidics, for example the values of velocity and temperature. Obviously the fluidics influences strongly the chemical composition of mixture in the deposition apparatus and thus the film properties. An important type of CVD technique is the Expanding Thermal Plasma (ETP) method [1] and [2] developed by van de Sanden and co-workers at the University of Eindhoven (the Netherlands).

1.3 Types of Deposition Chambers

Many types of deposition chamber are present in the world [3]. A complete classification is not possible but a short overview is now presented, starting by the:

Ion Beam Deposition

The Ion Beam deposition technique was developed in 1971 by Aisenberg and Chabot to deposit DLC films. This method produces hard, dense films with low surface roughness. For this reason these films are adapt for the protective coatings. In this type of deposition a beam of carbon or hydrocarbon ions characterized by energy ranging in the interval 10 eV – 100 eV is applied.

Mass Selected Ion Beam Deposition

The Mass Selected Ion Beam deposition presents a lot of advantages. In fact this technique is more controlled than the Ion Beam method because allows to select the ion species and their energies. Furthermore in this method it is possible to create films harder and more dense, the neutral species are filtered out and the film can be doped by switching to other ion species. The disadvantage is that the deposition rate is very low (order of 0.001 Å/s) and the apparatus cost is high. In Mass Selected Ion Beam technique the carbon ions are generated in an ion source. Successively these ions are accelerated to 5-40 keV and pass across a magnetic filter. After neutrals are filtered out and ions with an electron/mass ratio of atomic carbon ion are selected. By means of electrostatic lens the ions are decelerated to the desired ion energy. Finally the film is produced by focusing the resulting ion beam on the substrate in a vacuum.

Sputter Deposition

This type of deposition is the most common industrial deposition for amorphous carbons. The advantage is that putter sources generally are characterized by a rather low ion to neutral flux ratio towards the substrate. For this reason very hard films can not be produced in this way, but these

sources are very versatile and easy to scale up. Furthermore the deposition conditions can be monitored by the plasma power and pressure and they are rather independent of the substrate geometry.

The base of this deposition process is to sputter material from a graphite electrode which in turn can deposit on the substrate. The sputtering is completed by an Ar plasma. An Ar ion beam is used in the ion beam sputtering while in the Ion Beam Assisted Deposition a second Ar ion beam can be used to bombard the growing film. In the magnetron sputtering a magnetic field can be applied to increase the sputtering from the target. In the unbalanced magnetron the ion bombardment of the substrate can be further enhanced by configuring the magnetic fields across the substrate.

Plasma Enhanced Chemical Vapor Deposition

The Plasma Enhanced Chemical Vapor Deposition process creates an homogeneous film on large substrate and the set up of the system is quite simple. Films are medium hard with values of about 30 GPa. Different types of Plasma Enhanced Chemical Vapor Deposition technique are used and the most popular is the radio frequency Plasma Enhanced Chemical Vapor Deposition. The disadvantage of this process is that the ion energy and the ion current vary with the radio frequency power and thus it is not possible to obtain an independent control. To prevail over these disadvantages is possible, for example, to employ the microwave induced Plasma Enhanced Chemical Vapor Deposition.

1.4 Expanding Thermal Plasma

The ETP deposition process was developed by van de Sanden & co workers at the University of Eindhoven. This technique considers the deposition of a thin, amorphous film of C:H or of Si:H on a surface called substrate, using the Expanding Thermal arc Plasma method. The van de Sanden deposition apparatus is constituted of an electrical torch, a supersonic nozzle, a deposition chamber and a substrate holder, see Fig.1.1. The distance between the nozzle exit and the substrate can change because the group torch+nozzle can move, the diameter of the nozzle exit section and thus of the chamber inlet section is 0.032 m.

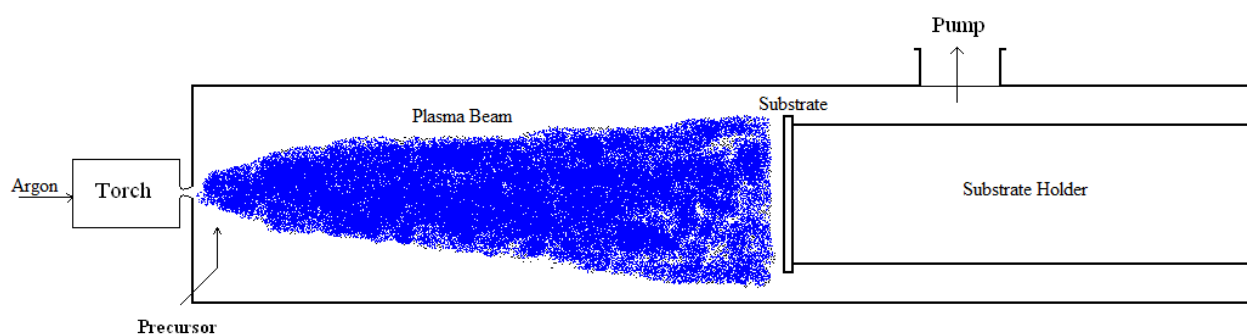


Fig 1.1 - Deposition apparatus at the University of Eindhoven

In this method Argon or a mixture of Argon and Hydrogen is ionized in a cascaded electrical torch at pressure of $10^4 \div 6 \times 10^4$ Pa forming thus a plasma. A precursor gas, like Acetylene (C_2H_2), or Methane (CH_4) or Sylane (SiH_4) is injected in the nozzle or directly in the chamber near the inlet section or directly into the background. The pressure in the chamber ($10 \div 10^2$ Pa) is obtained using a pump. Due to the high reactivity level of Argon ions, many complex chemical reactions take place forming a gas mixture made up of various radicals, ions and electrons. The gas mixture expands supersonically in the vessel and then is compressed by an abrupt shock wave. After the shock the various gases flow subsonically toward the exit slot and along the path some chemical species deposit on the substrate forming the thin film. At the substrate various surface reactions occur.

An important parameter is the sticking factor defined as the ratio of the number of deposited molecules to the number of total molecules arriving on the substrate.

Chapter 2

PLASMA CHEMISTRY

2.1 Introduction

Without any doubts chemical aspects play a central role in the life of each day. Man and woman live thanks to numerous and complex chemical reactions which happen in their body and with the external ambient. For example air molecules breathed react and generate the energy necessary to live. All objects, materials which are around us are generated thanks to many chemical (simply or complex) processes which are caused by nature or by the human actions. Obviously also the various materials produced by the film deposition processes are produced by means of numerous and also complex chemical reactions.

A lot of researchers studied deeply the chemistry just a lot of years ago and also nowadays many people work hard to understand the chemical processes. For example many aspects linked to gas behaviour, acids and bases in solutions, and determination of molecular weight were understood thanks to Avogadro, Arrhenius and Boltzmann in the 1700's and 1800's. In 1828 Wohler creating urea starting from inorganic materials understood that the organic and inorganic chemistries are strictly linked between them while at that time it was opinion that there are not connections. In the 1904 Thomson developed the "panettone" atomic model, Rutherford developed the "planetary" atomic model. A strong impulse in the atomic model was in the 1912 when Bohr explained the position of spectral lines of Hydrogen atom introducing the concept of quantization. The concept of electron cloud and atomic nucleus were used to explain in a more realistic and coherent way the chemical bound and the position of various elements in the periodic table, the chemistry and physics started to converge towards the same concept. In the 20th century, Perrin basing on numerous experiments and on theory of Albert Einstein to explain the Brownian motion, explained in a very clear way that the materials are made up of atoms.

As said before film deposition process is strongly influenced by a lot of multifaceted and complex chemical reactions. In fact, chemistry plays a key role because simple gases, like for instance Argon and Acetylene, due to chemical reactions generate new types of materials characterized by new physical and chemical properties. For this reason many researchers study hardly the chemistry in general and chemical reactions properties in particular. A very strong impulse in the study of chemistry for film deposition process is due principally to Benedikt [4], Mankelevich [5], Ariskin [6], Neyts [3] and Kuijlaars [7]. In fact Benedikt analyzed deeply plasma chemistry in an Argon/Acetylene expanding thermal plasma by means of various experimentally techniques, like for instance the residual gas analyzer and cavity ring down spectroscopy. Also

Mankelevich made numerous experimental analysis in order to obtain as many as possible important information on chemistry in an expanding thermal plasma apparatus.

The aim of this chapter is to make as possible a meticulous overview of chemical reactions and chemistry feature in the film deposition apparatus, explaining in particular the chemical models developed by Benedikt and Mankelevich.

2.2 Chemical Models

In this section the chemical models developed by Benedikt and Mankelevich are shown.

Benedikt Model

Benedikt made a lot of experimental measures in a film deposition apparatus by various technique, such as cavity ring down spectroscopy and residual gas analyzer. In particular he studied hardly the van de Sanden deposition apparatus at the University of Eindhoven where, as said before many complex chemical reactions occur. Starting from experimental results the researcher developed various chemical reactions and 24 of them are reported in Table 2.1 where is reported also the rate constant (K), the reaction yields and the heat of formation (ΔH_f) which is positive if the reaction is exothermic. It is easy to observe that there are:

- 5 charge transfer reactions (they are labeled by numbers 1, 7, 11, 13 and 15).
- 13 dissociative-recombination reactions (2, 3, 4, 5, 6, 8, 9, 10, 12, 14, 16, 17 and 18).
- 6 exothermic radical neutral reactions (19, 20, 21, 22, 23 and 24).

It is important to point out that the rate constant is not dependent by temperature. For completeness table 2.2 indicates the chemical species involved.

The chemical mechanisms and thus the mixture composition depend strongly on the Ar^+ molar fraction, because as reported in table 2.1 when Acetylene is injected in the nozzle the first reactions occurring is a charge transfer implying Ar^+ and C_2H_2 (reaction number 1). The Acetylene ions in turn will react with the electrons (reaction numbers 2, 3, 4, 5, 6) generating C_2H , C_2 , CH , CH_2 , C , H and H_2 in a quantity which is in accordance with the reaction yields. Some of these species in succession are initially ionized and after react with electrons forming different chemical species always in a quantity which is in accordance with the reaction yields. Exactly:

- 1) the species C_2H is ionized (reaction number 7) and the C_2H^+ reacts with electrons (reaction numbers 8 and 9) producing C_2 , H , C and CH .
- 2) The carbon molecule (C_2) is ionized (reaction number 11) and C_2^+ reacts with electron forming carbon atom (reaction number 12).

- 3) The species CH is ionized (reaction number 13) and the CH^+ reacts with electron (reaction number 14) producing C and H.
- 4) The species CH_2 is ionized (reaction number 15) and the CH_2^+ reacts with electrons (reaction numbers 16, 17 and 18) producing CH, H, C, H_2 .

Successively Acetylene reacts with C, CH, CH_2 , C_2 and C_2H (reaction numbers 19, 20, 21, 22, 23, 24) forming C_3 , C_3H , C_3H_3 , H, C_4H , C_4 , H_2 , C_4H_2 .

Table 2.1: Chemical Reactions by Benedikt analysis

N	Chemical Reaction	K [m ³ /s]	Reaction yields [-]	ΔH_f [ev]
1	$\text{Ar}^+ + \text{C}_2\text{H}_2 \rightarrow \text{Ar} + \text{C}_2\text{H}_2^+$	4.2×10^{-16}	1	0
2	$\text{C}_2\text{H}_2^+ + e \rightarrow \text{C}_2\text{H} + \text{H}$	9.5×10^{-14}	0.50	0
3	$\text{C}_2\text{H}_2^+ + e \rightarrow \text{C}_2 + \text{H} + \text{H}$	9.5×10^{-14}	0.30	0
4	$\text{C}_2\text{H}_2^+ + e \rightarrow \text{CH} + \text{CH}$	9.5×10^{-14}	0.13	0
5	$\text{C}_2\text{H}_2^+ + e \rightarrow \text{CH}_2 + \text{C}$	9.5×10^{-14}	0.05	0
6	$\text{C}_2\text{H}_2^+ + e \rightarrow \text{C}_2 + \text{H}_2$	9.5×10^{-14}	0.02	0
7	$\text{Ar}^+ + \text{C}_2\text{H} \rightarrow \text{Ar} + \text{C}_2\text{H}^+$	4.2×10^{-16}	1	0
8	$\text{C}_2\text{H}^+ + e \rightarrow \text{C}_2 + \text{H}$	7.2×10^{-14}	0.47	0
9	$\text{C}_2\text{H}^+ + e \rightarrow \text{C} + \text{CH}$	7.2×10^{-14}	0.38	0
10	$\text{C}_2\text{H}^+ + e \rightarrow \text{C} + \text{C} + \text{H}$	7.2×10^{-14}	0.15	0
11	$\text{Ar}^+ + \text{C}_2 \rightarrow \text{Ar} + \text{C}_2^+$	4.2×10^{-16}	1	0
12	$\text{C}_2^+ + e \rightarrow \text{C} + \text{C}$	6.0×10^{-14}	1	0
13	$\text{Ar}^+ + \text{CH} \rightarrow \text{Ar} + \text{CH}^+$	4.2×10^{-16}	1	0
14	$\text{CH}^+ + e \rightarrow \text{C} + \text{H}$	4.5×10^{-14}	1	0
15	$\text{Ar}^+ + \text{CH}_2 \rightarrow \text{Ar} + \text{CH}_2^+$	4.2×10^{-16}	1	0
16	$\text{CH}_2^+ + e \rightarrow \text{CH} + \text{H}$	5.2×10^{-14}	0.25	0
17	$\text{CH}_2^+ + e \rightarrow \text{C} + \text{H}_2$	5.2×10^{-14}	0.12	0
18	$\text{CH}_2^+ + e \rightarrow \text{C} + \text{H} + \text{H}$	5.2×10^{-14}	0.63	0
19	$\text{C} + \text{C}_2\text{H}_2 \rightarrow \text{C}_3 + \text{H}_2$	2.7×10^{-16}	1	1.28
20	$\text{CH} + \text{C}_2\text{H}_2 \rightarrow \text{C}_3\text{H} + \text{H}_2$	2.0×10^{-16}	1	1.91
21	$\text{CH}_2 + \text{C}_2\text{H}_2 \rightarrow \text{C}_3\text{H}_3 + \text{H}$	3.0×10^{-16}	1	0.56
22	$\text{C}_2 + \text{C}_2\text{H}_2 \rightarrow \text{C}_4\text{H} + \text{H}$	2.7×10^{-16}	0.5	0.42
23	$\text{C}_2 + \text{C}_2\text{H}_2 \rightarrow \text{C}_4 + \text{H}_2$	2.7×10^{-16}	0.5	0.97
24	$\text{C}_2\text{H} + \text{C}_2\text{H}_2 \rightarrow \text{C}_4\text{H}_2 + \text{H}$	1.3×10^{-16}	1	0.22

Table 2.2: Chemical Species by Benedikt

Ar	C ₂	C ₂ H ₂ ⁺	C ₄ H
Ar ⁺	C ₂ ⁺	C ₃	CH ₂ ⁺
C	C ₂ H	C ₃ H	C ₄ H ₂
CH	C ₂ H ⁺	C ₃ H ₃	H
CH ⁺	C ₂ H ₂	C ₄	H ₂
CH ₂			

An important parameter in the plasma chemistry of Ar/C₂H₂ mixture is the ratio (F) of the C₂H₂ molecular flux to the Ar⁺ molecular flux realized at the injection point of precursor. This ratio of molecular fluxes is equal to the ratio of their respective molar fractions at the injection point of Acetylene:

$$F = \frac{\alpha_{C_2H_2}}{\alpha_{Ar^+}} \quad (2.1)$$

According to Benedikt if $F < 1$ the charge transfer and dissociative-recombination reactions will dominate, if $F > 1$ the radical neutral reactions are dominant.

Mankelevich Model

Also Mankelevich analyzed hardly the chemistry in an Expanding Thermal Plasma deposition apparatus by means of various techniques both numerical and experimental. He studied especially the apparatus when methane is used as gas precursor. In his experiments CH₄ is injected into Ar/H₂ plasma through an annular injection ring positioned about 0.1 m downstream from the nozzle exit section. Experimentally measures made by cavity ring down spectroscopy technique at various station positioned at different stations from substrate are very useful to achieve the plasma-chemical transformations along the axis, both in the zone where flow field expand and in the so called “free plume region” where some flow parameters, like for instance pressure remain practically constant. Mankelevich studied a lot of chemical reactions involving many chemical species both radical, ions and electrons. Tables 2.3a, 2.3b and 2.3c report some chemical reactions analyzed by him (in table 2.3a there are only radicals, in table 2.3b there are radicals and ions and in table 2.3c there are

radicals, ions and electrons) where are written also the pre-exponential constant (A), the temperature constant (b), the activation energy (E_a) because he considered that chemical reactions can be written in the Arrhenius form:

$$K(T) = AT^b \exp\left(-\frac{E_a}{kT}\right) \quad (2.2)$$

where k is the Boltzmann constant. The physical dimension used by Mankelevich are cal, mol, K, cm and s.

Table 2.3a: Chemical Reactions by Mankelevich analysis

N	Chemical Reaction	A	b	E_A
1a	$C + CH_4 \Leftrightarrow C_2H_3 + H$	5×10^{13}	0	0
2a	$C + C_2H \Leftrightarrow C_3 + H$	1.6×10^{14}	0	0
3a	$C + C_2H_2 \Leftrightarrow C_3H + H$	1.6×10^{14}	0	0
4a	$CH + C_2H \Leftrightarrow C_3H + H$	2×10^{14}	0	0
5a	$CH + C_2H_2 \Leftrightarrow C_3H_2 + H$	2×10^{14}	0	0
6a	$C_2H + C_2H \Leftrightarrow C_4H + H$	1×10^{14}	0	0
7a	$C_2H + C_2H \Leftrightarrow C_4H_2$	8.32×10^{21}	-3	0
8a	$C_2H + CH_4 \Leftrightarrow C_3H_4 + H$	1.2×10^{14}	0	0
9a	$C_2H + CH_3 \Leftrightarrow C_3H_3 + H$	1.2×10^{14}	0	0
10a	$C_3 + CH \Leftrightarrow C_4 + H$	2×10^{14}	0	0
11a	$C_3 + CH_2 \Leftrightarrow C_4H + H$	2×10^{14}	0	0
12a	$C_3 + CH_3 \Leftrightarrow C_4H_2 + H$	2×10^{14}	0	0
13a	$C_3 + CH_4 \Leftrightarrow C_4H_3 + H$	3×10^{18}	0	0
14a	$C_3H + H \Leftrightarrow C_3 + H_2$	1×10^{14}	0	0
15a	$C_3H_2 + H \Leftrightarrow C_3H + H_2$	1×10^{14}	0	0
16a	$C_2 + M \Leftrightarrow C + C + M$	1.5×10^{16}	0	142400
17a	$CH_2 + CH_2 \Leftrightarrow C_2H_2 + H + H$	1.2×10^{14}	0	800
18a	$C_2H_2 + C_2H_2 \Leftrightarrow C_4H_4$	3.9×10^{12}	0	32600
19a	$C_2H_2 + C_2H_2 \Leftrightarrow C_4H_2 + H_2$	1×10^{14}	0	52200
20a	$C_2H_2 + C_2H_2 \Leftrightarrow C_4H_3 + H$	1.4×10^{15}	0	65500

21a	$C_4H_4 \Leftrightarrow C_4H_2 + H_2$	1.1×10^{13}	0	75000
22a	$C_4H_3 + H \Leftrightarrow C_4H_2 + H_2$	8.1×10^{13}	0	0
23a	$C_2H + C_2H_2 \Leftrightarrow C_4H_2 + H$	1.2×10^{14}	0	0
24a	$C_2H + C_4H_2 \Leftrightarrow C_6H_2 + H$	1.2×10^{14}	0	0
25a	$C_4H_2 \Leftrightarrow C_4H + H$	8.9×10^{17}	0	131600
26a	$C_6H_2 \Leftrightarrow C_6H + H$	8.9×10^{13}	0	112100
27a	$C_4H + C_2H_2 \Leftrightarrow C_6H_2 + H$	1.2×10^{14}	0	0
28a	$C_4H + H_2 \Leftrightarrow C_4H_2 + H$	4.1×10^5	2.4	200
29a	$C_6H + H_2 \Leftrightarrow C_6H_2 + H$	4.1×10^5	2.4	200
30a	$C_4H_2 + C_2H_2 \Leftrightarrow C_6H_2 + H_2$	1×10^{14}	0	52200
31a	$C_3H_3 + CH_2 \Leftrightarrow C_4H_4 + H$	4×10^{13}	0	0

Table 2.3b: Chemical Reactions by Mankelevich analysis

N	Chemical Reaction	A	b	E_A
1b	$Ar^+ + H_2 \Leftrightarrow ArH^+ + H$	6×10^{14}	0	0
2b	$Ar^+ + C_2H_2 \Leftrightarrow Ar + C_2H_2^+$	1×10^{14}	0	0
3b	$Ar^+ + C_2H \Leftrightarrow Ar + C_2H^+$	1×10^{14}	0	0
4b	$Ar^+ + CH \Leftrightarrow Ar + CH^+$	1×10^{14}	0	0
5b	$Ar^+ + C \Leftrightarrow Ar + C^+$	1×10^9	0	0

Table 2.3c: Chemical Reactions by Mankelevich analysis

N	Chemical Reaction	A	b	E_A
1c	$ArH^+ + e \Leftrightarrow Ar + H$	3.6×10^{16}	0	0
2c	$C_2H_2^+ + e \Leftrightarrow C_2H + H$	1.58×10^{19}	-0.68	0
3c	$C_2H^+ + e \Leftrightarrow CH + C$	1.41×10^{18}	-0.5	0
4c	$CH^+ + e \Leftrightarrow C + H$	9.39×10^{17}	-0.42	0
5c	$C_2^+ + e \Leftrightarrow C + C$	3.13×10^{18}	-0.5	0
6c	$H^+ + e + e \Leftrightarrow H + e$	1.15×10^{39}	-4.3	0
7c	$Ar^+ + e + e \Leftrightarrow Ar + e$	1.15×10^{39}	-4.3	0
8c	$C^+ + e + e \Leftrightarrow C + e$	1.15×10^{39}	-4.3	0

9c	$H^+ + e + M \Leftrightarrow H + M$	5.6×10^{27}	-2.5	0
10c	$Ar^+ + e + M \Leftrightarrow Ar + M$	5.6×10^{27}	-2.5	0
11c	$C^+ + e + M \Leftrightarrow C + M$	5.6×10^{27}	-2.5	0

It is possible to say that:

- From table 2.3a it is evident that there are 31 reactions involving only radicals based on carbon and hydrogen. Furthermore 12 equations (7a, 16a, 17a, 18a, 19a, 20a, 21a, 25a, 26a, 28a, 29a, 30a) are temperature dependent while the remaining are temperature independent. It is also to point out that all chemical reactions are dissociation-recombination except for equation 18a which is only of recombination, for equations 16a, 21a, 25a and 26a which are only dissociation. Besides in equ. 16a there is also the third body (M) which assumes the role of catalyst. All of these 31 reactions are characterized by two reagents and two yields except for equations 7a and 18a in which there is only 1 yields, for equations 21a, 25a and 26a in which there is only one reagent, for equations 16a and 17a in which there are 3 yields. It is to point out also that reactions 2a and 3a are characterized by the same value of rate constant at fixed temperature because A, b and E_A assume the same values, as well as reactions 4a, 5a, 10a, 11a and 12a are characterized by the same value of rate constant at fixed temperature because A, b and E_A assume the same values, as well as reactions 6a, 14a and 15a are characterized by the same value of rate constant at fixed temperature because A, b and E_A assume the same values, as well as reactions 8a, 9a, 23a, 24a and 27a are characterized by the same value of rate constant at fixed temperature because A, b and E_A assume the same values, as well as reactions 28a and 29a are characterized by the same value of rate constant at fixed temperature because A, b and E_A assume the same values. Activation energy is always zero except for reactions number 16a, 17a, 18a, 19a, 20a, 21a, 25a, 26a, 28a, 29a and 30a.
- From table 2.3b it is evident that there are 5 reactions implying ions. All reactions are temperature independent. Furthermore, except for equ. 1b which is a dissociation-recombination reaction, all reactions are charge transfer. However all reactions are characterized by two reagents and two yields. The third body is not present. It is to point out also that reactions 2b, 3b and 4b are characterized by the same value of rate constant at fixed temperature because A, b and E_A assume the same values. Activation energy is always zero
- From table 2.3c it is evident that there are 11 reactions in which also electrons are involved. Except for reaction 1c which is temperature independent, all reactions are temperature

dependent because the exponential temperature constant is nonzero, while the activation energy is always zero. As the b value is negative the rate constant in each equation is inversely proportional to temperature. Reactions 1c, 2c, 3c, 4c and 5c are dissociation-recombination reactions. In particular the electron recombines with ion which is thus transformed in a radical. Successively the radical dissociates in two radicals. The remaining reactions (6c, 7c, 8c, 9c, 10c and 11c) are recombination reactions and there are three reagents. In particular in equations 9c, 10c and 11c there are electron and third body in the reagents, while in equations 6c, 7c and 8c there are two electrons in the reagents and one electron plays the role of third body. It is to point out also that reactions 6c, 7c and 8c are characterized by the same value of rate constant at fixed temperature because A, b and E_A assume the same values, as well as reactions 9c, 10c and 11c are characterized by the same value of rate constant at fixed temperature because A, b and E_A assume the same values. Activation energy is always zero.

For completeness table 2.4 reports the chemical species involved in the various chemical reactions considered by Mankelevich analysis.

Table 2.4: Chemical Species by Mankelevic analysis

Ar	C_2^+	C_4
Ar^+	C_2H	C_4H
ArH^+	C_2H^+	C_4H_2
C	C_2H_2	C_4H_3
C^+	$C_2H_2^+$	C_4H_4
CH	C_2H_3	C_6H
CH^+	C_3	C_6H_2
CH_2	C_3H	H
CH_3	C_3H_2	H^+
CH_4	C_3H_3	H_2
C_2	C_3H_4	

The dependence of C, C_2 and C_3 hydrocarbon species concentrations with CH_4 flow rate is the result of a complex balance between the above chemical reactions. The most significant reactions are those:

- regarding the shifting of Hydrogen atom ($C_xH_y + H \Leftrightarrow C_xH_{y-1} + H_2$), i.e. reactions number 14a, 15a, 22a,
- linking the C, C₂ and C₃ hydrocarbon groups like in equations 2a, 3a, 4a and 5a.

The high values of concentrations of C and H atoms and of H/H₂ ratio cause the high grow rates showed for diamond film growth by means of d.c.-arc jet reactors.

Confronting reactions by Benedikt and Mankelevich it is clear that 8 chemical reactions are the same. These reactions are:

- 3 charge transfer reactions (equations 1, 7 and 13 from Benedikt table).
- 4 reactions involving electrons (equations 2, 9, 12 and 14 from Benedikt table)
- 1 reaction implying only radicals (equation 24)

At temperature typical for deposition apparatus (around 2000 K) the difference in the values of rate constant by Benedikt and Mankelevich analysis is negligible. However the chemistry by Benedikt is simulated, i.e. the chemical species considered are those reported in table 2.2 and chemical reactions implemented are those written in table 2.1.

Chapter 3

RAREFIED FLOW FIELDS

3.1 Introduction

The rarefaction flow fields are extremely important because they are widely present in many and significant different topics, from industrial to aerospace applications [8] and a lot of researchers studied and study hardly this particular regime. At the beginning of the 20th century Knudsen, Weber and other illustrious researchers started to analyze the rarefied gas dynamics.

In particular Knudsen, for example, examined the mass flow rate in a pipe, discovered the transitional regime and formulate the well-known Knudsen number which, as we will see later, is a particular dimensionless number that characterize if a flow field is continuum or rarefied. From about the 1960's, due to the interest in the space missions, the rarefied regime was studied also in space applications because during the re-entry path at "high" altitude the flow field is not longer continuum. In the same period Bird gave a fundamental contribution to rarefied analysis and invented the DSMC method [9], that is also nowadays the unique reliable method to examine correctly the rarefied flow fields. In fact in these flows the Navier-Stokes equations are correct but can not be used because the phenomenological transport equations of Newton, Fourier and Fick fail. Besides, the Boltzmann Equation is valid (it is valid in all types of regimes) but it is impossible to solve.

From 1980's thanks to the creation of very complicate/special industrial products, such as for example of micro-electronic-mechanical systems, the scientific community discovered the great importance of rarefied flow field in a lot of different industrial applications. Also today due to the importance of micro/nano technologies the rarefaction flows are widely diffused. In fact, for example, the rarefied flow field are obtained:

- in the region between the read/write head and the hard disk of a computer. The rarefaction condition is obtained because even if air is at ambient conditions, the distance between these two elements is of the order of 50 nm.
- in the thin film deposition apparatus. In fact for the creation of thin films the pressure in the deposition chamber has to be of the order of 10-100 Pa and thus the rarefaction conditions are easily obtained.

The aim of this chapter is to illustrate the most diffuse parameters which characterize if a flow field can be considered rarefied or continuum.

3.2 Rarefaction Parameters

In literature there are a lot of parameters to quantify the rarefaction level in the flow field. Some parameters represent the rarefaction degree of the whole flow field, while others analyze only a small/big part of the flow field and thus denote merely the local rarefaction level. The most popular parameters are the P parameter of Bird, the local Knudsen number (Kn_G) based on gradient length scale of a generic thermo-fluid-dynamic quantity and the Cheng and Chang parameter.

The P parameter of Bird is defined as:

$$P = \frac{\sqrt{\pi}}{2} S \frac{\lambda}{\rho} \left| \frac{d\rho}{ds} \right| \quad (3.2.1)$$

where:

- λ is the local mean free path,
- ρ is the local density,
- $\frac{d\rho}{ds}$ is the derivative of density along the direction defined by the curvilinear abscissa s ,
- S is the speed ratio, defined as:

$$S = \frac{V}{c} \quad (3.2.2)$$

In the definition of the speed ratio, V is the macroscopic velocity and c is the most probable thermal velocity equal to:

$$c = \sqrt{\frac{2kT}{m}} \quad (3.2.3)$$

where k is the Boltzmann constant, T is the temperature and m is the physical mass of molecule.

In literature the Speed ratio is often identified as “molecular Mach number”. In fact, as the ratio k/m is equal to the gas constant (R), then the most probable thermal velocity can be expressed as:

$$c = \sqrt{2RT} \quad (3.2.4)$$

And thus substituting the formula (3.2.4) in the (3.2.2), the speed ratio is equal to:

$$S = \frac{V}{\sqrt{2RT}} \quad (3.2.5)$$

Multiplying and dividing equation (3.2.5) by the root square of the ratio of specific heat:

$$S = \frac{\sqrt{\gamma}}{\sqrt{\gamma}} \frac{V}{\sqrt{2RT}} \quad (3.2.6)$$

and thus:

$$S = \frac{\sqrt{\gamma}}{\sqrt{2}} \frac{V}{\sqrt{\gamma RT}} \quad (3.2.7)$$

as $\sqrt{\gamma RT}$ is the laplacian velocity of the sound, the ratio $\frac{V}{\sqrt{\gamma RT}}$ is equal to the Mach number and therefore there is the link between the speed ratio and the mach number:

$$S = \frac{\sqrt{\gamma}}{\sqrt{2}} M \quad (3.2.8)$$

The difference is that the Mach number measures the relative importance of the convective velocity with respect to the sound velocity; the speed ratio measures the relative importance of convective velocity with respect to the mean thermal velocity.

Bird suggests to use the value of $P = 0.02$ as the value of continuum break-down parameter and therefore a molecular approach is necessary if $P > 0.02$ while for $P < 0.02$ the Navier-Stokes equations can be used.

The local Knudsen number based on gradient length scale of a generic thermo-fluid-dynamic quantity (G) is equal to the ratio of mean free path to the gradient length scale of G :

$$\text{Kn}_G = \frac{\lambda}{\left(\frac{\partial G}{\partial s}\right)} \quad (3.2.9)$$

where $(\partial G/\partial s)$ is the spatial derivative of G along the s direction. If we consider for example the flow speed (V), then Kn_G identified as $\text{Kn}_G = \text{Kn}_V = \frac{\lambda}{\partial V/\partial s}$.

According to Bird the flow field:

- is continuum and there is the necessity to use the Navier-Stokes Equations if $\text{Kn}_G < 0.1$,
- is continuum without the necessity to use the Navier-Stokes Equations (continuum low density) if $0.1 < \text{Kn}_G < 0.2$,
- is rarefied and a molecular approach (based for example to Direct Simulation Monte Carlo approach) is necessary if $\text{Kn}_G > 0.2$.

The classification of flow field rarefaction level as function both of Kn_G and P is shown in Fig.3.1.

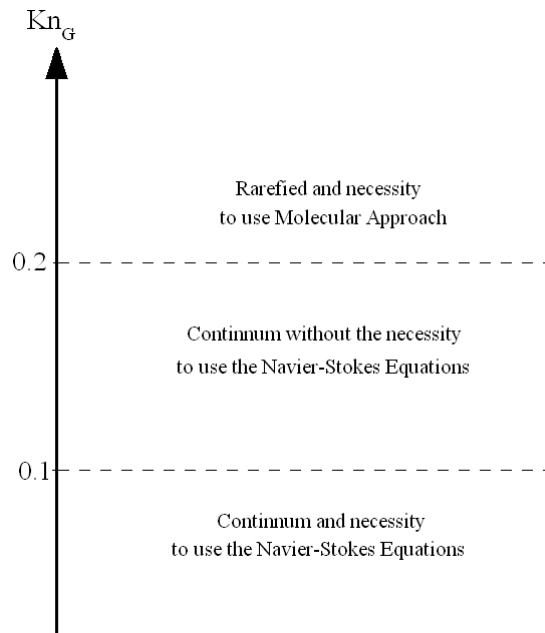


Fig.3.1: Classification of flow field rarefaction levels based on Kn_G

Both P and Kn_G characterize the rarefaction degree in a local zone and not the entire flow field. For rarefaction of whole flow field the overall Knudsen number is a widely accepted parameter and it is equal to the ratio of the mean free path to a characteristic dimension (L_{car}) of the flow field:

$$Kn = \frac{\lambda}{L_{car}} \quad (3.2.10)$$

In particular flow field is:

- continuum if $Kn \ll 1$,
- in transitional regime if $Kn \approx O(1)$,
- in free molecule flow if $Kn \gg 1$.

Obviously other particular formulations of the Knudsen number are possible, according to the choice of λ and/or L_{car} . For instance, λ could be the mean free stream path, the mean free path of the molecules remitted by the body surface, the mean free path down-stream a shock wave, etc. L_{car} could be a geometrical dimension of the body, the boundary layer thickness, the shock wave thickness, the stand-off distance, etc. If Knudsen number based on mean free stream path (Kn_∞) is used, the classification suggested by Moss is useful. This classification says that flow field is:

- 1) Continuum if $Kn_\infty < 0.001$,
- 2) In transitional regime if $0.001 < Kn_\infty < 50$,
- 3) In Free Molecule Flow if $Kn_\infty > 50$.

As said before, another important rarefaction parameter is the Cheng and Chang parameter (K_r^2) which is equal to [10]:

$$K_r^2 = \varepsilon \frac{\rho_\infty V_\infty D T^*}{\mu^* T_0} \quad (3.2.11)$$

where the subscripts ∞ denotes free stream conditions, D is the diameter of body and:

$$\varepsilon = \frac{\gamma - 1}{4\gamma} \quad (3.2.12)$$

$$T^* = \frac{T_0 + T_w}{2} \quad (3.2.13)$$

where T_0 is the stagnation temperature and T_w is the wall temperature. The viscosity μ^* is evaluated by the Sutherland law as:

$$\mu^* = \mu \left(\frac{T^*}{T} \right)^\omega \quad (3.2.14)$$

The Cheng and Chang parameter is used especially to analyze the flow field rarefaction for a capsule during the re-entry path. Furthermore K_r^2 is strictly linked to Reynolds number after a normal shock wave:

$$Re_2 = \frac{\rho_\infty V_\infty D}{\mu_2} \quad (3.2.15)$$

where μ_2 is the viscosity evaluated after a normal shock wave.

Chapter 4

PREPROCESSOR

4.1 Introduction

A pre-processor code is written in order to simulate flow field in the zones of Expanding Thermal Plasma deposition apparatus where there is a continuum regime. More specifically the pre-processor consider the flow field in the torch and in the divergent part of nozzle (exactly from throat until to 90% of length). The use of pre-processor is extremely important because the characterization of the different thermo-fluid-dynamic parameters in a gas influenced by elevated values of temperature is very difficult (in some condition is impossible) by means of experimental measures. In fact in the torch also at low electrical power (around 1 kW) a strong electrical discharge takes place and the “usual” gas is transformed in a plasma at elevated temperature (higher than 10000 K) in which there are radicals, ions and electrons. The gas is not in thermodynamic equilibrium because Ar is destroyed and Ar^+ is created. The flow field is incompressible ($M \ll 1$) at torch inlet section, is subsonic ($M < 1$) at torch exit section and becomes supersonic in the nozzle (clearly in divergent part). Furthermore at 90% of nozzle divergent part due to injection of Acetylene as gas precursor, many chemical reactions, involving both radicals, ions and electrons take place. These reaction are very complex and change continuously chemical composition of plasma mixture and thus the chemical-physical properties of plasma mixture.

The present pre-processor code is written using the Microsoft QuickBASIC language and it is made up of 4 different sub-codes which work in tandem, i.e. the output from a code is the input to the following code. Figure 4.1 describes the scheme of the used codes.

In particular:

- by INPUTVS.BAS user can fix some useful parameters, such as for example the electrical power supplied to torch.
- HEATVS.BAS is a sub-code which simulates flow field in entire torch. Flow field is made up of inert Argon, the ionization effect by means of the Saha's equation is considered.
- NOZVS.BAS is a sub-code which simulates flow field in divergent part of nozzle (from throat until to 90% of nozzle axis). Flow field is made up of Ar and Ar^+ .
- CHIBEVS.BAS is a sub-code which simulates flow field from 90% of nozzle for a very short space (10^{-5} m). Presence of Acetylene as gas precursor is considered and in particular

it is injected at velocity of 100 m/s. Chemical reactions generate a plasma mixture made up of 21 chemical species (15 radical and 6 ions).

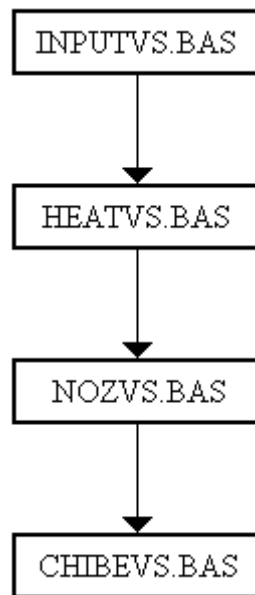


Fig. 4.1 - Scheme of pre-processor code

A complex mathematical model is developed to characterize the complex aero-thermo-chemic behavior of flow field. The aim of this chapter is to explain in a clear way the various thermo-fluid-dynamic laws used.

4.2 Basic Equations

In torch and in nozzle the flow field is considered for hypothesis:

- 1) Quasi 1D, i.e. the flow field is considered only along the axis centerline.
- 2) Time independent, thus time derivative is equal to zero $\left(\frac{\partial}{\partial t} = 0\right)$.
- 3) Not viscous and not thermally conductive.
- 4) Each gas constituting the plasma mixture is a perfect gas ($P=\rho RT$).
- 5) Validity of the Dalton law, therefore pressure of whole mixture is equal to sum of pressure of each single gas.
- 6) Chemically reactive when precursor (Acetylene) at 90% of nozzle axis is injected. Therefore chemical reactions occur.

The variability with temperature of degrees of freedom and of specific heats are also taken into account. It is to point out that flow field along torch and nozzle is very complex for many reason and a rapid thermo-fluid-dynamic evolution occurs. For the solution of the various unknown parameters, such as for example velocity, pressure and density the following equations must be taken into account:

- 3 equations related to thermo-fluid-dynamics (conservative equations of mass, momentum and energy).
- State equation of plasma mixture written in terms of pressure.
- State equation of plasma mixture written in terms of specific energy.

The three thermo-fluid-dynamic equations are:

$$\rho u A = \text{const} \quad (4.2.1)$$

$$p + \rho u^2 = \text{const} \quad (4.2.2)$$

$$h + \frac{u^2}{2} = \text{const} \quad (4.2.3)$$

where obviously ρ is density, u is velocity component along the x direction, A is area section of conduct which changes along x axis, p is pressure and h is enthalpy.

In order to obtain the state equation of plasma mixture written in terms of pressure, the Dalton law is used. By this law the total pressure of the whole mixture is equal to the sum of pressure of each single gas constituting the mixture:

$$p = \sum_{i=1}^{21} p_i \quad (4.2.4)$$

writing the pressure linked to the 21 chemical species it results:

$$p = p_{Ar} + p_{Ar^+} + p_{C_2H_2} + p_{C_2H_2^+} + p_{C_2H} + p_H + p_{C_2} + p_{CH} + p_{C_2H^+} + p_C + p_{C_2^+} + p_{CH^+} + \\ p_{CH_2} + p_{CH_2^+} + p_{H_2} + p_{C_3} + p_{C_3H} + p_{C_3H_3} + p_{C_4H} + p_{C_4} + p_{C_4H_2} \quad (4.2.5)$$

State equation is valid for pressure of each gas:

$$p = \frac{\text{Num}}{\text{Vol}} k T \quad (4.2.6)$$

where obviously Num is the number of molecules of the mixture, Vol is the volume occupied by the mixture and k is the Boltzmann constant (about 1.38×10^{-23} J/k). Thus:

$$p = \frac{kT}{\text{Vol}} (\text{Num}_{Ar} + \text{Num}_{Ar^+} + \text{Num}_{C_2H_2} + \text{Num}_{C_2H_2^+} + \text{Num}_{C_2H} + \text{Num}_H + \text{Num}_{C_2} + \text{Num}_{CH} + \\ \text{Num}_{C_2H^+} + \text{Num}_C + \text{Num}_{C_2^+} + \text{Num}_{CH^+} + \text{Num}_{CH_2} + \text{Num}_{CH_2^+} + \text{Num}_{H_2} + \text{Num}_{C_3} + \\ \text{Num}_{C_3H} + \text{Num}_{C_3H_3} + \text{Num}_{C_4H} + \text{Num}_{C_4} + \text{Num}_{C_4H_2}) \quad (4.2.7)$$

Now multiply and divide each number of atoms for the physical mass (in [kg]) of the related chemical species:

$$\begin{aligned}
p = T k \frac{1}{\text{Vol}} & \left(\text{Num}_{\text{Ar}} \frac{m_{\text{Ar}}}{m_{\text{Ar}}} + \text{Num}_{\text{Ar}^+} \frac{m_{\text{Ar}^+}}{m_{\text{Ar}^+}} + \text{Num}_{\text{C}_2\text{H}_2} \frac{m_{\text{C}_2\text{H}_2}}{m_{\text{C}_2\text{H}_2}} + \text{Num}_{\text{C}_2\text{H}_2^+} \frac{m_{\text{C}_2\text{H}_2^+}}{m_{\text{C}_2\text{H}_2^+}} + \text{Num}_{\text{C}_2\text{H}} \frac{m_{\text{C}_2\text{H}}}{m_{\text{C}_2\text{H}}} + \right. \\
& \text{Num}_{\text{H}} \frac{m_{\text{H}}}{m_{\text{H}}} + \text{Num}_{\text{C}_2} \frac{m_{\text{C}_2}}{m_{\text{C}_2}} + \text{Num}_{\text{CH}} \frac{m_{\text{CH}}}{m_{\text{CH}}} + \text{Num}_{\text{C}_2\text{H}^+} \frac{m_{\text{C}_2\text{H}^+}}{m_{\text{C}_2\text{H}^+}} + \text{Num}_{\text{C}} \frac{m_{\text{C}}}{m_{\text{C}}} + \text{Num}_{\text{C}_2^+} \frac{m_{\text{C}_2^+}}{m_{\text{C}_2^+}} + \\
& \text{Num}_{\text{CH}^+} \frac{m_{\text{CH}^+}}{m_{\text{CH}^+}} + \text{Num}_{\text{CH}_2} \frac{m_{\text{CH}_2}}{m_{\text{CH}_2}} + \text{Num}_{\text{CH}_2^+} \frac{m_{\text{CH}_2^+}}{m_{\text{CH}_2^+}} + \text{Num}_{\text{H}_2} \frac{m_{\text{H}_2}}{m_{\text{H}_2}} + \text{Num}_{\text{C}_3} \frac{m_{\text{C}_3}}{m_{\text{C}_3}} + \\
& \left. \text{Num}_{\text{C}_3\text{H}} \frac{m_{\text{C}_3\text{H}}}{m_{\text{C}_3\text{H}}} + \text{Num}_{\text{C}_3\text{H}_3} \frac{m_{\text{C}_3\text{H}_3}}{m_{\text{C}_3\text{H}_3}} + \text{Num}_{\text{C}_4\text{H}} \frac{m_{\text{C}_4\text{H}}}{m_{\text{C}_4\text{H}}} + \text{Num}_{\text{C}_4} \frac{m_{\text{C}_4}}{m_{\text{C}_4}} + \text{Num}_{\text{C}_4\text{H}_2} \frac{m_{\text{C}_4\text{H}_2}}{m_{\text{C}_4\text{H}_2}} \right) \quad (4.2.8)
\end{aligned}$$

The product of number of atoms of a generic chemical species with the physical mass of the same single atom is the physical mass (M) of that chemical species present in the mixture. Therefore:

$$\begin{aligned}
p = T k \frac{1}{\text{Vol}} & \left(M_{\text{Ar}} \frac{1}{m_{\text{Ar}}} + M_{\text{Ar}^+} \frac{1}{m_{\text{Ar}^+}} + M_{\text{C}_2\text{H}_2} \frac{1}{m_{\text{C}_2\text{H}_2}} + M_{\text{C}_2\text{H}_2^+} \frac{1}{m_{\text{C}_2\text{H}_2^+}} + M_{\text{C}_2\text{H}} \frac{1}{m_{\text{C}_2\text{H}}} + M_{\text{H}} \frac{1}{m_{\text{H}}} + \right. \\
& M_{\text{C}_2} \frac{1}{m_{\text{C}_2}} + M_{\text{CH}} \frac{1}{m_{\text{CH}}} + M_{\text{C}_2\text{H}^+} \frac{1}{m_{\text{C}_2\text{H}^+}} + M_{\text{C}} \frac{1}{m_{\text{C}}} + M_{\text{C}_2^+} \frac{1}{m_{\text{C}_2^+}} + M_{\text{CH}^+} \frac{1}{m_{\text{CH}^+}} + \\
& M_{\text{CH}_2} \frac{1}{m_{\text{CH}_2}} + M_{\text{CH}_2^+} \frac{1}{m_{\text{CH}_2^+}} + M_{\text{H}_2} \frac{1}{m_{\text{H}_2}} + M_{\text{C}_3} \frac{1}{m_{\text{C}_3}} + M_{\text{C}_3\text{H}} \frac{1}{m_{\text{C}_3\text{H}}} + \\
& \left. M_{\text{C}_3\text{H}_3} \frac{1}{m_{\text{C}_3\text{H}_3}} + M_{\text{C}_4\text{H}} \frac{1}{m_{\text{C}_4\text{H}}} + M_{\text{C}_4} \frac{1}{m_{\text{C}_4}} + M_{\text{C}_4\text{H}_2} \frac{1}{m_{\text{C}_4\text{H}_2}} \right) \quad (4.2.9)
\end{aligned}$$

It is to point out that, for example the difference between m_{Ar} and M_{Ar} is that m_{Ar} is the physical mass (in [kg]) of a single Ar atom while M_{Ar} is the physical mass (always in [kg]) of all the Ar atoms present in the mixture. The same reasoning is valid for each other chemical species. Now multiply and divide equ.(4.2.9) for physical mass of whole plasma mixture (M_{TOT}):

$$\begin{aligned}
p = T k \frac{M_{\text{TOT}}}{\text{Vol}} & \left(\frac{M_{\text{Ar}}}{M_{\text{TOT}}} \frac{1}{m_{\text{Ar}}} + \frac{M_{\text{Ar}^+}}{M_{\text{TOT}}} \frac{1}{m_{\text{Ar}^+}} + \frac{M_{\text{C}_2\text{H}_2}}{M_{\text{TOT}}} \frac{1}{m_{\text{C}_2\text{H}_2}} + \frac{M_{\text{C}_2\text{H}_2^+}}{M_{\text{TOT}}} \frac{1}{m_{\text{C}_2\text{H}_2^+}} + \frac{M_{\text{C}_2\text{H}}}{M_{\text{TOT}}} \frac{1}{m_{\text{C}_2\text{H}}} + \right. \\
& \frac{M_{\text{H}}}{M_{\text{TOT}}} \frac{1}{m_{\text{H}}} + \frac{M_{\text{C}_2}}{M_{\text{TOT}}} \frac{1}{m_{\text{C}_2}} + \frac{M_{\text{CH}}}{M_{\text{TOT}}} \frac{1}{m_{\text{CH}}} + \frac{M_{\text{C}_2\text{H}^+}}{M_{\text{TOT}}} \frac{1}{m_{\text{C}_2\text{H}^+}} + \frac{M_{\text{C}}}{M_{\text{TOT}}} \frac{1}{m_{\text{C}}} + \frac{M_{\text{C}_2^+}}{M_{\text{TOT}}} \frac{1}{m_{\text{C}_2^+}} + \\
& \frac{M_{\text{CH}^+}}{M_{\text{TOT}}} \frac{1}{m_{\text{CH}^+}} + \frac{M_{\text{CH}_2}}{M_{\text{TOT}}} \frac{1}{m_{\text{CH}_2}} + \frac{M_{\text{CH}_2^+}}{M_{\text{TOT}}} \frac{1}{m_{\text{CH}_2^+}} + \frac{M_{\text{H}_2}}{M_{\text{TOT}}} \frac{1}{m_{\text{H}_2}} + \frac{M_{\text{C}_3}}{M_{\text{TOT}}} \frac{1}{m_{\text{C}_3}} + \\
& \left. \frac{M_{\text{C}_3\text{H}}}{M_{\text{TOT}}} \frac{1}{m_{\text{C}_3\text{H}}} + \frac{M_{\text{C}_3\text{H}_3}}{M_{\text{TOT}}} \frac{1}{m_{\text{C}_3\text{H}_3}} + \frac{M_{\text{C}_4\text{H}}}{M_{\text{TOT}}} \frac{1}{m_{\text{C}_4\text{H}}} + \frac{M_{\text{C}_4}}{M_{\text{TOT}}} \frac{1}{m_{\text{C}_4}} + \frac{M_{\text{C}_4\text{H}_2}}{M_{\text{TOT}}} \frac{1}{m_{\text{C}_4\text{H}_2}} \right) \quad (4.2.10)
\end{aligned}$$

obviously the ratio M_{TOT} to the volume is the density of plasma mixture, while the ratio of the mass of each chemical species to M_{TOT} is the mass fraction (β) linked to each chemical species:

$$\begin{aligned}
 p = T k \rho \left(\beta_{Ar} \frac{1}{m_{Ar}} + \beta_{Ar+} \frac{1}{m_{Ar+}} + \beta_{C2H2} \frac{1}{m_{C2H2}} + \beta_{C2H2+} \frac{1}{m_{C2H2+}} + \beta_{C2H} \frac{1}{m_{C2H}} + \beta_H \frac{1}{m_H} + \right. \\
 \beta_{C2} \frac{1}{m_{C2}} + \beta_{CH} \frac{1}{m_{CH}} + \beta_{C2H+} \frac{1}{m_{C2H+}} + \beta_C \frac{1}{m_C} + \beta_{C2+} \frac{1}{m_{C2+}} + \beta_{CH+} \frac{1}{m_{CH+}} + \beta_{CH2} \frac{1}{m_{CH2}} + \\
 \beta_{CH2+} \frac{1}{m_{CH2+}} + \beta_{H2} \frac{1}{m_{H2}} + \beta_{C3} \frac{1}{m_{C3}} + \beta_{C3H} \frac{1}{m_{C3H}} + \beta_{C3H3} \frac{1}{m_{C3H3}} + \beta_{C4H} \frac{1}{m_{C4H}} + \\
 \left. \beta_{C4} \frac{1}{m_{C4}} + \beta_{C4H2} \frac{1}{m_{C4H2}} \right) \quad (4.2.11)
 \end{aligned}$$

Now multiply and divide equ. (4.2.11) for m_{Ar} :

$$\begin{aligned}
 p = T \frac{k}{m_{Ar}} \rho \left(\beta_{Ar} \frac{m_{Ar}}{m_{Ar}} + \beta_{Ar+} \frac{m_{Ar}}{m_{Ar+}} + \beta_{C2H2} \frac{m_{Ar}}{m_{C2H2}} + \beta_{C2H2+} \frac{m_{Ar}}{m_{C2H2+}} + \beta_{C2H} \frac{m_{Ar}}{m_{C2H}} + \beta_H \frac{m_{Ar}}{m_H} + \right. \\
 \beta_{C2} \frac{m_{Ar}}{m_{C2}} + \beta_{CH} \frac{m_{Ar}}{m_{CH}} + \beta_{C2H+} \frac{m_{Ar}}{m_{C2H+}} + \beta_C \frac{m_{Ar}}{m_C} + \beta_{C2+} \frac{m_{Ar}}{m_{C2+}} + \beta_{CH+} \frac{m_{Ar}}{m_{CH+}} + \beta_{CH2} \frac{m_{Ar}}{m_{CH2}} + \\
 \beta_{CH2+} \frac{m_{Ar}}{m_{CH2+}} + \beta_{H2} \frac{m_{Ar}}{m_{H2}} + \beta_{C3} \frac{m_{Ar}}{m_{C3}} + \beta_{C3H} \frac{m_{Ar}}{m_{C3H}} + \beta_{C3H3} \frac{m_{Ar}}{m_{C3H3}} + \beta_{C4H} \frac{m_{Ar}}{m_{C4H}} + \\
 \left. \beta_{C4} \frac{m_{Ar}}{m_{C4}} + \beta_{C4H2} \frac{m_{Ar}}{m_{C4H2}} \right) \quad (4.2.12)
 \end{aligned}$$

placing for convenience:

$$Z_{Ar} = \frac{m_{Ar}}{m_{Ar}} = 1 \quad (4.2.13a)$$

$$Z_{Ar+} = \frac{m_{Ar}}{m_{Ar+}} = 1 \quad (4.2.13b)$$

because it is approximated that Ar and Ar⁺ have got the same physical mass. In fact the physical mass of electron (about 9.109×10⁻³¹ kg) can be neglected because very small in comparison with that of Argon (about 6.64×10⁻²⁸ kg).

$$Z_{C_2H_2} = \frac{m_{Ar}}{m_{C_2H_2}} \quad (4.2.13c)$$

$$Z_{C_2H_2^+} = \frac{m_{Ar}}{m_{C_2H_2^+}} \quad (4.2.13d)$$

$$Z_{C_2H} = \frac{m_{Ar}}{m_{C_2H}} \quad (4.2.13e)$$

$$Z_H = \frac{m_{Ar}}{m_H} \quad (4.2.13f)$$

$$Z_{C_2} = \frac{m_{Ar}}{m_{C_2}} \quad (4.2.13g)$$

$$Z_{CH} = \frac{m_{Ar}}{m_{CH}} \quad (4.2.13h)$$

$$Z_{C_2H^+} = \frac{m_{Ar}}{m_{C_2H^+}} \quad (4.2.13i)$$

$$Z_C = \frac{m_{Ar}}{m_C} \quad (4.2.13j)$$

$$Z_{C_2^+} = \frac{m_{Ar}}{m_{C_2^+}} \quad (4.2.13k)$$

$$Z_{CH^+} = \frac{m_{Ar}}{m_{CH^+}} \quad (4.2.13m)$$

$$Z_{CH_2} = \frac{m_{Ar}}{m_{CH_2}} \quad (4.2.13n)$$

$$Z_{CH_2^+} = \frac{m_{Ar}}{m_{CH_2^+}} \quad (4.2.13p)$$

$$Z_{H_2} = \frac{m_{Ar}}{m_{H_2}} \quad (4.2.13q)$$

$$Z_{C_3} = \frac{m_{Ar}}{m_{C_3}} \quad (4.2.13r)$$

$$Z_{C_3H} = \frac{m_{Ar}}{m_{C_3H}} \quad (4.2.13s)$$

$$Z_{C_3H_3} = \frac{m_{Ar}}{m_{C_3H_3}} \quad (4.2.13t)$$

$$Z_{C_4H} = \frac{m_{Ar}}{m_{C_4H}} \quad (4.2.13u)$$

$$Z_{C_4} = \frac{m_{Ar}}{m_{C_4}} \quad (4.2.13v)$$

$$Z_{C_4H_2} = \frac{m_{Ar}}{m_{C_4H_2}} \quad (4.2.13z)$$

clearly these 21 parameters are all dimensionless. Therefore equation (4.2.12) becomes:

$$p = T \frac{k}{m_{Ar}} \rho (\beta_{Ar} + \beta_{Ar^+} + \beta_{C_2H_2} Z_{C_2H_2} + \beta_{C_2H_2^+} Z_{C_2H_2^+} + \beta_{C_2H} Z_{C_2H} + \beta_H Z_H + \beta_{C_2} Z_{C_2} + \beta_{CH} Z_{CH} + \beta_{C_2H^+} Z_{C_2H^+} + \beta_C Z_C + \beta_{C_2^+} Z_{C_2^+} + \beta_{CH^+} Z_{CH^+} + \beta_{CH_2} Z_{CH_2} + \beta_{CH_2^+} Z_{CH_2^+} + \beta_{H_2} Z_{H_2} + \beta_{C_3} Z_{C_3} + \beta_{C_3H} Z_{C_3H} + \beta_{C_3H_3} Z_{C_3H_3} + \beta_{C_4H} Z_{C_4H} + \beta_{C_4} Z_{C_4} + \beta_{C_4H_2} Z_{C_4H_2}) \quad (4.2.14)$$

Always for simplicity, it is opportune to consider the following dimensionless parameter:

$$\begin{aligned}
Z_1 = & \beta_{Ar} + \beta_{Ar^+} + \beta_{C_2H_2} Z_{C_2H_2} + \beta_{C_2H_2^+} Z_{C_2H_2^+} + \beta_{C_2H} Z_{C_2H} + \beta_H Z_H + \beta_{C_2} Z_{C_2} + \beta_{CH} Z_{CH} + \\
& \beta_{C_2H^+} Z_{C_2H^+} + \beta_C Z_C + \beta_{C_2^+} Z_{C_2^+} + \beta_{CH^+} Z_{CH^+} + \beta_{CH_2} Z_{CH_2} + \beta_{CH_2^+} Z_{CH_2^+} + \beta_{H_2} Z_{H_2} + \\
& \beta_{C_3} Z_{C_3} + \beta_{C_3H} Z_{C_3H} + \beta_{C_3H_3} Z_{C_3H_3} + \beta_{C_4H} Z_{C_4H} + \beta_{C_4} Z_{C_4} + \beta_{C_4H_2} Z_{C_4H_2}
\end{aligned} \tag{4.2.15}$$

Thus equation (4.2.14) is equal to the following:

$$p = T \frac{k}{m_{Ar}} \rho Z_1 \tag{4.2.16}$$

As the ratio of Boltzmann constant to m_{Ar} is the constant of Argon (R_{Ar}), it results:

$$p = R_{Ar} T \rho Z_1 \tag{4.2.17}$$

In order to obtain the state equation of plasma mixture written in terms of specific energy the form of total energy is used. Obviously this total energy is equal to the sum of energy of each single chemical species multiplied with the linked number of molecules:

$$\begin{aligned}
E_{TOT} = & E_{Ar} Num_{Ar} + E_{Ar^+} Num_{Ar^+} + E_{C_2H_2} Num_{C_2H_2} + E_{C_2H_2^+} Num_{C_2H_2^+} + E_{C_2H} Num_{C_2H} + E_H Num_H + \\
& E_{C_2} Num_{C_2} + E_{CH} Num_{CH} + E_{C_2H^+} Num_{C_2H^+} + E_C Num_C + E_{C_2^+} Num_{C_2^+} + E_{CH^+} Num_{CH^+} + \\
& E_{CH_2} Num_{CH_2} + E_{CH_2^+} Num_{CH_2^+} + E_{H_2} Num_{H_2} + E_{C_3} Num_{C_3} + E_{C_3H} Num_{C_3H} + E_{C_3H_3} Num_{C_3H_3} + \\
& E_{C_4H} Num_{C_4H} + E_{C_4} Num_{C_4} + E_{C_4H_2} Num_{C_4H_2}
\end{aligned} \tag{4.2.18}$$

It is to point out that E_{TOT} is total energy which is different from specific total energy (e_{TOT}), more specifically $e_{TOT} = E_{TOT}/M_{TOT}$. However total energy of a single chemical species is defined as:

$$E_{TOT} = \frac{n}{2} kT \tag{4.2.19}$$

where n is the number of degree of freedom of chemical species. For this reason the following equation of total energy is obtained considering equ. (4.2.19) for each chemical species:

$$\begin{aligned}
E_{\text{TOT}} = kT & \left(\text{Num}_{\text{Ar}} \frac{n_{\text{Ar}}}{2} + \text{Num}_{\text{Ar}^+} \frac{n_{\text{Ar}^+}}{2} + \text{Num}_{\text{C}_2\text{H}_2} \frac{n_{\text{C}_2\text{H}_2}}{2} + \text{Num}_{\text{C}_2\text{H}_2^+} \frac{n_{\text{C}_2\text{H}_2^+}}{2} + \text{Num}_{\text{C}_2\text{H}} \frac{n_{\text{C}_2\text{H}}}{2} + \right. \\
& \text{Num}_{\text{H}} \frac{n_{\text{H}}}{2} + \text{Num}_{\text{C}_2} \frac{n_{\text{C}_2}}{2} + \text{Num}_{\text{CH}} \frac{n_{\text{CH}}}{2} + \text{Num}_{\text{C}_2\text{H}} \frac{n_{\text{C}_2\text{H}}}{2} + \text{Num}_{\text{C}} \frac{n_{\text{C}}}{2} + \text{Num}_{\text{C}_2^+} \frac{n_{\text{C}_2^+}}{2} + \\
& \text{Num}_{\text{CH}^+} \frac{n_{\text{CH}^+}}{2} + \text{Num}_{\text{CH}_2} \frac{n_{\text{CH}_2}}{2} + \text{Num}_{\text{CH}_2^+} \frac{n_{\text{CH}_2^+}}{2} + \text{Num}_{\text{H}_2} \frac{n_{\text{H}_2}}{2} + \text{Num}_{\text{C}_3} \frac{n_{\text{C}_3}}{2} + \\
& \left. \text{Num}_{\text{C}_3\text{H}} \frac{n_{\text{C}_3\text{H}}}{2} + \text{Num}_{\text{C}_3\text{H}_3} \frac{n_{\text{C}_3\text{H}_3}}{2} + \text{Num}_{\text{C}_4\text{H}} \frac{n_{\text{C}_4\text{H}}}{2} + \text{Num}_{\text{C}_4} \frac{n_{\text{C}_4}}{2} + \text{Num}_{\text{C}_4\text{H}_2} \frac{n_{\text{C}_4\text{H}_2}}{2} \right) \quad (4.2.20)
\end{aligned}$$

Similar to what made for pressure (see eq.(4.2.12)), multiply and divide each number of atoms for the physical mass (in [kg]) of the corresponding chemical species:

$$\begin{aligned}
E_{\text{TOT}} = kT & \left(\text{Num}_{\text{Ar}} \frac{n_{\text{Ar}}}{2} \frac{m_{\text{Ar}}}{m_{\text{Ar}}} + \text{Num}_{\text{Ar}^+} \frac{n_{\text{Ar}^+}}{2} \frac{m_{\text{Ar}^+}}{m_{\text{Ar}^+}} + \text{Num}_{\text{C}_2\text{H}_2} \frac{n_{\text{C}_2\text{H}_2}}{2} \frac{m_{\text{C}_2\text{H}_2}}{m_{\text{C}_2\text{H}_2}} + \right. \\
& \text{Num}_{\text{C}_2\text{H}_2^+} \frac{n_{\text{C}_2\text{H}_2^+}}{2} \frac{m_{\text{C}_2\text{H}_2^+}}{m_{\text{C}_2\text{H}_2^+}} + \text{Num}_{\text{C}_2\text{H}} \frac{n_{\text{C}_2\text{H}}}{2} \frac{m_{\text{C}_2\text{H}}}{m_{\text{C}_2\text{H}}} + \text{Num}_{\text{H}} \frac{n_{\text{H}}}{2} \frac{m_{\text{H}}}{m_{\text{H}}} + \text{Num}_{\text{C}_2} \frac{n_{\text{C}_2}}{2} \frac{m_{\text{C}_2}}{m_{\text{C}_2}} + \\
& \text{Num}_{\text{CH}} \frac{n_{\text{CH}}}{2} \frac{m_{\text{CH}}}{m_{\text{CH}}} + \text{Num}_{\text{C}_2\text{H}^+} \frac{n_{\text{C}_2\text{H}^+}}{2} \frac{m_{\text{C}_2\text{H}^+}}{m_{\text{C}_2\text{H}^+}} + \text{Num}_{\text{C}} \frac{n_{\text{C}}}{2} \frac{m_{\text{C}}}{m_{\text{C}}} + \text{Num}_{\text{C}_2^+} \frac{n_{\text{C}_2^+}}{2} \frac{m_{\text{C}_2^+}}{m_{\text{C}_2^+}} + \\
& \text{Num}_{\text{CH}^+} \frac{n_{\text{CH}^+}}{2} \frac{m_{\text{CH}^+}}{m_{\text{CH}^+}} + \text{Num}_{\text{CH}_2} \frac{n_{\text{CH}_2}}{2} \frac{m_{\text{CH}_2}}{m_{\text{CH}_2}} + \text{Num}_{\text{CH}_2^+} \frac{n_{\text{CH}_2^+}}{2} \frac{m_{\text{CH}_2^+}}{m_{\text{CH}_2^+}} + \text{Num}_{\text{H}_2} \frac{n_{\text{H}_2}}{2} \frac{m_{\text{H}_2}}{m_{\text{H}_2}} + \\
& \text{Num}_{\text{C}_3} \frac{n_{\text{C}_3}}{2} \frac{m_{\text{C}_3}}{m_{\text{C}_3}} + \text{Num}_{\text{C}_3\text{H}} \frac{n_{\text{C}_3\text{H}}}{2} \frac{m_{\text{C}_3\text{H}}}{m_{\text{C}_3\text{H}}} + \text{Num}_{\text{C}_3\text{H}_3} \frac{n_{\text{C}_3\text{H}_3}}{2} \frac{m_{\text{C}_3\text{H}_3}}{m_{\text{C}_3\text{H}_3}} + \text{Num}_{\text{C}_4\text{H}} \frac{n_{\text{C}_4\text{H}}}{2} \frac{m_{\text{C}_4\text{H}}}{m_{\text{C}_4\text{H}}} + \\
& \left. \text{Num}_{\text{C}_4} \frac{n_{\text{C}_4}}{2} \frac{m_{\text{C}_4}}{m_{\text{C}_4}} + \text{Num}_{\text{C}_4\text{H}_2} \frac{n_{\text{C}_4\text{H}_2}}{2} \frac{m_{\text{C}_4\text{H}_2}}{m_{\text{C}_4\text{H}_2}} \right) \quad (4.2.21)
\end{aligned}$$

Once again the product of number of atoms of a chemical species with the physical mass of a single atom is M. Therefore:

$$\begin{aligned}
E_{\text{TOT}} = kT & \left(M_{\text{Ar}} \frac{n_{\text{Ar}}}{2} \frac{1}{m_{\text{Ar}}} + M_{\text{Ar}^+} \frac{n_{\text{Ar}^+}}{2} \frac{1}{m_{\text{Ar}^+}} + M_{\text{C}_2\text{H}_2} \frac{n_{\text{C}_2\text{H}_2}}{2} \frac{1}{m_{\text{C}_2\text{H}_2}} + M_{\text{C}_2\text{H}_2^+} \frac{n_{\text{C}_2\text{H}_2^+}}{2} \frac{1}{m_{\text{C}_2\text{H}_2^+}} + \right. \\
& M_{\text{C}_2\text{H}} \frac{n_{\text{C}_2\text{H}}}{2} \frac{1}{m_{\text{C}_2\text{H}}} + M_{\text{H}} \frac{n_{\text{H}}}{2} \frac{1}{m_{\text{H}}} + M_{\text{C}_2} \frac{n_{\text{C}_2}}{2} \frac{1}{m_{\text{C}_2}} + M_{\text{CH}} \frac{n_{\text{CH}}}{2} \frac{1}{m_{\text{CH}}} + M_{\text{C}_2\text{H}^+} \frac{n_{\text{C}_2\text{H}^+}}{2} \frac{1}{m_{\text{C}_2\text{H}^+}} + \\
& M_{\text{C}} \frac{n_{\text{C}}}{2} \frac{1}{m_{\text{C}}} + M_{\text{C}_2^+} \frac{n_{\text{C}_2^+}}{2} \frac{1}{m_{\text{C}_2^+}} + M_{\text{CH}^+} \frac{n_{\text{CH}^+}}{2} \frac{1}{m_{\text{CH}^+}} + M_{\text{CH}_2} \frac{n_{\text{CH}_2}}{2} \frac{1}{m_{\text{CH}_2}} + M_{\text{CH}_2^+} \frac{n_{\text{CH}_2^+}}{2} \frac{1}{m_{\text{CH}_2^+}} +
\end{aligned}$$

$$\begin{aligned}
& M_{H_2} \frac{n_{H_2}}{2} \frac{1}{m_{H_2}} + M_{C_3} \frac{n_{C_3}}{2} \frac{1}{m_{C_3}} + M_{C_3H} \frac{n_{C_3H}}{2} \frac{1}{m_{C_3H}} + M_{C_3H_3} \frac{n_{C_3H_3}}{2} \frac{1}{m_{C_3H_3}} + \\
& \left. M_{C_4H} \frac{n_{C_4H}}{2} \frac{1}{m_{C_4H}} + M_{C_4} \frac{n_{C_4}}{2} \frac{1}{m_{C_4}} + M_{C_4H_2} \frac{n_{C_4H_2}}{2} \frac{1}{m_{C_4H_2}} \right) \quad (4.2.22)
\end{aligned}$$

Now multiply and divide the equ.(4.2.22) by M_{TOT} :

$$\begin{aligned}
E_{TOT} = k T M_{TOT} & \left(\frac{M_{Ar}}{M_{TOT}} \frac{n_{Ar}}{2} \frac{1}{m_{Ar}} + \frac{M_{Ar+}}{M_{TOT}} \frac{n_{Ar+}}{2} \frac{1}{m_{Ar+}} + \frac{M_{C_2H_2}}{M_{TOT}} \frac{n_{C_2H_2}}{2} \frac{1}{m_{C_2H_2}} + \frac{M_{C_2H_2+}}{M_{TOT}} \frac{n_{C_2H_2+}}{2} \frac{1}{m_{C_2H_2+}} + \right. \\
& \frac{M_{C_2H}}{M_{TOT}} \frac{n_{C_2H}}{2} \frac{1}{m_{C_2H}} + \frac{M_H}{M_{TOT}} \frac{n_H}{2} \frac{1}{m_H} + \frac{M_{C_2}}{M_{TOT}} \frac{n_{C_2}}{2} \frac{1}{m_{C_2}} + \frac{M_{CH}}{M_{TOT}} \frac{n_{CH}}{2} \frac{1}{m_{CH}} + \frac{M_{C_2H+}}{M_{TOT}} \frac{n_{C_2H+}}{2} \frac{1}{m_{C_2H+}} + \\
& \frac{M_C}{M_{TOT}} \frac{n_C}{2} \frac{1}{m_C} + \frac{M_{C_2+}}{M_{TOT}} \frac{n_{C_2+}}{2} \frac{1}{m_{C_2+}} + \frac{M_{CH+}}{M_{TOT}} \frac{n_{CH+}}{2} \frac{1}{m_{CH+}} + \frac{M_{CH_2}}{M_{TOT}} \frac{n_{CH_2}}{2} \frac{1}{m_{CH_2}} + \frac{M_{CH_2+}}{M_{TOT}} \frac{n_{CH_2+}}{2} \frac{1}{m_{CH_2+}} + \\
& \frac{M_{H_2}}{M_{TOT}} \frac{n_{H_2}}{2} \frac{1}{m_{H_2}} + \frac{M_{C_3}}{M_{TOT}} \frac{n_{C_3}}{2} \frac{1}{m_{C_3}} + \frac{M_{C_3H}}{M_{TOT}} \frac{n_{C_3H}}{2} \frac{1}{m_{C_3H}} + \frac{M_{C_3H_3}}{M_{TOT}} \frac{n_{C_3H_3}}{2} \frac{1}{m_{C_3H_3}} + \\
& \left. \frac{M_{C_4H}}{M_{TOT}} \frac{n_{C_4H}}{2} \frac{1}{m_{C_4H}} + \frac{M_{C_4}}{M_{TOT}} \frac{n_{C_4}}{2} \frac{1}{m_{C_4}} + \frac{M_{C_4H_2}}{M_{TOT}} \frac{n_{C_4H_2}}{2} \frac{1}{m_{C_4H_2}} \right) \quad (4.2.23)
\end{aligned}$$

obviously the ratio of the mass of each chemical species to M_{TOT} is the mass fraction linked to each chemical species:

$$\begin{aligned}
E_{TOT} = k T M_{TOT} & \left(\beta_{Ar} \frac{n_{Ar}}{2} \frac{1}{m_{Ar}} + \beta_{Ar+} \frac{n_{Ar+}}{2} \frac{1}{m_{Ar+}} + \beta_{C_2H_2} \frac{n_{C_2H_2}}{2} \frac{1}{m_{C_2H_2}} + \beta_{C_2H_2+} \frac{n_{C_2H_2+}}{2} \frac{1}{m_{C_2H_2+}} + \right. \\
& \beta_{C_2H} \frac{n_{C_2H}}{2} \frac{1}{m_{C_2H}} + \beta_H \frac{n_H}{2} \frac{1}{m_H} + \beta_{C_2} \frac{n_{C_2}}{2} \frac{1}{m_{C_2}} + \beta_{CH} \frac{n_{CH}}{2} \frac{1}{m_{CH}} + \beta_{C_2H+} \frac{n_{C_2H+}}{2} \frac{1}{m_{C_2H+}} + \\
& \beta_C \frac{n_C}{2} \frac{1}{m_C} + \beta_{C_2+} \frac{n_{C_2+}}{2} \frac{1}{m_{C_2+}} + \beta_{CH+} \frac{n_{CH+}}{2} \frac{1}{m_{CH+}} + \beta_{CH_2} \frac{n_{CH_2}}{2} \frac{1}{m_{CH_2}} + \beta_{CH_2+} \frac{n_{CH_2+}}{2} \frac{1}{m_{CH_2+}} + \\
& \beta_{H_2} \frac{n_{H_2}}{2} \frac{1}{m_{H_2}} + \beta_{C_3} \frac{n_{C_3}}{2} \frac{1}{m_{C_3}} + \beta_{C_3H} \frac{n_{C_3H}}{2} \frac{1}{m_{C_3H}} + \beta_{C_3H_3} \frac{n_{C_3H_3}}{2} \frac{1}{m_{C_3H_3}} + \\
& \left. \beta_{C_4H} \frac{n_{C_4H}}{2} \frac{1}{m_{C_4H}} + \beta_{C_4} \frac{n_{C_4}}{2} \frac{1}{m_{C_4}} + \beta_{C_4H_2} \frac{n_{C_4H_2}}{2} \frac{1}{m_{C_4H_2}} \right) \quad (4.2.24)
\end{aligned}$$

Now multiply and divide the equ.(4.2.24) by m_{Ar} :

$$\begin{aligned}
E_{\text{TOT}} = \frac{k}{m_{\text{Ar}}} T M_{\text{TOT}} \left(\beta_{\text{Ar}} \frac{n_{\text{Ar}}}{2} \frac{m_{\text{Ar}}}{m_{\text{Ar}}} + \beta_{\text{Ar}^+} \frac{n_{\text{Ar}^+}}{2} \frac{m_{\text{Ar}}}{m_{\text{Ar}^+}} + \beta_{\text{C}_2\text{H}_2} \frac{n_{\text{C}_2\text{H}_2}}{2} \frac{m_{\text{Ar}}}{m_{\text{C}_2\text{H}_2}} + \beta_{\text{C}_2\text{H}_2^+} \frac{n_{\text{C}_2\text{H}_2^+}}{2} \frac{m_{\text{Ar}}}{m_{\text{C}_2\text{H}_2^+}} + \right. \\
\beta_{\text{C}_2\text{H}} \frac{n_{\text{C}_2\text{H}}}{2} \frac{m_{\text{Ar}}}{m_{\text{C}_2\text{H}}} + \beta_{\text{H}} \frac{n_{\text{H}}}{2} \frac{m_{\text{Ar}}}{m_{\text{H}}} + \beta_{\text{C}_2} \frac{n_{\text{C}_2}}{2} \frac{m_{\text{Ar}}}{m_{\text{C}_2}} + \beta_{\text{CH}} \frac{n_{\text{CH}}}{2} \frac{m_{\text{Ar}}}{m_{\text{CH}}} + \beta_{\text{C}_2\text{H}^+} \frac{n_{\text{C}_2\text{H}^+}}{2} \frac{m_{\text{Ar}}}{m_{\text{C}_2\text{H}^+}} + \\
\beta_{\text{C}} \frac{n_{\text{C}}}{2} \frac{m_{\text{Ar}}}{m_{\text{C}}} + \beta_{\text{C}_2^+} \frac{n_{\text{C}_2^+}}{2} \frac{m_{\text{Ar}}}{m_{\text{C}_2^+}} + \beta_{\text{CH}^+} \frac{n_{\text{CH}^+}}{2} \frac{m_{\text{Ar}}}{m_{\text{CH}^+}} + \beta_{\text{CH}_2} \frac{n_{\text{CH}_2}}{2} \frac{m_{\text{Ar}}}{m_{\text{CH}_2}} + \beta_{\text{CH}_2^+} \frac{n_{\text{CH}_2^+}}{2} \frac{m_{\text{Ar}}}{m_{\text{CH}_2^+}} + \\
\beta_{\text{H}_2} \frac{n_{\text{H}_2}}{2} \frac{m_{\text{Ar}}}{m_{\text{H}_2}} + \beta_{\text{C}_3} \frac{n_{\text{C}_3}}{2} \frac{m_{\text{Ar}}}{m_{\text{C}_3}} + \beta_{\text{C}_3\text{H}} \frac{n_{\text{C}_3\text{H}}}{2} \frac{m_{\text{Ar}}}{m_{\text{C}_3\text{H}}} + \beta_{\text{C}_3\text{H}_3} \frac{n_{\text{C}_3\text{H}_3}}{2} \frac{m_{\text{Ar}}}{m_{\text{C}_3\text{H}_3}} + \\
\left. \beta_{\text{C}_4\text{H}} \frac{n_{\text{C}_4\text{H}}}{2} \frac{m_{\text{Ar}}}{m_{\text{C}_4\text{H}}} + \beta_{\text{C}_4} \frac{n_{\text{C}_4}}{2} \frac{m_{\text{Ar}}}{m_{\text{C}_4}} + \beta_{\text{C}_4\text{H}_2} \frac{n_{\text{C}_4\text{H}_2}}{2} \frac{m_{\text{Ar}}}{m_{\text{C}_4\text{H}_2}} \right) \quad (4.2.25)
\end{aligned}$$

It is easy to see the constant of Argon and the dimensionless parameters (from 4.2.13a to 4.2.13z) used also before for pressure:

$$\begin{aligned}
E_{\text{TOT}} = R_{\text{Ar}} T M_{\text{TOT}} \left(\beta_{\text{Ar}} \frac{n_{\text{Ar}}}{2} + \beta_{\text{Ar}^+} \frac{n_{\text{Ar}^+}}{2} + \beta_{\text{C}_2\text{H}_2} \frac{n_{\text{C}_2\text{H}_2}}{2} Z_{\text{C}_2\text{H}_2} + \beta_{\text{C}_2\text{H}_2^+} \frac{n_{\text{C}_2\text{H}_2^+}}{2} Z_{\text{C}_2\text{H}_2^+} + \beta_{\text{C}_2\text{H}} \frac{n_{\text{C}_2\text{H}}}{2} Z_{\text{C}_2\text{H}} + \right. \\
\beta_{\text{H}} \frac{n_{\text{H}}}{2} Z_{\text{H}} + \beta_{\text{C}_2} \frac{n_{\text{C}_2}}{2} Z_{\text{C}_2} + \beta_{\text{CH}} \frac{n_{\text{CH}}}{2} Z_{\text{CH}} + \beta_{\text{C}_2\text{H}^+} \frac{n_{\text{C}_2\text{H}^+}}{2} Z_{\text{C}_2\text{H}^+} + \beta_{\text{C}} \frac{n_{\text{C}}}{2} Z_{\text{C}} + \beta_{\text{C}_2^+} \frac{n_{\text{C}_2^+}}{2} Z_{\text{C}_2^+} + \\
\beta_{\text{CH}^+} \frac{n_{\text{CH}^+}}{2} Z_{\text{CH}^+} + \beta_{\text{CH}_2} \frac{n_{\text{CH}_2}}{2} Z_{\text{CH}_2} + \beta_{\text{CH}_2^+} \frac{n_{\text{CH}_2^+}}{2} Z_{\text{CH}_2^+} + \beta_{\text{H}_2} \frac{n_{\text{H}_2}}{2} Z_{\text{H}_2} + \beta_{\text{C}_3} \frac{n_{\text{C}_3}}{2} Z_{\text{C}_3} + \\
\left. \beta_{\text{C}_3\text{H}} \frac{n_{\text{C}_3\text{H}}}{2} Z_{\text{C}_3\text{H}} + \beta_{\text{C}_3\text{H}_3} \frac{n_{\text{C}_3\text{H}_3}}{2} Z_{\text{C}_3\text{H}_3} + \beta_{\text{C}_4\text{H}} \frac{n_{\text{C}_4\text{H}}}{2} Z_{\text{C}_4\text{H}} + \beta_{\text{C}_4} \frac{n_{\text{C}_4}}{2} Z_{\text{C}_4} + \beta_{\text{C}_4\text{H}_2} \frac{n_{\text{C}_4\text{H}_2}}{2} Z_{\text{C}_4\text{H}_2} \right) \quad (4.2.26)
\end{aligned}$$

Dividing equ.(4.2.26) by M_{TOT} , the form of specific energy is obtained:

$$\begin{aligned}
e_{\text{TOT}} = R_{\text{Ar}} T \left(\beta_{\text{Ar}} \frac{n_{\text{Ar}}}{2} + \beta_{\text{Ar}^+} \frac{n_{\text{Ar}^+}}{2} + \beta_{\text{C}_2\text{H}_2} \frac{n_{\text{C}_2\text{H}_2}}{2} Z_{\text{C}_2\text{H}_2} + \beta_{\text{C}_2\text{H}_2^+} \frac{n_{\text{C}_2\text{H}_2^+}}{2} Z_{\text{C}_2\text{H}_2^+} + \beta_{\text{C}_2\text{H}} \frac{n_{\text{C}_2\text{H}}}{2} Z_{\text{C}_2\text{H}} + \right. \\
\beta_{\text{H}} \frac{n_{\text{H}}}{2} Z_{\text{H}} + \beta_{\text{C}_2} \frac{n_{\text{C}_2}}{2} Z_{\text{C}_2} + \beta_{\text{CH}} \frac{n_{\text{CH}}}{2} Z_{\text{CH}} + \beta_{\text{C}_2\text{H}^+} \frac{n_{\text{C}_2\text{H}^+}}{2} Z_{\text{C}_2\text{H}^+} + \beta_{\text{C}} \frac{n_{\text{C}}}{2} Z_{\text{C}} + \beta_{\text{C}_2^+} \frac{n_{\text{C}_2^+}}{2} Z_{\text{C}_2^+} + \\
\beta_{\text{CH}^+} \frac{n_{\text{CH}^+}}{2} Z_{\text{CH}^+} + \beta_{\text{CH}_2} \frac{n_{\text{CH}_2}}{2} Z_{\text{CH}_2} + \beta_{\text{CH}_2^+} \frac{n_{\text{CH}_2^+}}{2} Z_{\text{CH}_2^+} + \beta_{\text{H}_2} \frac{n_{\text{H}_2}}{2} Z_{\text{H}_2} + \beta_{\text{C}_3} \frac{n_{\text{C}_3}}{2} Z_{\text{C}_3} + \\
\left. \beta_{\text{C}_3\text{H}} \frac{n_{\text{C}_3\text{H}}}{2} Z_{\text{C}_3\text{H}} + \beta_{\text{C}_3\text{H}_3} \frac{n_{\text{C}_3\text{H}_3}}{2} Z_{\text{C}_3\text{H}_3} + \beta_{\text{C}_4\text{H}} \frac{n_{\text{C}_4\text{H}}}{2} Z_{\text{C}_4\text{H}} + \beta_{\text{C}_4} \frac{n_{\text{C}_4}}{2} Z_{\text{C}_4} + \beta_{\text{C}_4\text{H}_2} \frac{n_{\text{C}_4\text{H}_2}}{2} Z_{\text{C}_4\text{H}_2} \right) \quad (4.2.27)
\end{aligned}$$

For brevity, it is opportune to consider the following dimensionless parameter:

$$\begin{aligned}
Z_2 = & \frac{n_{Ar}}{2} \beta_{Ar} + \frac{n_{Ar+}}{2} \beta_{Ar+} + \frac{n_{C2H2}}{2} \beta_{C2H2} Z_{C2H2} + \frac{n_{C2H2+}}{2} \beta_{C2H2+} Z_{C2H2+} + \frac{n_{C2H}}{2} \beta_{C2H} Z_{C2H} + \\
& \frac{n_H}{2} \beta_H Z_H + \frac{n_{C2}}{2} \beta_{C2} Z_{C2} + \frac{n_{CH}}{2} \beta_{CH} Z_{CH} + \frac{n_{C2H+}}{2} \beta_{C2H+} Z_{C2H+} + \frac{n_C}{2} \beta_C Z_C + \frac{n_{C2+}}{2} \beta_{C2+} Z_{C2+} + \\
& \frac{n_{CH+}}{2} \beta_{CH+} Z_{CH+} + \frac{n_{CH2}}{2} \beta_{CH2} Z_{CH2} + \frac{n_{CH2+}}{2} \beta_{CH2+} Z_{CH2+} + \frac{n_{H2}}{2} \beta_{H2} Z_{H2} + \frac{n_{C3}}{2} \beta_{C3} Z_{C3} + \\
& \frac{n_{C3H}}{2} \beta_{C3H} Z_{C3H} + \frac{n_{C3H3}}{2} \beta_{C3H3} Z_{C3H3} + \frac{n_{C4H}}{2} \beta_{C4H} Z_{C4H} + \frac{n_{C4}}{2} \beta_{C4} Z_{C4} + \frac{n_{C4H2}}{2} \beta_{C4H2} Z_{C4H2} \quad (4.2.28)
\end{aligned}$$

thus equ.(4.2.27) is equal to:

$$e_{TOT} = R_{Ar} T Z_2 \quad (4.2.29)$$

The contribution of energy (Δe) due to exothermic reactions must be also implemented:

$$e_{TOT} = e_{TOT} + \Delta e \quad (4.2.30)$$

Now it is shown how obtain the three thermo-fluid-dynamic equations. It is easy to see that the system of equations is not possible to solve in an analytical way because it is not linear and for this reason a numerical procedure is strictly necessary. In order to solve it numerically, the differentiation procedure is used. In particular, differentiating equ. (4.2.1) in a logarithmic way:

$$\frac{d\rho}{\rho} + \frac{du}{u} + \frac{dA}{A} = 0 \quad (4.2.31)$$

equivalently:

$$\frac{d\rho}{\rho} = -\left(\frac{du}{u} + \frac{dA}{A}\right) \quad (4.2.32)$$

that can be written as:

$$d\rho = -\rho \left(\frac{du}{u} + \frac{dA}{A}\right) \quad (4.2.33)$$

Equation (4.2.2) differentiated is equal to:

$$dp + u^2 d\rho + 2(\rho u) du = 0 \quad (4.2.34)$$

remaining only dp at the first term:

$$dp = -u^2 d\rho - 2\rho u du \quad (4.2.35)$$

or:

$$dp = -\rho u \left(2du + \frac{u}{\rho} d\rho \right) \quad (4.2.36)$$

substituting equ. (4.2.32) into (4.2.36):

$$dp = -\rho u \left[2du + u \left(-\frac{du}{u} - \frac{dA}{A} \right) \right] \quad (4.2.37)$$

equivalently, solving the round brackets:

$$dp = -\rho u \left(2du - du - u \frac{dA}{A} \right) \quad (4.2.38)$$

i.e.:

$$dp = -\rho u \left(du - u \frac{dA}{A} \right) \quad (4.2.39)$$

Differentiating equ. (4.2.3) it results:

$$dh + \frac{2u du}{2} = 0 \quad (4.2.40)$$

simplifying the number 2:

$$dh + u du = 0 \quad (4.2.41)$$

moving (u du) at the second term:

$$dh = -u du \quad (4.2.42)$$

enthalpy is defined as:

$$h = e_{TOT} + \frac{p}{\rho} + \Delta e \quad (4.2.43)$$

and thus placing equations (4.2.29) and (4.2.17):

$$h = R_{Ar} T Z_2 + R_{Ar} T Z_1 + \Delta e \quad (4.2.44)$$

putting $R_{Ar}T$ in evidence:

$$h = R_{Ar} T (Z_1 + Z_2) + \Delta e \quad (4.2.45)$$

differentiating:

$$dh = R_{Ar} dT (Z_1 + Z_2) + R_{Ar} T (dZ_1 + dZ_2) + \Delta e \quad (4.2.46)$$

where:

$$\begin{aligned} dZ_1 = & \frac{d\beta_{Ar}}{dx} + \frac{d\beta_{Ar+}}{dx} + \frac{d\beta_{C_2H_2}}{dx} Z_{C_2H_2} + \frac{d\beta_{C_2H_2+}}{dx} Z_{C_2H_2+} + \frac{d\beta_{C_2H}}{dx} Z_{C_2H} + \frac{d\beta_H}{dx} Z_H + \frac{d\beta_{C_2}}{dx} Z_{C_2} + \frac{d\beta_{CH}}{dx} Z_{CH} + \\ & \frac{d\beta_{C_2H+}}{dx} Z_{C_2H+} + \frac{d\beta_C}{dx} Z_C + \frac{d\beta_{C_2+}}{dx} Z_{C_2+} + \frac{d\beta_{CH+}}{dx} Z_{CH+} + \frac{d\beta_{CH_2}}{dx} Z_{CH_2} + \frac{d\beta_{CH_2+}}{dx} Z_{CH_2+} + \frac{d\beta_{H_2}}{dx} Z_{H_2} + \\ & \frac{d\beta_{C_3}}{dx} Z_{C_3} + \frac{d\beta_{C_3H}}{dx} Z_{C_3H} + \frac{d\beta_{C_3H_3}}{dx} Z_{C_3H_3} + \frac{d\beta_{C_4H}}{dx} Z_{C_4H} + \frac{d\beta_{C_4}}{dx} Z_{C_4} + \frac{d\beta_{C_4H_2}}{dx} Z_{C_4H_2} \end{aligned} \quad (4.2.47)$$

$$dZ_2 = \frac{n_{Ar}}{2} \frac{d\beta_{Ar}}{dx} + \frac{n_{Ar+}}{2} \frac{d\beta_{Ar+}}{dx} + \frac{n_{C_2H_2}}{2} \frac{d\beta_{C_2H_2}}{dx} Z_{C_2H_2} + \frac{n_{C_2H_2+}}{2} \frac{d\beta_{C_2H_2+}}{dx} Z_{C_2H_2+} + \frac{n_{C_2H}}{2} \frac{d\beta_{C_2H}}{dx} Z_{C_2H} +$$

$$\begin{aligned}
& \frac{n_H}{2} \frac{d\beta_H}{dx} Z_H + \frac{n_{C2}}{2} \frac{d\beta_{C2}}{dx} Z_{C2} + \frac{n_{CH}}{2} \frac{d\beta_{CH}}{dx} Z_{CH} + \frac{n_{C2H+}}{2} \frac{d\beta_{C2H+}}{dx} Z_{C2H+} + \frac{n_C}{2} \frac{d\beta_C}{dx} Z_C + \\
& \frac{n_{C2+}}{2} \frac{d\beta_{C2+}}{dx} Z_{C2+} + \frac{n_{CH+}}{2} \frac{d\beta_{CH+}}{dx} Z_{CH+} + \frac{n_{CH2}}{2} \frac{d\beta_{CH2}}{dx} Z_{CH2} + \frac{n_{CH2+}}{2} \frac{d\beta_{CH2+}}{dx} Z_{CH2+} + \\
& \frac{n_{H2}}{2} \frac{d\beta_{H2}}{dx} Z_{H2} + \frac{n_{C3}}{2} \frac{d\beta_{C3}}{dx} Z_{C3} + \frac{n_{C3H}}{2} \frac{d\beta_{C3H}}{dx} Z_{C3H} + \frac{n_{C3H3}}{2} \frac{d\beta_{C3H3}}{dx} Z_{C3H3} + \\
& \frac{n_{C4H}}{2} \frac{d\beta_{C4H}}{dx} Z_{C4H} + \frac{n_{C4}}{2} \frac{d\beta_{C4}}{dx} Z_{C4} + \frac{n_{C4H2}}{2} \frac{d\beta_{C4H2}}{dx} Z_{C4H2}
\end{aligned} \tag{4.2.48}$$

It results that dZ_1 and dZ_2 are characterized by the physical dimension of [1/m]. For convenience of writing put $dZ_2=Z_3$ and $dZ_1=Z_4$. Therefore:

$$dh = R_{Ar} dT (Z_1 + Z_2) + R_{Ar} T (Z_3 + Z_4) + \Delta e \tag{4.2.49}$$

Thus, putting in evidence R_{Ar} :

$$dh = R_{Ar} \left[dT (Z_1 + Z_2) + T (Z_3 + Z_4) + \frac{\Delta e}{R_{Ar}} \right] \tag{4.2.50}$$

At first term placing dh by equation (4.2.42):

$$-u du = R_{Ar} \left[dT (Z_1 + Z_2) + T (Z_3 + Z_4) + \frac{\Delta e}{R_{Ar}} \right] \tag{4.2.51}$$

Term dT is achieved differentiating equation (4.2.17). In fact:

$$dp = R_{Ar} dT \rho Z_1 + R_{Ar} T d\rho Z_1 + R_{Ar} T \rho dZ_4 \tag{4.2.52}$$

Dividing by R_{Ar} :

$$\frac{dp}{R_{Ar}} = dT \rho Z_1 + T d\rho Z_1 + T \rho dZ_4 \tag{4.2.53}$$

Inverting first and second terms:

$$dT\rho Z_1 + Td\rho Z_1 + T\rho Z_4 = \frac{dp}{R_{Ar}} \quad (4.2.54)$$

Leaving only $dT\rho Z_1$ at first term:

$$dT\rho Z_1 = \frac{dp}{R_{Ar}} - Td\rho Z_1 - T\rho Z_4 \quad (4.2.55)$$

Dividing by ρZ_1 :

$$dT = \frac{\frac{dp}{R_{Ar}} - Td\rho Z_1 - T\rho Z_4}{\rho Z_1} \quad (4.2.56)$$

equally:

$$dT = \frac{dp}{R_{Ar} \rho Z_1} - T \frac{d\rho}{\rho} - T \frac{Z_4}{Z_1} \quad (4.2.57)$$

placing equ. (4.2.57) in equ. (4.2.51):

$$-u du = R_{Ar} \left[\left(\frac{dp}{R_{Ar} \rho Z_1} - T \frac{d\rho}{\rho} - T \frac{Z_4}{Z_1} \right) (Z_1 + Z_2) + T(Z_3 + Z_4) + \frac{\Delta e}{R_{Ar}} \right] \quad (4.2.58)$$

placing (4.2.39) and (4.2.32) in (4.2.58):

$$-u du = R_{Ar} \left[\left(\frac{-\rho u \left(du - u \frac{dA}{A} \right)}{R_{Ar} \rho Z_1} + T \left(\frac{du}{u} + \frac{dA}{A} \right) - T \frac{Z_4}{Z_1} \right) (Z_1 + Z_2) + T(Z_3 + Z_4) + \frac{\Delta e}{R_{Ar}} \right] \quad (4.2.59)$$

Solving the “small” round brackets in the “big” round brackets:

$$-u \, du = R_{Ar} \left[\left(-\frac{u \, du}{R_{Ar} Z_1} + \frac{u^2}{R_{Ar} Z_1} \frac{dA}{A} + T \frac{du}{u} + T \frac{dA}{A} - T \frac{Z_4}{Z_1} \right) (Z_1 + Z_2) + T (Z_3 + Z_4) + \frac{\Delta e}{R_{Ar}} \right] \quad (4.2.60)$$

dividing by $R_{Ar}(Z_1+Z_2)$:

$$-\frac{u \, du}{R_{Ar}(Z_1 + Z_2)} = -\frac{u \, du}{R_{Ar} Z_1} + \frac{u^2}{R_{Ar} Z_1} \frac{dA}{A} + T \frac{du}{u} + T \frac{dA}{A} - T \frac{Z_4}{Z_1} + T \frac{(Z_3 + Z_4)}{(Z_1 + Z_2)} + \frac{\Delta e}{R_{Ar}(Z_1 + Z_2)} \quad (4.2.61)$$

placing all terms containing du at first term:

$$-\frac{u \, du}{R_{Ar}(Z_1 + Z_2)} + \frac{u \, du}{R_{Ar} Z_1} - T \frac{du}{u} = \frac{u^2}{R_{Ar} Z_1} \frac{dA}{A} + T \frac{dA}{A} - T \frac{Z_4}{Z_1} + T \frac{(Z_3 + Z_4)}{(Z_1 + Z_2)} + \frac{\Delta e}{R_{Ar}(Z_1 + Z_2)} \quad (4.2.62)$$

placing in evidence dA/A and T :

$$-\frac{u \, du}{R_{Ar}(Z_1 + Z_2)} + \frac{u \, du}{R_{Ar} Z_1} - T \frac{du}{u} = \left(\frac{u^2}{R_{Ar} Z_1} + T \right) \frac{dA}{A} + \left(\frac{Z_3 + Z_4}{Z_1 + Z_2} - \frac{Z_4}{Z_1} \right) T + \frac{\Delta e}{R_{Ar}(Z_1 + Z_2)} \quad (4.2.63)$$

placing in evidence du :

$$\left(-\frac{u}{R_{Ar}(Z_1 + Z_2)} + \frac{u}{R_{Ar} Z_1} - T \frac{1}{u} \right) du = \left(\frac{u^2}{R_{Ar} Z_1} + T \right) \frac{dA}{A} + \left(\frac{Z_3 + Z_4}{Z_1 + Z_2} - \frac{Z_4}{Z_1} \right) T + \frac{\Delta e}{R_{Ar}(Z_1 + Z_2)} \quad (4.2.64)$$

and therefore the final form of du :

$$du = \frac{\left(\frac{u^2}{R_{Ar} Z_1} + T \right) \frac{dA}{A} + \left(\frac{Z_3 + Z_4}{Z_1 + Z_2} - \frac{Z_4}{Z_1} \right) T + \frac{\Delta e}{R_{Ar}(Z_1 + Z_2)}}{\left(-\frac{u}{R_{Ar}(Z_1 + Z_2)} + \frac{u}{R_{Ar} Z_1} - T \frac{1}{u} \right)} \quad (4.2.65)$$

In addition to equations (4.2.33), (4.2.52), (4.2.57) and (4.2.65) the equations linked to chemical reactions are implemented (see table 2.1).

4.3 Torch

The sub-code HEATVS.BAS is developed in order to simulate the flow field in the torch. In addition to hypothesis linked to flow field written in section 4.2 it is to point out that electrical power is supposed to be distributed uniformly along the torch conduct. Torch simulated is the PERKIN-EMLER 9MB-M torch installed at the “Small Planetary Entry Simulator” [11] and [12] at the University of Naples “Federico II”. It is schematized as a convergent nozzle (inlet diameter 13×10^{-3} m, length 9×10^{-3} m, exit diameter 8×10^{-3} m) followed by a conduct at constant area (diameter 8×10^{-3} m, length 2.3×10^{-2} m), see Fig.4.2.

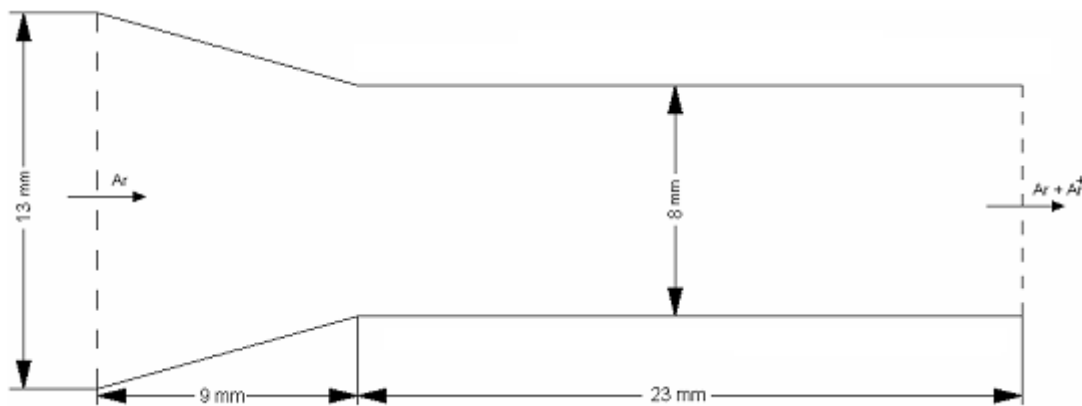


Fig. 4.2 – Scheme of the Torch Perkin-Emler 9 Mb

The codes read in input a file generated by INPUTVS.BAS sub-code. Obviously the thermo-fluid-dynamic equations used by HEATVS.BAS are the same seen in section 4.2 (equations (4.2.33), (4.2.52), (4.2.57) and (4.2.65)), but in that equations only Ar and Ar^+ molar fraction are different by zero. More specifically at initial section of torch only inert Argon is injected and thus only Ar molar fraction is not zero while all the other molar fractions linked to the remaining 20 chemical species are zero. However, due to electrical power supplied to torch, the ionization effects occur and thus at torch exit section there is a plasma mixture highly energized made up of Ar, Ar^+ and electrons. For this reason at torch section exit also Ar^+ molar fraction is not zero (obviously the sum of Ar and Ar^+ molar fractions is equal to one). The first ionization of Argon is considered and quantified by means of Ar^+ molar fraction. At each point of torch conduct this fraction is computed as the ratio of

number of Ar^+ molecules to the number of initial Ar molecules and is evaluated by the Saha's equation [13]:

$$\log_{10}\left(\frac{\alpha_{\text{ions}}^2}{1-\alpha_{\text{ions}}^2}p\right) = \frac{-5050 E_{\text{ion}}}{T} + 2.5 \log_{10}(T) - 6.5 \quad (4.3.1)$$

where:

- 1) α_{ions} is molar fraction of ions. In this analysis corresponds to the molar fraction of Ar^+ ($\alpha_{\text{ions}} = \alpha_{\text{Ar}^+}$).
- 2) p is pressure in Pa.
- 3) T is temperature in K.
- 4) E_{ion} is the first ionization energy in eV. For Argon $E_{\text{ion}} = 15.8$ eV.

To evaluate the form of α_{ions} solve the logarithm:

$$\left(\frac{\alpha_{\text{ions}}^2}{1-\alpha_{\text{ions}}^2}p\right) = 10^{\frac{-5050 E_{\text{ion}}}{T} + 2.5 \log_{10}(T) - 6.5} \quad (4.3.2)$$

multiply each term by $\frac{1-\alpha_{\text{ions}}^2}{p}$:

$$\alpha_{\text{ions}}^2 = \frac{1-\alpha_{\text{ions}}^2}{p} 10^{\frac{-5050 E_{\text{ion}}}{T} + 2.5 \log_{10}(T) - 6.5} \quad (4.3.3)$$

explicating the ratio:

$$\alpha_{\text{ions}}^2 = \frac{10^{\frac{-5050 E_{\text{ion}}}{T} + 2.5 \log_{10}(T) - 6.5}}{p} - \frac{10^{\frac{-5050 E_{\text{ion}}}{T} + 2.5 \log_{10}(T) - 6.5}}{p} \alpha_{\text{ions}}^2 \quad (4.3.4)$$

placing all terms containing α_{ions}^2 at first term:

$$\alpha_{\text{ions}}^2 + \frac{10^{\frac{-5050 E_{\text{ion}} + 2.5 \log_{10}(T) - 6.5}{T}}}{p} \alpha_{\text{ions}}^2 = \frac{10^{\frac{-5050 E_{\text{ion}} + 2.5 \log_{10}(T) - 6.5}{T}}}{p} \quad (4.3.5)$$

grouping terms containing α_{ions}^2 :

$$\left(1 + \frac{10^{\frac{-5050 E_{\text{ion}} + 2.5 \log_{10}(T) - 6.5}{T}}}{p} \right) \alpha_{\text{ions}}^2 = \frac{10^{\frac{-5050 E_{\text{ion}} + 2.5 \log_{10}(T) - 6.5}{T}}}{p} \quad (4.3.6)$$

and thus:

$$\alpha_{\text{ions}}^2 = \frac{10^{\frac{-5050 E_{\text{ion}} + 2.5 \log_{10}(T) - 6.5}{T}}}{p} \cdot \left(1 + \frac{10^{\frac{-5050 E_{\text{ion}} + 2.5 \log_{10}(T) - 6.5}{T}}}{p} \right)^{-1} \quad (4.3.7)$$

The final form of α_{ions} is achieved by the root square:

$$\alpha_{\text{ions}} = \sqrt{\frac{10^{\frac{-5050 E_{\text{ion}} + 2.5 \log_{10}(T) - 6.5}{T}}}{p} \cdot \left(1 + \frac{10^{\frac{-5050 E_{\text{ion}} + 2.5 \log_{10}(T) - 6.5}{T}}}{p} \right)^{-1}} = \alpha_{\text{Ar+}} \quad (4.3.8)$$

The influence of the electrical power is pretty strong as it is easy to verify in next sections.

The velocity at torch exit (V_{Exit}) is measured experimentally and change linearly with Argon mass flow rate (\dot{m}). More specifically velocity is zero when mass flow rate is zero and is equal to 50 m/s when mass flow rate is equal to 1.5 g/s. Thus the following law can be applied:

$$V_{\text{Exit}} = \frac{50}{0.0015} \dot{m} \quad (4.3.9)$$

The velocity at torch inlet (V_{Inlet}) is computed starting from V_{Exit} using the area section at exit (A_{Exit}) and at inlet (A_{Inlet}) of torch:

$$V_{\text{Inlet}} = V_{\text{Exit}} \frac{A_{\text{Exit}}}{A_{\text{Inlet}}} \quad (4.3.10)$$

Density at torch inlet section is evaluated by means of mass flow rate and velocity:

$$\rho_{\text{Inlet}} = \frac{\dot{m}}{V_{\text{Inlet}}} \quad (4.3.11)$$

Pressure at torch inlet section is easily computed using the state equation:

$$p_{\text{Inlet}} = \rho_{\text{Inlet}} T_{\text{Inlet}} R_{\text{Ar}} \quad (4.3.12)$$

Number Density (N_{inlet}) at torch inlet section is achieved starting from density:

$$N_{\text{Inlet}} = \frac{\rho_{\text{Inlet}}}{m_{\text{Ar}}} \quad (4.3.13)$$

To avoid numerical instability the various thermo-fluid-dynamic parameters are divided by the respective parameters of reference. Integration step is equal to 3.2×10^{-6} m.

The sub-codes generates in output two different files, one useful for user to plot the various parameters along torch axis and one which is used as input for the following sub-code. Both output files are written in the same path used by INPUTVS.BAS.

4.4 NOZZLE

Flow field in nozzle is simulated by NOZVS.BAS sub-code. Three different supersonic conical nozzles (in this work labeled A, B and C) are taken into account and Table 4.1 shows the characteristic dimensions of them, i.e. convergent length (CL), divergent length (DL), radius of throat (R_T), radius of exit section (R_E), area of throat (A_{Throat}), area of exit section (A_{Exit}). Moreover it are reported also ratio A_{Exit}/A_{Throat} and the opening angle (Θ) of cone equal to:

$$\Theta = 57.3 \frac{R_E - R_T}{DL} \quad (4.4.1)$$

Obviously the number 57.3 is used to convert the physical dimension in degree. Radius of inlet section is equal to 0.011 m for all nozzles and thus Area of inlet section corresponds to $3.8013 \times 10^{-4} \text{ m}^2$ for all nozzles.

Table 4.1: Geometrical Characteristics of nozzles

Nozzle	CL [m]	DL [m]	R_T [m]	R_E [m]	A_{Throat} [m ²]	A_{Exit} [m ²]	A_{Exit}/A_{Throat} [-]	Θ [deg]
A	0.046	0.061	5.5×10^{-3}	0.011	9.5×10^{-5}	3.8×10^{-4}	4	5.2
B	0.046	0.1553	5.5×10^{-3}	0.025	9.5×10^{-5}	2.0×10^{-3}	20	7.2
C	0.025	0.1983	4.0×10^{-3}	0.03	5.03×10^{-5}	2.8×10^{-3}	56	7.5

As typical example Fig. 4.3 reports the section of nozzle C.

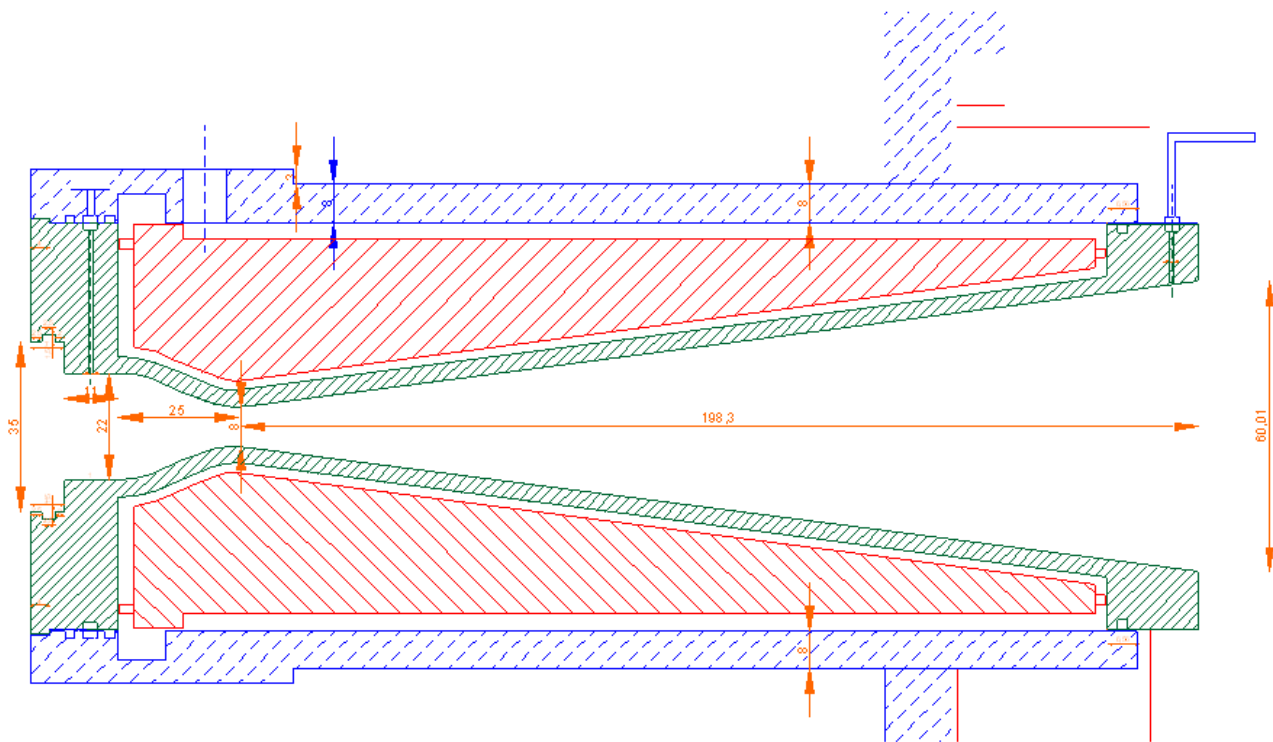


Fig. 4.3: Scheme of Nozzle C

Even if in table 4.1 the nozzle convergent length is reported, as said before NOZVS.BAS sub-code simulates flow field from throat until to 90% of divergent part of nozzle axis and the convergent part is not simulated. This means that the length of divergent part simulated by NOZVS.BAS is equal to 0.05 m, 0.13 m and 0.17 m for nozzles A, B and C respectively. The various thermo-fluid-dynamic parameters at throat are easily computed by conservation of mass flow rate, putting the condition of sonic flow at throat.

Obviously the thermo-fluid-dynamic equations used by HEATVS.BAS are the same seen in section 4.2 (equations (4.2.33), (4.2.52), (4.2.57) and (4.2.65)), but in that equations only Ar and Ar^+ molar fraction are different by zero. To avoid numerical instability the various thermo-fluid-dynamic parameters are divided by the respective parameters of reference.

The sub-codes generate in output two different files, one useful for user to plot the various parameters along nozzle axis and one which is used as input for CHIBEVS.BAS. Both output files are written in the same path used by INPUTVS.BAS.

CHIBEVS.BAS sub-code reads in input the file generated by NOZVS.BAS and simulates flow field from the 90% of nozzle (where C_2H_2) is injected for a short space (10^{-5} m). Acetylene is injected at velocity of 100 m/s at 300 K. The various chemical reactions (see table 2.1) are implemented. Obviously the thermo-fluid-dynamic equations used by this sub-code are the same seen in section 4.2 (equations (4.2.33), (4.2.52), (4.2.57) and (4.2.65) plus equations linked to chemical reactions).

Due to chemistry the molar fractions of chemical species are all not zero. In order to avoid numerical instability CHIBEVS.BAS sub-code considers an integration step equal to 10^{-16} m. The specific heat at constant pressure, the ratio of specific heats and the degree of freedom for mono-atomic species are constant with temperature, in particular:

For chemical species Ar it results:

$$c_{p_{Ar}} = 520.0254 \text{ [J/(kg*K)]}$$

$$\gamma_{Ar} = \frac{5}{3}$$

$$n_{Ar} = 3$$

Chemical species Ar^+ is characterized by the same properties of Ar:

$$c_{p_{Ar^+}} = 520.0254 \text{ [J/(kg*K)]}$$

$$\gamma_{Ar^+} = \frac{5}{3}$$

$$n_{Ar^+} = 3$$

For chemical species C it results:

$$c_{p_C} = 1736.583 \text{ [J/(kg*K)]}$$

$$\gamma_C = \frac{5}{3}$$

$$n_C = 3$$

For chemical species H, it results:

$$c_{p_H} = 20786 \text{ [J/(kg}\cdot\text{K)]}$$

$$\gamma_H = \frac{5}{3}$$

$$n_H = 3$$

Chemical species C_3H is polyatomic, however an average value is taken into account:

$$c_{p_{C_3H}} = 1444.054 \text{ [J/(kg}\cdot\text{K)]}$$

$$\gamma_{C_3H} = 1.18428$$

$$n_C = \frac{2}{\gamma_{C_3H} - 1}$$

The variation with temperature of specific heat at constant pressure and of degree of freedom for the other poly-atomic species are considered. More specifically the specific heat c_p is written in a polynomial form. The polynomial by NIST database is in the following form:

$$c_p = \frac{1000}{m} \left[a + b \frac{T}{1000} + c \left(\frac{T}{1000} \right)^2 + d \left(\frac{T}{1000} \right)^3 + e \left(\frac{T}{1000} \right)^{-2} \right] \quad (4.4.2)$$

while by Fluent database it results:

$$c_p = a + b \cdot T + c \cdot T^2 + d \cdot T^3 + e \cdot T^4 \quad (4.4.3)$$

Knowing c_p is easy to calculate n . In fact:

$$\gamma = \frac{n+2}{n} \quad (4.4.4)$$

writing at first term γ as ratio of specific heats:

$$\frac{c_p}{c_v} = \frac{n+2}{n} \quad (4.4.5)$$

Specific heat at volume constant is equal to $c_p - R$ (because $R = c_p - c_v$):

$$\frac{c_p}{c_p - R} = \frac{n+2}{n} \quad (4.4.6)$$

Multiplying each term by n:

$$\frac{c_p}{c_p - R} n = n + 2 \quad (4.4.7)$$

writing all terms containing n at first term:

$$\frac{c_p}{c_p - R} n - n = 2 \quad (4.4.8)$$

putting n in evidence:

$$\left(\frac{c_p}{c_p - R} - 1 \right) n = 2 \quad (4.4.9)$$

Solving the round brackets:

$$\frac{c_p - c_p + R}{c_p - R} n = 2 \quad (4.4.10)$$

simplifying c_p :

$$\frac{R}{c_p - R} n = 2 \quad (4.4.11)$$

multiplying each term by $(c_p - R)/R$:

$$n = 2 \frac{c_p - R}{R} \quad (4.4.12)$$

and finally formula linking n with c_p :

$$n = 2 \frac{c_p}{R} - 2 \quad (4.4.13)$$

The values of constants to evaluate c_p are reported for all poly-atomic species in such a way that the physical dimension of c_p is $J/(kg \cdot K)$.

Chemical species H_2 (by NIST database):

For temperature until but not equal to 1000 K the polynomial constants are:

$$\begin{aligned} a &= 33.066178 \\ b &= -11.363417 \\ c &= 11.432816 \\ d &= -2.772874 \\ e &= -0.158558 \end{aligned}$$

For temperature in range of [1000 K, 2500 K[the polynomial constants are:

$$\begin{aligned} a &= 18.563083 \\ b &= 12.257357 \\ c &= -2.859786 \\ d &= 0.268238 \\ e &= 1.97799 \end{aligned}$$

For temperature above or equal to 2500 K the polynomial constants are:

$$\begin{aligned} a &= 43.41356 \\ b &= -4.293079 \\ c &= 1.272428 \\ d &= -0.096876 \end{aligned}$$

$$e = -20.533862$$

Chemical Specie C₂H (by Nist database)

For temperature until but not equal to 1200 K the polynomial constants are:

$$a_{C_2H} = 33.40916$$

$$b_{C_2H} = 24.11331$$

$$c_{C_2H} = -6.600595$$

$$d_{C_2H} = 0.278912$$

$$e_{C_2H} = -0.259459$$

For temperature above or equal to 6000 K the polynomial constants are:

$$a_{C_2H} = 39.2922$$

$$b_{C_2H} = 13.32081$$

$$c_{C_2H} = -1.952364$$

$$d_{C_2H} = 0.08629$$

$$e_{C_2H} = 0.978203$$

Chemical Species C₂H⁺ is characterized by the same form of C₂H.

For temperature until but not equal to 1200 K the polynomial constants are:

$$a_{C_2H^+} = 33.40916$$

$$b_{C_2H^+} = 24.11331$$

$$c_{C_2H^+} = -6.600595$$

$$d_{C_2H^+} = 0.278912$$

$$e_{C_2H^+} = -0.259459$$

For temperature above or equal to 6000 K the polynomial constants are:

$$a_{C_2H^+} = 39.2922$$

$$b_{C_2H^+} = 13.32081$$

$$c_{C_2H^+} = -1.952364$$

$$d_{C_2H^+} = 0.08629$$

$$e_{C_2H^+} = 0.978203$$

Chemical Specie C₂ (by NIST database)

For temperature until but not equal to 700 K the polynomial constants are:

$$\begin{aligned}a_{C_2} &= 123.9092 \\b_{C_2} &= -348.0067 \\c_{C_2} &= 485.0971 \\d_{C_2} &= -232.7994 \\e_{C_2} &= -1.240298\end{aligned}$$

For temperature above or equal to 6000 K the polynomial constants are:

$$\begin{aligned}a_{C_2} &= 30.50408 \\b_{C_2} &= 5.445811 \\c_{C_2} &= -0.853373 \\d_{C_2} &= 0.065641 \\e_{C_2} &= 0.81475\end{aligned}$$

Chemical Specie C_2^+ is characterized by the same properties of C_2 :

For temperature until but not equal to 700 K the polynomial constants are:

$$\begin{aligned}a_{C_2^+} &= 123.9092 \\b_{C_2^+} &= -348.0067 \\c_{C_2^+} &= 485.0971 \\d_{C_2^+} &= -232.7994 \\e_{C_2^+} &= -1.240298\end{aligned}$$

For temperature above or equal to 6000 K the polynomial constants are:

$$\begin{aligned}a_{C_2^+} &= 30.50408 \\b_{C_2^+} &= 5.445811 \\c_{C_2^+} &= -0.853373 \\d_{C_2^+} &= 0.065641 \\e_{C_2^+} &= 0.81475\end{aligned}$$

Chemical Specie CH by NIST database:

For temperature until but not equal to 1100 K the polynomial constants are:

$$\begin{aligned}a_{CH} &= 32.9421 \\b_{CH} &= -16.71056 \\c_{CH} &= 24.18595 \\d_{CH} &= -7.784709\end{aligned}$$

$$e_{\text{CH}} = -0.065198$$

For temperature in range above or equal to 6000 K the polynomial constants are:

$$a_{\text{CH}} = 30.15367$$

$$b_{\text{CH}} = 8.455112$$

$$c_{\text{CH}} = -1.969644$$

$$d_{\text{CH}} = 0.15427$$

$$e_{\text{CH}} = -4.98009$$

Chemical Specie CH_2 by NIST database:

For temperature until but not equal to 1400 K the polynomial constants are:

$$a_{\text{CH}_2} = 31.96823$$

$$b_{\text{CH}_2} = 6.783603$$

$$c_{\text{CH}_2} = 12.5189$$

$$d_{\text{CH}_2} = -5.696265$$

$$e_{\text{CH}_2} = -0.031115$$

For temperature above or equal to 6000 K the polynomial constants are:

$$a_{\text{CH}_2} = 51.55901$$

$$b_{\text{CH}_2} = 3.876975$$

$$c_{\text{CH}_2} = -0.649608$$

$$d_{\text{CH}_2} = 0.037901$$

$$e_{\text{CH}_2} = -10.72589$$

Chemical Species CH_2^+ is characterized by the same properties of CH_2 :

For temperature until but not equal to 1400 K the polynomial constants are:

$$a_{\text{CH}_2^+} = 31.96823$$

$$b_{\text{CH}_2^+} = 6.783603$$

$$c_{\text{CH}_2^+} = 12.5189$$

$$d_{\text{CH}_2^+} = -5.696265$$

$$e_{\text{CH}_2^+} = -0.031115$$

For temperature above or equal to 6000 K the polynomial constants are:

$$a_{\text{CH}_2^+} = 51.55901$$

$$\begin{aligned}b_{\text{CH}_2^+} &= 3.876975 \\c_{\text{CH}_2^+} &= -0.649608 \\d_{\text{CH}_2^+} &= 0.037901 \\e_{\text{CH}_2^+} &= -10.72589\end{aligned}$$

Chemical Specie C₃ by NIST database:

For temperature until but not equal to 1000 K the polynomial constants are:

$$\begin{aligned}a_{\text{C}_3} &= 26.33364 \\b_{\text{C}_3} &= 20.2683 \\c_{\text{C}_3} &= 2.788842 \\d_{\text{C}_3} &= -5.049168 \\e_{\text{C}_3} &= 0.466985\end{aligned}$$

For temperature above or equal to 6000 K the polynomial constants are:

$$\begin{aligned}a_{\text{C}_3} &= 43.89853 \\b_{\text{C}_3} &= 5.491207 \\c_{\text{C}_3} &= -0.819001 \\d_{\text{C}_3} &= 0.048698 \\e_{\text{C}_3} &= -3.879841\end{aligned}$$

Chemical Species C₄ by NIST database

For temperature until but not equal to 1200 K the polynomial constants are:

$$\begin{aligned}a_{\text{C}_4} &= 34.8664 \\b_{\text{C}_4} &= 84.34818 \\c_{\text{C}_4} &= -55.64804 \\d_{\text{C}_4} &= 13.82762 \\e_{\text{C}_4} &= -0.468144\end{aligned}$$

For temperature above or equal to 6000 K the polynomial constants are:

$$\begin{aligned}a_{\text{C}_4} &= 84.02309 \\b_{\text{C}_4} &= 1.74647 \\c_{\text{C}_4} &= -0.340843 \\d_{\text{C}_4} &= 0.022954 \\e_{\text{C}_4} &= -8.928448\end{aligned}$$

Chemical Specie C_2H_2 by NIST database.

For temperature until but not equal to 1100 K the polynomial constants are:

$$a_{C_2H_2} = 40.68697$$

$$b_{C_2H_2} = 40.73279$$

$$c_{C_2H_2} = -16.1784$$

$$d_{C_2H_2} = 3.669741$$

$$e_{C_2H_2} = -0.658411$$

For temperature above or equal to 6000 K the polynomial constants are:

$$a_{C_2H_2} = 67.47244$$

$$b_{C_2H_2} = 11.7511$$

$$c_{C_2H_2} = -2.02147$$

$$d_{C_2H_2} = 0.136195$$

$$e_{C_2H_2} = -9.806418$$

Chemical Species of $C_2H_2^+$ is characterized by the same properties of C_2H_2

Chemical Specie C_4H by Fluent database

For temperature until but not equal to 1000 K the polynomial constants are:

$$a_{C_4H} = 851.4331$$

$$b_{C_4H} = 1.202147$$

$$c_{C_4H} = -1.029494 \times 10^{-6}$$

$$d_{C_4H} = 0$$

$$e_{C_4H} = 0$$

For temperature above or equal to 5000 K the polynomial constants are:

$$a_{C_4H} = 1058.16$$

$$b_{C_4H} = 1.04982$$

$$c_{C_4H} = -0.0003535623$$

$$d_{C_4H} = 5.22429 \times 10^{-8}$$

$$e_{C_4H} = -2.773814 \times 10^{-12}$$

Chemical Specie C_4H_2 by Fluent database

For temperature until but not equal to 1000 K the polynomial constants are:

$$a_{C_4H_2} = 665.2049$$

$$b_{C_4H_2} = 3.290158$$

$$c_{C_4H_2} = -0.001638581$$

$$d_{C_4H_2} = -1.102005 \times 10^{-6}$$

$$e_{C_4H_2} = 1.009371 \times 10^{-9}$$

For temperature above or equal to 5000 K the polynomial constants are:

$$a_{C_4H_2} = 1499.988$$

$$b_{C_4H_2} = 1.004362$$

$$c_{C_4H_2} = -0.0003236658$$

$$d_{C_4H_2} = 4.575433 \times 10^{-8}$$

$$e_{C_4H_2} = -2.301297 \times 10^{-12}$$

Chemical Specie CH^+ by Fluent database

For temperature until but not equal to 1000 K the polynomial constants are:

$$a_{CH^+} = 2124.927$$

$$b_{CH^+} = 0.8602966$$

$$c_{CH^+} = -0.0024881$$

$$d_{CH^+} = 3.275895 \times 10^{-6}$$

$$e_{CH^+} = -1.312159 \times 10^{-9}$$

For temperature above or equal to 5000 K the polynomial constants are:

$$a_{CH^+} = 1758.438$$

$$b_{CH^+} = 0.9917626$$

$$c_{CH^+} = -0.0003428573$$

$$d_{CH^+} = 5.697908 \times 10^{-8}$$

$$e_{CH^+} = -3.459451 \times 10^{-12}$$

Chemical Specie C_3H_3 by Fluent Database

For temperature until but not equal to 1000 K the polynomial constants are:

$$a_{C_3H_3} = 389.236$$

$$b_{C_3H_3} = 5.06317$$

$$c_{C_3H_3} = -0.00466698$$

$$d_{C_3H_3} = 2.13026 \times 10^{-6}$$

$$e_{C_3H_3} = -2.95874 \times 10^{-10}$$

For temperature above or equal to 1000 K the polynomial constants are:

$$a_{C_3H_3} = 1413.91$$

$$b_{C_3H_3} = 1.72134$$

$$c_{C_3H_3} = -0.000606263$$

$$d_{C_3H_3} = 9.65477 \times 10^{-8}$$

$$e_{C_3H_3} = -5.72398 \times 10^{-12}$$

The specific heat at constant pressure of whole mixture is computed easily as an average value of specific heats at constant pressure of each chemical species by means of respective mass fractions:

$$\begin{aligned} c_{p_{\text{Mix}}} = & \beta_{Ar} c_{p_{Ar}} + \beta_{Ar^+} c_{p_{Ar^+}} + \beta_{C_2H_2^+} c_{p_{C_2H_2^+}} + \beta_{C_2H_2} c_{p_{C_2H_2}} + \beta_{CH_2^+} c_{p_{CH_2^+}} + \beta_{CH_2} c_{p_{CH_2}} + \beta_{C_2H} c_{p_{C_2H}} + \\ & \beta_H c_{p_H} + \beta_{C_2} c_{p_{C_2}} + \beta_{CH} c_{p_{CH}} + \beta_{C_2H^+} c_{p_{C_2H^+}} + \beta_C c_{p_C} + \beta_{C_2^+} c_{p_{C_2^+}} + \beta_{CH^+} c_{p_{CH^+}} + \beta_{H_2} c_{p_{H_2}} + \\ & \beta_{C_3} c_{p_{C_3}} + \beta_{C_3H} c_{p_{C_3H}} + \beta_{C_3H_3} c_{p_{C_3H_3}} + \beta_{C_4H} c_{p_{C_4H}} + \beta_{C_4} c_{p_{C_4}} + \beta_{C_4H_2} c_{p_{C_4H_2}} \end{aligned} \quad (4.4.14)$$

Similarly the ratio of specific heats for mixture is computed as an average value of ratio of specific heats of each chemical species by means of respective mass fractions:

$$\begin{aligned} \gamma_{\text{Mix}} = & \beta_{Ar} \gamma_{Ar} + \beta_{Ar^+} \gamma_{Ar^+} + \beta_{C_2H_2^+} \gamma_{C_2H_2^+} + \beta_{C_2H_2} \gamma_{C_2H_2} + \beta_{CH_2^+} \gamma_{CH_2^+} + \beta_{CH_2} \gamma_{CH_2} + \beta_{C_2H} \gamma_{C_2H} + \\ & \beta_H \gamma_H + \beta_{C_2} \gamma_{C_2} + \beta_{CH} \gamma_{CH} + \beta_{C_2H^+} \gamma_{C_2H^+} + \beta_C \gamma_C + \beta_{C_2^+} \gamma_{C_2^+} + \beta_{CH^+} \gamma_{CH^+} + \beta_{H_2} \gamma_{H_2} + \\ & \beta_{C_3} \gamma_{C_3} + \beta_{C_3H} \gamma_{C_3H} + \beta_{C_3H_3} \gamma_{C_3H_3} + \beta_{C_4H} \gamma_{C_4H} + \beta_{C_4} \gamma_{C_4} + \beta_{C_4H_2} \gamma_{C_4H_2} \end{aligned} \quad (4.4.15)$$

The molecular weight of entire mixture is easy computed as an average value of molecular weights of each chemical species by means of respective molar fractions:

$$\begin{aligned} pm_{\text{Mix}} = & \alpha_{Ar} pm_{Ar} + \alpha_{Ar^+} pm_{Ar^+} + \alpha_{C_2H_2^+} pm_{C_2H_2^+} + \alpha_{C_2H_2} pm_{C_2H_2} + \alpha_{CH_2^+} pm_{CH_2^+} + \alpha_{CH_2} pm_{CH_2} + \\ & \alpha_{C_2H} pm_{C_2H} + \alpha_H pm_H + \alpha_{C_2} pm_{C_2} + \alpha_{CH} pm_{CH} + \alpha_{C_2H^+} pm_{C_2H^+} + \alpha_C pm_C + \alpha_{C_2^+} pm_{C_2^+} + \\ & \alpha_{CH^+} pm_{CH^+} + \alpha_{H_2} pm_{H_2} + \alpha_{C_3} pm_{C_3} + \alpha_{C_3H} pm_{C_3H} + \alpha_{C_3H_3} pm_{C_3H_3} + \\ & \alpha_{C_4H} pm_{C_4H} + \alpha_{C_4} pm_{C_4} + \alpha_{C_4H_2} pm_{C_4H_2} \end{aligned} \quad (4.4.16)$$

The average physical mass of mixture corresponds to an average value of physical mass of each chemical species by means of respective molar fractions:

$$\begin{aligned}
 m_{\text{Mix}} = & \alpha_{\text{Ar}} m_{\text{Ar}} + \alpha_{\text{Ar}^+} m_{\text{Ar}^+} + \alpha_{\text{C}_2\text{H}_2^+} m_{\text{C}_2\text{H}_2^+} + \alpha_{\text{C}_2\text{H}_2} m_{\text{C}_2\text{H}_2} + \alpha_{\text{CH}_2^+} m_{\text{CH}_2^+} + \alpha_{\text{CH}_2} m_{\text{CH}_2} + \alpha_{\text{C}_2\text{H}} m_{\text{C}_2\text{H}} + \\
 & \alpha_{\text{H}} m_{\text{H}} + \alpha_{\text{C}_2} m_{\text{C}_2} + \alpha_{\text{CH}} m_{\text{CH}} + \alpha_{\text{C}_2\text{H}^+} m_{\text{C}_2\text{H}^+} + \alpha_{\text{C}} m_{\text{C}} + \alpha_{\text{C}_2^+} m_{\text{C}_2^+} + \alpha_{\text{CH}^+} m_{\text{CH}^+} + \alpha_{\text{H}_2} m_{\text{H}_2} + \\
 & \alpha_{\text{C}_3} m_{\text{C}_3} + \alpha_{\text{C}_3\text{H}} m_{\text{C}_3\text{H}} + \alpha_{\text{C}_3\text{H}_3} m_{\text{C}_3\text{H}_3} + \alpha_{\text{C}_4\text{H}} m_{\text{C}_4\text{H}} + \alpha_{\text{C}_4} m_{\text{C}_4} + \alpha_{\text{C}_4\text{H}_2} m_{\text{C}_4\text{H}_2}
 \end{aligned} \tag{4.4.17}$$

The constant of gas of whole mixture (R_{Mix}) is equal to:

$$R_{\text{Mix}} = \frac{R}{\rho m_{\text{Mix}}} \tag{4.4.18}$$

where R is the universal constant of gas (about 8314 J/(kmol*K)).

Chapter 5

DIRECT SIMULATION MONTE CARLO METHOD

5.1 Introduction

The Direct Simulation Monte Carlo method was developed by Bird in the 1960's and until now is the unique reliable method to solve in an accurate way the rarefied flow fields. In fact in rarefaction regimes the phenomenological equations of Newton, Fourier and Fick fail and thus the "classical" Navier-Stokes equations can not be used. Also the Boltzmann equation is correct but its solution is unknown. Many researchers tried and try to solve it by a numerical, computational and/or analytical way but they obtained results only in very simple conditions. Furthermore Navier-Stokes and Boltzmann equations can not take into account many physical aspects of profound importance such as, for example, the excitation of internal degrees of freedom (rotation and vibration) and the chemical reactions that are, on the contrary, considered successfully in the DSMC.

The DSMC method developed by Bird is labelled "basic DSMC" because nowadays the method is improved by means of new procedures and the improved method is labelled "sophisticated DSMC".

Many researchers work hard to amplify the capability of this method from different point of view. This improvement is linked both to the method and to its computational implementation. In particular, the aims are, for example i) to extend the possibility to use the DSMC method also in other regimes, such as the continuum and the free molecular flow, ii) to improve the method also in the solution of rarefied flow fields, obtaining, for example, solutions in a faster way, iii) to consider different particular aspects until now unknown such as for example the quantum effects, iv) to analyze not only gases but also various types of fluids which are of the same great interest, such as for examples water.

It has to point out that a solution by the DSMC approach can be obtained only by the flow field simulations and thus the use of a computer code is essential. Different codes based on DSMC approach able to analyze 2D and 3D flows also around or inner complex bodies are present and in this thesis the sophisticated and worldwide accepted DS2V (Ver.4.5.06) code by Bird is employed. The aim of this chapter is to illustrate in general the characteristics of the DSMC method (both basic and sophisticated) and of the DS2V code.

5.2 Basic DSMC method

The gas simulated is considered made up of an high number (also millions) of simulated molecules, each one representing a number of real molecules. Evolution of each molecule is due to collisions with other molecules and/or with the body under study. Thanks to collision there is an exchanging of momentum and energy, thus velocity changes in modulus and in direction. Excitation of internal degrees of freedom (rotation and vibration) are taken into account and chemical reactions (dissociation, recombination and exchange) can be considered. The DSMC method is statistical and stochastic. It is statistical because the macroscopic thermo-fluid-dynamic quantities like for instance velocity, temperature, density are evaluated as averages of microscopic quantities as per velocity and mass of a single molecule. It is stochastic because its procedure relies on sampling probability functions by means of random numbers.

The computational domain, including the body, is divided in various cells. Position, velocity and internal state of each molecule in each cell are computed concurrently. DSMC uses the cells only for sampling the macroscopic properties and for selecting the colliding molecules. Thermo-fluid-dynamic quantities are computed in each cell and located in its center. Each dimension of a cell must be smaller than the local mean free path. Movement of each molecule from a cell to another one is the product of the velocity (that is the sum of convective and thermal velocities) with the time step. In order to uncouple molecular motion and collisions, the time step has to be less than the mean collision time, i.e. the time step between two successive collisions.

DSMC is a computational method which implements equations derived by kinetic theory of gases. In fact, it does not rely on any numerical procedures as per, solution of differential equations, integration, interpolation and so on. The most important advantage is that DSMC does not suffer from numerical instabilities and is valid in each type of flow field (from ipo-sonic to iper-sonic) and for each value of Mach and Reynolds numbers. On the other hand gas density must be sufficiently low. Statistical fluctuations and statistical errors are intrinsic in the DSMC simulations which are also intrinsically not steady state. Generally a steady state condition can be considered obtained when the simulation time is sufficiently large and the variation of some thermo-fluid-dynamic parameters, as for example the heat flux, between two successive time steps is small. Furthermore the computer core storage has to be large enough for simulating an appropriate number of molecules.

The different macroscopic properties are evaluated in each cell as average of microscopic quantities.

5.3 “Sophisticated” DSMC method

According to Bird the DSMC method is sophisticated [14], [15] if

- 1) it relies on two separated types of cells (collision and sampling cells) with the related cell adaptation. The collision cells are characterized by a dense space resolution much higher than the sampling cell. As suggested by the name the collision cells are used to choose the molecules involved in the collision while the sampling cells are used to compute the macroscopic flow quantities like for instance pressure and temperature. As shown in fig. 5.1 the adaptation process consists in transforming a system made up of rectangular cells into a system made up of not rectangular cells but in a form which contains a given number of molecules. Bird suggests to put 8 molecules in each adapted cell.

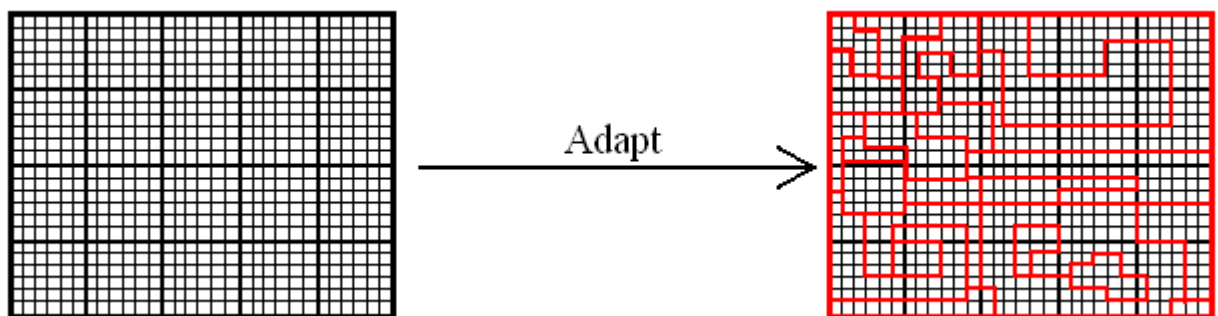


Fig. 5.1: Schematization of adaptation

- 2) it implements methods promoting nearest neighbor collisions, thus the first molecule is chosen randomly in the cell, the collision partner is the nearest molecule.
- 3) the same pair of molecules can not collide in sequential collisions,
- 4) it generates automatically computational parameters such as numbers of cells and of simulated molecules by the input number of megabytes and to the free stream density,
- 5) It uses the radial weighting factor in the solution of axial-symmetric flow fields, where if the cells are evenly spaced in the radial direction, the cells closer to the axis are smaller.
- 6) Thus the radial weighting factor, defined as the ratio of the radial position r of a molecule to the reference radius, tends to equalize the number of simulated molecules in each cell layer.

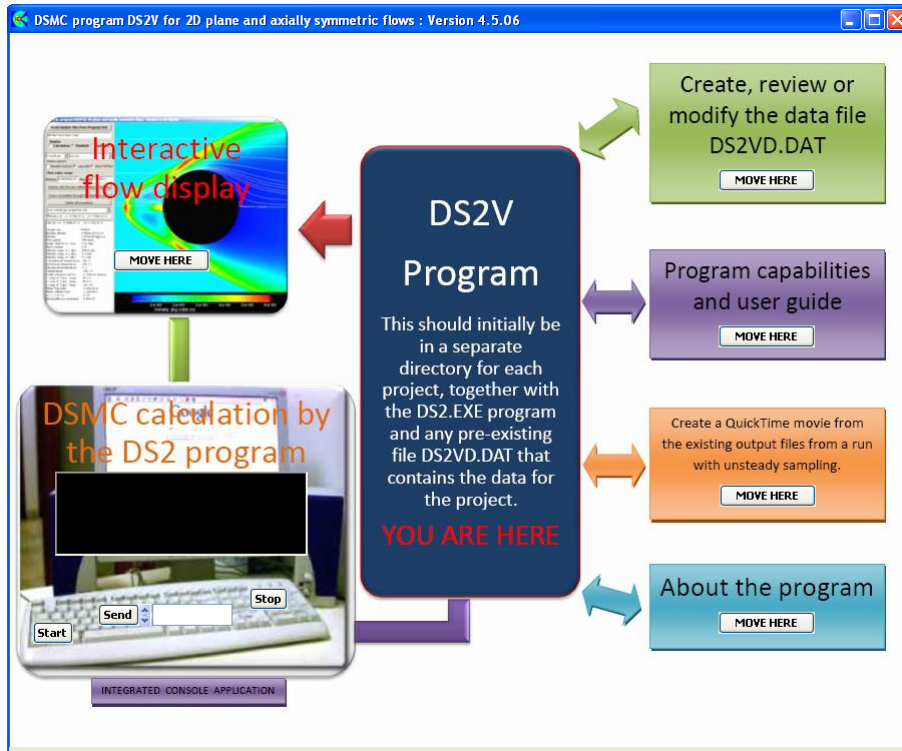
7) it provides optimal time step. Using a single constant value of the time step in every collision cell is not efficient. In fact, the time step could be too short for cells where density is low and too long for cells where density is high. The adaptive procedure of time step consists in fixing, in each cell, a local time step (Δt_l) as a fraction of the local collision time (Δt_c), generally $\Delta t_l = \Delta t_c / 5$. This value is used to compute the number of collisions in each cell.

5.4 DS2V Code

DS2V code [16] described in this section is related to version 4.5.06. This code simulates 2-D plane/axi-symmetric flow fields. A body can be taken into account and flow field can be inner or outer the body. DS2V is a very user friendly DSMC code and it is particularly suitable for the present application because can consider chemical reactions involving electrons and ions. This DSMC code is sophisticated because is characterized by all the properties written in section 5.3 and besides it is also advanced because furnishes on-line to user some parameters useful to understand if the simulation is correct. For example DS2V gives the number of simulated molecules and the ratio of the mean separation of the colliding molecules to the local mean free path. For correct results, the value of this ratio which is indicative of the proper number of simulated molecules has to be less than 1, more specifically Bird suggests that the ratio must be less than 0.2.

The main window of the code is shown in Fig.5.2. To generate an input is necessary to push to “green” radio button (Create, review or modify the data file DS2V.DAT).

Fig. 5.2: Main Window of DS2V



Thus the window in Fig.5.3 is shown. User must insert a lot of parameters like for instance the dimension of computational domain, the chemical species, the chemical reactions and the free stream thermo-fluid-dynamic parameters like for example velocity, temperature, number density.

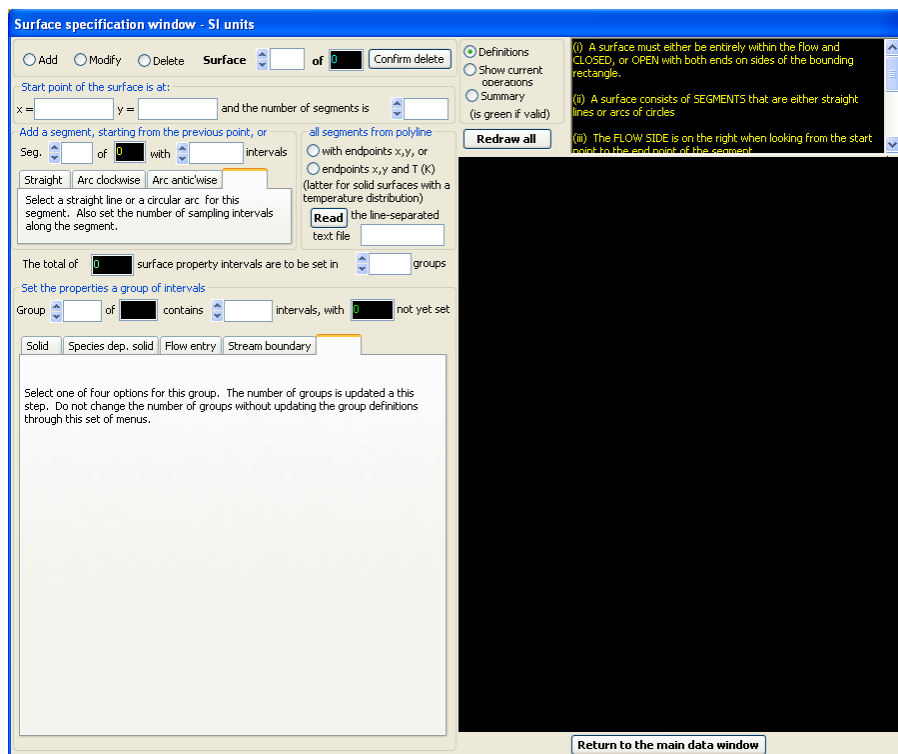
Fig. 5.3: Window to generate input file

The screenshot shows the 'Main data input window - SI units' with the following sections and controls:

- File Management:** Buttons for 'Review/modify the existing file D52VD.DAT', 'Set completely new data', and 'Write this data as the new file D52VD.DAT'.
- Calculation Parameters:** 'Magnitude of the calculation' (input field), 'Estimate fraction of bounding rectangle that is occupied by flowfield' (input field), and 'Estimate ratio of final average flowfield density to stream or reference gas density' (input field).
- Flow Quantities:** Radio buttons for 'Steady flow at large times' and 'Continuing unsteady flow'. Input fields for 'Minimum x', 'Maximum x', 'Minimum y', and 'Maximum y'.
- Flowfield State:** Radio buttons for 'Vacuum', 'Main stream', and 'Both main and secondary streams'. 'Initial separation plane at constant' with radio buttons for 'x' and 'y' and an input field for 'm'.
- Stream and Reference Gas:** 'Main stream and/or reference gas' and 'Optional secondary stream' sections. Fields for 'Number density (/cu m)', 'Temperature (K)', 'Vib. Temp. (K)', and velocity components in x, y, and z directions.
- Molecular Species:** 'Add', 'Review/modify species', and 'Description (no spaces)' fields. 'Reference diameter (m)', 'At ref. temperature (K)', 'Viscosity-temp. power law w', 'VSS param. (1 for VHS model)', 'Molecular mass (kg)', and 'Rotational deg. of freedom'.
- Rotation and Vibration:** Radio buttons for 'const. rotl. collision no. Zr =', 'For Zr=a+b*T+c*T^2 with coeff. a in polynomial =', 'coeff. b =', and 'and coeff. c ='. 'Vibration' section with 'Set mode of' and 'with characteristic vibrational temperature (K)'. Radio buttons for 'constant' and 'reference Zv = at reference temperature (K)'. 'Characteristic dissociation temperature (K) to species and'.
- Electronic:** 'Electric charge (integer multiple of the elementary charge 1.60218e-19 C)'.
- Input File:** 'Molecular input file DSMIF.DAT (A renamed DSMOF.DAT)'. 'Check if present' with 'mols. / record' and 'records' fields. Note: 'The generation of the DSMOF.DAT file is a run-time option.'
- Options:** Radio buttons for 'Use standard options' and 'Use custom options (experienced users)'. Buttons for 'Go to the surface specification window' and 'Return to the main D52V Program window'.
- Custom Parameters:** 'Optional custom adjustment of the automatically set computational parameters'. Buttons for 'Weight. factors', 'Division size', 'Element size', 'Initial mols.', 'Time step', 'Sampling int.', 'Output int.', 'Unsteady samp.', 'Dup. buffer', 'Near. neigh.', and 'Chemistry'. A note about radial weighting factors and a 'Change the value of this ratio to:-' input field.

After that it is necessary to push “Go to the surface specification window” and the window in Fig. 5.4 is shown. In this window user must insert the coordination of the segments forming the geometry and select the type of segment (straight or arc line). Furthermore the user must fix the type of interaction surface-molecule. Geometry can contain holes in which flow field enter or exit from geometry.

Fig. 5.4: Window to create geometry



Finally user pushing to “Return to the main data window” goes back to window shown in Fig. 5.3. Now he must push “write this data as the new file DS2V.DAT” to generate the file containing the input data.

Chapter 6

POSTPROCESSORS

6.1 Introduction

Obviously the results furnished in output by DS2V have to be analyzed in the most suitable way. In order to obtain this aim two post-processor codes have been written. In particular the first post-processor is written in Microsoft QuickBASIC language (PARRAR.BAS) and evaluates the rarefaction degree along the chamber axis using the P parameter of Bird and different local Knudsen numbers. The second one is written in Fortran language (ELDASU.FOR) and computes the thin film distribution on the substrate surface. Both the codes are user friendly.

The post-run rarefaction analysis is very important because justifies the use of a DSMC code in the chamber deposition without the necessity to utilize a continuum approach. As well as the computation of thin film distribution is essential because, as said before, together with the study of fluidics in the deposition apparatus is a fundamental objective of the present Ph.D thesis.

The aim of this section is to explain in more detail these 2 post-processor codes.

6.2 Rarefaction parameters

PARRAR.BAS code is user friendly. The users must sort the output from DS2V (DS2FF.dat) in a file containing:

- 1) along the columns the variables in the order of abscissa, ordinate, number density, density, velocity component along x, velocity component along y, velocity component along z, translational temperature, rotational temperature, vibrational temperature, overall temperature, Mach number, mean collision, mean collision separation, mean free path, ratio of mean collision separation to mean free path, velocity, **angular degree**, pressure.
- 2) along the rows the values of the different parameters along the chamber axis (from x = 0.45 m until to x = 0 m).

PARRAR.BAS reads in input this new file and evaluates the rarefaction degree along the chamber axis by means of:

- 1) P parameter of Bird. Numerically the formula (3.2.1) at each point i is written as:

$$P_i = \frac{\sqrt{\pi}}{2} S_i \frac{\lambda_i}{\rho_i} \left| \frac{d\rho}{ds} \right|_i \quad (6.2.1)$$

where the mean free path and density at each point i are provided in output by DS2V. The speed ratio at each point i is computed by:

$$S = \frac{V_i}{\sqrt{\frac{2kT_i}{m}}} \quad (6.2.2)$$

where the velocity and temperature at each point i are present in output by DS2V. The derivative in (6.2.1) at each point i is approximated numerically by:

$$\left| \frac{d\rho}{ds} \right|_i = \left| \frac{\rho_{i+1} - \rho_i}{s_{i+1} - s_i} \right| = \left| \frac{\rho_{i+1} - \rho_i}{x_{i+1} - x_i} \right| \quad (6.2.3)$$

where obviously x is the abscissa.

- 2) The local Knudsen number based on the local gradient length scale of a generic thermo-fluid-dynamic quantity. Numerically the formula (3.2.9) at each point i is written as:

$$\text{Kn}_{G_i} = \frac{\lambda_i}{\left(\frac{\partial G}{\partial s} \right)_i} \quad (6.2.4)$$

where, as said before, the mean free path at each point i is given in output by DS2V. The derivative in (6.2.4) at each point i is approximated numerically by:

$$\left(\frac{dG}{ds} \right)_i = \frac{G_{i+1} - G_i}{s_{i+1} - s_i} = \frac{G_{i+1} - G_i}{x_{i+1} - x_i} \quad (6.2.5)$$

where the parameter G , which can be for example velocity or temperature, at each point i is furnished in output by DS2V. More specifically considering velocity, temperature, density and pressure, the local Knudsen numbers are respectively computed numerically at each point i by:

$$\text{Kn}_{V_i} = \frac{\lambda_i}{\frac{V_{i+1} - V_i}{x_{i+1} - x_i}} \quad (6.2.6)$$

$$\text{Kn}_{T_i} = \frac{\lambda_i}{\frac{T_{i+1} - T_i}{x_{i+1} - x_i}} \quad (6.2.7)$$

$$\text{Kn}_{\rho_i} = \frac{\lambda_i}{\frac{\rho_{i+1} - \rho_i}{x_{i+1} - x_i}} \quad (6.2.8)$$

$$\text{Kn}_{p_i} = \frac{\lambda_i}{\frac{p_{i+1} - p_i}{x_{i+1} - x_i}} \quad (6.2.9)$$

The user assigns the name of file where PARRAR.BAS writes the parameter of rarefaction and the values of abscissa x.

6.3 Film

ELDASU.FOR code is an user friendly code. DS2V code does not provide the film distribution but the value of the molecule number flux on a surface. This flux is equal to the number of molecules which arrive to a surface element per unit of time and per unit of surface and thus is characterized by the physical dimension of $[1/s/m^2]$. For this reason, in order to simulate the film configuration, the substrate temperature is put equal to 10^{-3} K (practically zero) and a totally accommodate diffusive reflection is taken into account only for the four species (C, C₂, CH and C₂H) constituting the film, while a specular reflection is considered for all the other chemical species. In this way C, C₂, CH and C₂H remain attached on the substrate because the re-emitted velocity is close to zero and form the film, while the other chemical species come back to the flow field and do not deposit. It results that the sticking probability of C, C₂, CH and C₂H are equal to one, while the sticking probability of each remaining species is zero. The sticking probability of a single species is defined as the ratio of the number of molecules of the single species which deposit to the total number of the single species which arrive to the substrate. Therefore in a first, preliminary and simple analysis of film properties, the molecule number fluxes of C, C₂, CH and C₂H on the substrate can be considered as a rough estimation of the film distribution. More specifically the film is considered to be equal to the sum (here labeled N_f) of the number fluxes of C (N_{fC}), C₂ (N_{fC2}), CH (N_{fCH}) and C₂H (N_{fC2H}):

$$N_f = N_{fC} + N_{fC2} + N_{fCH} + N_{fC2H} \quad (6.3.1)$$

In the present DSMC simulation the substrate surface (length 0.05 m) is divided in 500 parts characterized by the same length (10^{-4} m). The DS2V code provides in output (file DS2SU.dat) for the mid-point of each single part the value of the molecule number flux of whole mixture (N_{fTOT}) equal to the sum of the molecule number fluxes of all 21 chemical species constituting the plasma mixtures. This means that N_{fTOT} is the sum of molecule number flux of Ar (N_{fAr}), Ar⁺ (N_{fAr+}), C₂H₂ (N_{fC2H2}), C₂H₂⁺ (N_{fC2H2+}), C₂H (N_{fC2H}), H (N_{fH}), C₂ (N_{fC2}), CH (N_{fCH}), C₂H⁺ (N_{fC2H+}), C (N_{fC}), C₂⁺ (N_{fC2+}), CH⁺ (N_{fCH+}), CH₂ (N_{fCH2}), CH₂⁺ (N_{fCH2+}), H₂ (N_{fH2}), C₃ (N_{fC3}), C₃H (N_{fC3H}), C₃H₃ (N_{fC3H3}), C₄H (N_{fC4H}), C₄ (N_{fC4}) and C₄H₂ (N_{fC4H2}):

$$N_{\text{fTOT}} = N_{\text{fAr}} + N_{\text{fAr}^+} + N_{\text{fC}_2\text{H}_2} + N_{\text{fC}_2\text{H}_2^+} + N_{\text{fC}_2\text{H}} + N_{\text{fH}} + N_{\text{fC}_2} + N_{\text{fCH}} + N_{\text{fC}_2\text{H}^+} + N_{\text{fC}} + N_{\text{fC}_2^+} + N_{\text{fCH}^+} + N_{\text{fCH}_2} + N_{\text{fCH}_2^+} + N_{\text{fH}_2} + N_{\text{fC}_3} + N_{\text{fC}_3\text{H}} + N_{\text{fC}_3\text{H}_3} + N_{\text{fC}_4\text{H}} + N_{\text{fC}_4} + N_{\text{fC}_4\text{H}_2} \quad (6.3.2)$$

DS2V furnishes also the number of molecules sample of all 21 chemical species constituting the mixture. Furthermore DS2V provides in output for the entire surface of the simulated body some useful parameters. The user must organize the DS2SU.dat file in a new file having in order the curvilinear abscissa, Cartesian abscissa, Cartesian ordinate, N_{fTOT} , pressure, normal component of shear stress, tangential component of shear stress, incident energy, re-emitted energy, total energy (sum of incident with re-emitted energy), temperature of surface, velocity slip, translational temperature slip, rotational temperature slip, samples of Ar, Ar⁺, C₂H₂, C₂H₂⁺, C₂H, H, C₂, CH, C₂H⁺, C, C₂⁺, CH⁺, CH₂, CH₂⁺, H₂, C₃, C₃H, C₃H₃, C₄H, C₄, C₄H₂, related only to the substrate surface, i.e. for the parts characterized by $x = 0.45$ m and y in the range 5×10^{-5} - 4.995×10^{-5} m (interval is not equal to 0-0.05 m due to the mesh).

ELDASU.FOR evaluates the molar fractions of C (α_{C}), C₂ (α_{C_2}), CH (α_{CH}) and C₂H ($\alpha_{\text{C}_2\text{H}}$). This evaluation is made as the ratio of sample of each of the above single species to the total sample of all 21 chemical species. However, after this computation ELDASU.FOR computes the molecule number flux of C (N_{fC}), C₂ (N_{fC_2}), CH (N_{fCH}) and C₂H ($N_{\text{fC}_2\text{H}}$) as:

$$N_{\text{fC}} = \alpha_{\text{C}} N_{\text{fTOT}} \quad (6.3.3)$$

$$N_{\text{fC}_2} = \alpha_{\text{C}_2} N_{\text{fTOT}} \quad (6.3.4)$$

$$N_{\text{fCH}} = \alpha_{\text{CH}} N_{\text{fTOT}} \quad (6.3.5)$$

$$N_{\text{fC}_2\text{H}} = \alpha_{\text{C}_2\text{H}} N_{\text{fTOT}} \quad (6.3.6)$$

and finally evaluates the “film” applying the formula (6.3.1).

At the end of computations the post-processor writes a file (format .dat) where there are the ordinate of the substrate and the values of N_{fC} , N_{fC_2} , N_{fCH} , $N_{\text{fC}_2\text{H}}$ and N_{f} (obviously corresponding to each substrate ordinate).

Chapter 7

ANALYSIS OF THE RESULTS

7.1 Introduction

In this section the analysis of the results linked to simulation of the flow field in an Expanding Thermal Plasma deposition apparatus, made up of an electrical torch, a supersonic conical nozzle and the van de Sanden deposition chamber is evaluated [17]. All these data have been obtained after numerous preliminary runs computed in order to verify the real practicability of tests conditions, to take confidence with the codes, to make a sensitivity analysis and to choose the best methodology and geometry configuration [18]. The preliminary tests consider the thermo-fluid-dynamic evolution and thin film deposition characteristics using in the deposition apparatus only inert, not diffusive Argon and thus without any type of chemical reactions, in brief Argon has been considered just as a simple tracer.

In the present study, as said before, the simulation is achieved using first a continuum pre-processor code, for the torch and for the divergent part of nozzle (from the throat until to the 90% of nozzle axis) and then by means of the widely accepted 2-D axis-symmetric DSMC code by Bird (DS2V, Ver. 4.5.06) for the remaining part of the nozzle and for the entire deposition chamber. Figure 7.1 shows in a schematic way the zones where the two different codes are applied. Also in the convergent part of the nozzle the flow field is continuum but it is not necessary to simulate it because the thermo-fluid-dynamic conditions at the throat are easily evaluated by the conservation of mass flow rate and putting the condition of sonic flow (Mach number equal to 1) without using complex computational procedures.

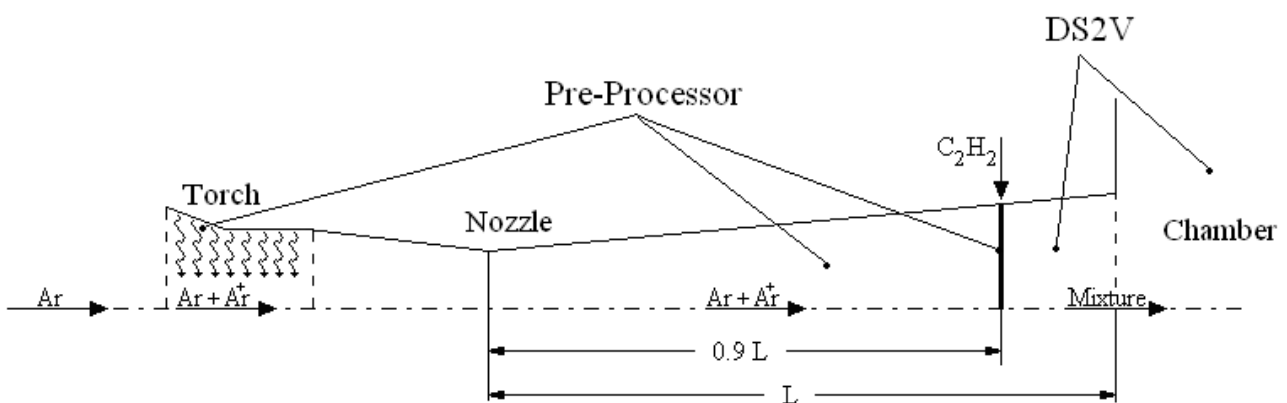


Fig. 7.1 – Scheme representing where the codes are used

The choice to use in the initial part of the apparatus a continuum approach and in the remaining part a molecular approach is justified by the fact that the rarefaction analysis and also other researchers

[19] and [20] demonstrated that typically the rarefaction condition is really obtained only in a part of the chamber. However the version of DS2V used in these runs can simulate accurately the entire chamber and also the last part of nozzle because it is advanced and sophisticated and not basic thus can work correctly in conditions where the Knudsen number is not so high. More over the use of a DSMC code is proper because, simulating the thermo-fluid-dynamic evolution of each single molecule constituting the flow field, is based on a molecular approach and thus well suitable to reproduce the deposition process in which the film formation is obtained by the stick of each single atom on the substrate. The use of the DSMC code in the last part of nozzle is made up to get better the computation of DS2V in the chamber. In fact in this way the flow field expands more precisely in the nozzle, furnishing a detailed profile of various thermo-fluid-dynamic parameters at the exit section while the pre-processor is 1-D and furnishes in output a single value and not a profile at the exit section.

The influences on the thermo-fluid-dynamic evolution of gases in the chamber and on thin film properties deposited on the substrate surface due to different:

- 1) electrical power provided to the torch,
- 2) precursor mass flow rate (Argon mass flow rate is constant in all runs),
- 3) thermo-fluid-dynamic conditions at the chamber inlet by the use of supersonic conical nozzles characterized by different geometry,

are estimated and the analysis of the results is showed.

In the present runs the flow field simulations involve Ar which is ionized in the torch (the first ionization is modelled by the Saha equation) forming thus a plasma mixture made up of Ar, Ar⁺ and electrons which flows in the nozzle. As said before the pre-processor does not evaluate the flow field evolution of electrons, for this reason in fig. 7.1 there are written only Ar and Ar⁺ while the electrons are not signed on the arrows in torch and in the divergent part of nozzle. Furthermore the chemical composition of the plasma in the nozzle, i.e. the molar fractions of Ar and Ar⁺, remains constant and equal to those obtained at the torch exit section. At the 90% of nozzle axis the precursor Acetylene is injected. After the nozzle exit the plasma mixture goes in the chamber where it first supersonically expands and after it is compressed by a barrel shock wave. Successively the gases proceed subsonically towards the substrate and a hydrogenated amorphous carbon (a-C:H) thin film is generated on the substrate surface thanks to the deposition of C, C₂, CH and C₂H. Also DS2V considers the chemical reactions. In input are given all the necessary data to evaluate them using the steric factor procedure, such as the parameters in the rate constant expressed by an

Arrhenius form. Initially in the vessel the gas is stationary (velocity equal to zero) and the pressure is maintained low (about 30 Pa) by means of pumps at the chamber exit. The value of temperature is unknown because very difficult to measure accurately and to determine numerically. In fact, an instrument can not entry because it can be destructed or seriously damaged, the measurements by not-intrusive methods are not precise. More over also the temperature evaluated numerically is inaccurate because the numerical simulations imply many unknown parameters. For this reason a value of temperature equal to one obtained at the 90% of nozzle axis, output by the pre-processor is used. Also the density is equal to one achieved at the 90% of nozzle axis. In this way the velocity (V_E) at the chamber exit slot is evaluated by means of mass flow rate conservation considering the exit, which in reality is a hole, as an annulus with area equal to 0.01 m^2 .

7.2 Heater

The heater in the ETP deposition apparatus is extremely important because thanks to it a part of inert Argon is ionized ($\text{Ar} \rightarrow \text{Ar}^+ + \text{e}^-$) forming a plasma made up of inert Argon, Argon ions and electrons. The presence of Argon ions is fundamental to the occurrence of chemical reactions and thus on the mixture composition, because, as shown in chapter 2, when Acetylene will be injected in the nozzle it first will react chemically with Ar^+ by the following reaction:



The Acetylene ions in turn will react with the electrons generating “new” different chemical species which in turn will react chemically together, changing the chemical composition of plasma mixture. The various chemical reactions implemented in the present computations are reported in table 2.1.

The heater analyzed is the electrical torch Perkin-Emler 9MB-M (see section 4.3). The electrical power supplied to the torch ranges in the interval 1÷13 kW and it is obtained by different combinations of current voltage and intensity of electric current (see table 7.1), at each test the Argon mass flow rate is constant and equal to 100 sccs (standard cubic centimeter per second, 1 sccs = 2.69×10^{19} particles/s).

Table 7.1 – Electrical parameters input to the torch

V	I	P
[V]	[A]	[kW]
220	61	13.42
220	48	10.56
220	22	4.84
200	10	2
50	20	1

The influence of the electrical power is pretty strong on ionization level as it is easy to verify by fig. 7.2 where α_{Ar^+} along the torch axis is reported at different electrical power. It results that when the electrical power is high (13 kW) Argon is completely ionized already near the torch inlet section

($\alpha_{Ar^+} \approx 1$). When the electrical power is low (1 kW) it results $\alpha_{Ar^+} \approx 0.02$ at the torch exit.

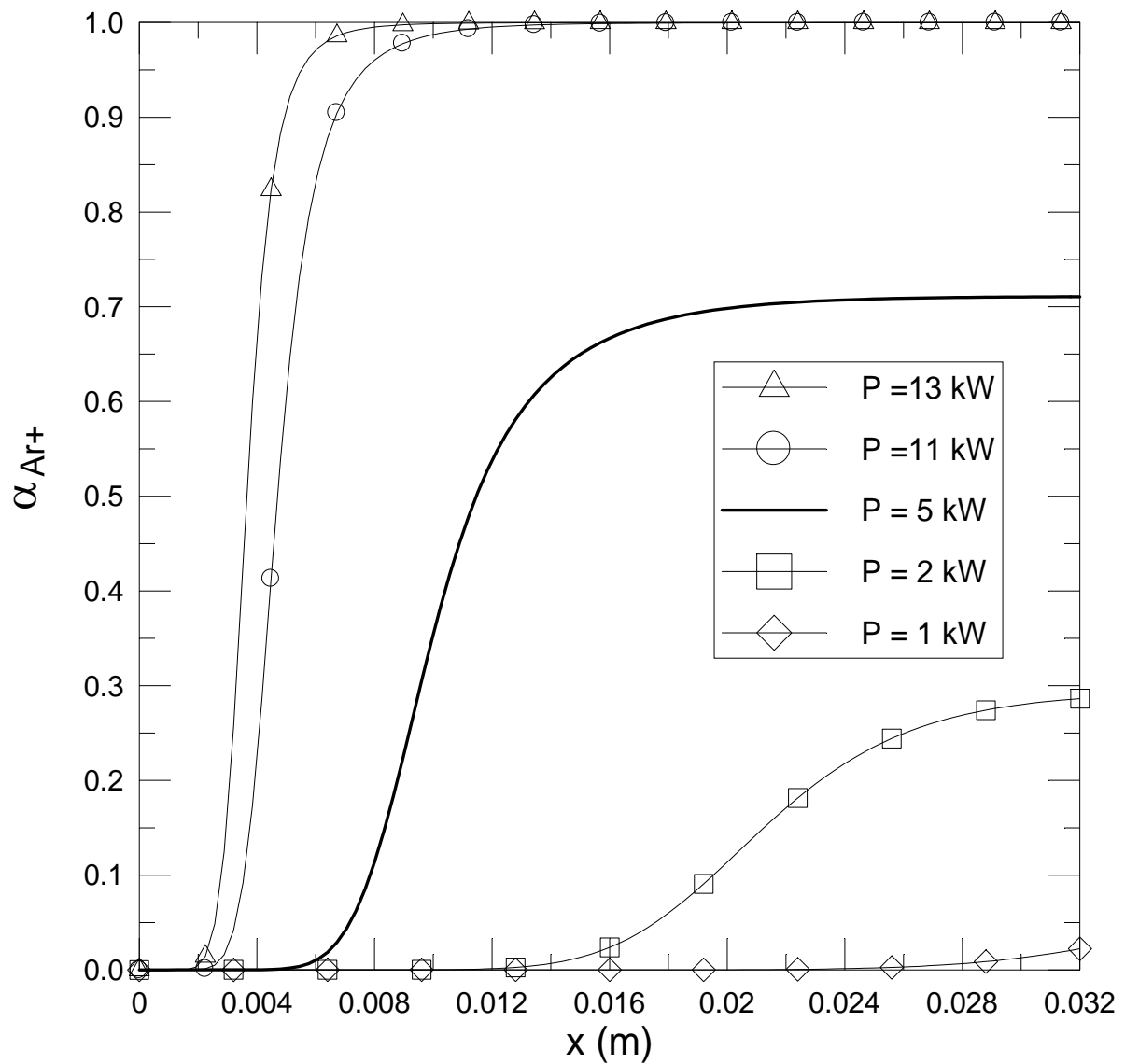


Fig. 7.2 – Profiles of Argon ionization degree along the torch axis

Figures 7.3a, 7.3b, 7.3c and 7.3d show the profiles of Mach number, velocity, temperature and density along the torch axis at different electrical power. At the torch inlet the Mach number is incompressible ($M \approx 7.1 \times 10^{-3}$) in every tests and then increases both in the convergent part and in the conduct with constant area. The Mach number increases in the nozzle due to the effect of area ratio changing while it increases in conduct with constant area due to the effect of power given to the gas. The higher is the electrical power, the higher is the value of Mach number. In fact the maximum value ($M \approx 0.36$) is obtained at the torch exit when $P = 13$ kW. As expected increasing the electrical power either temperature and velocity increases while the density decreases. This is due to the fact that when the electrical power is high, the energy given to the gas is high. This energy is distributed in thermal energy represented by temperature and kinetic energy represented by velocity. Thus the molecules of the gas characterized by high energy move faster, the distance between them increases and the density decreases. The maximum values both of velocity and of temperature are obtained at the torch exit when the electrical power is equal to 13 kW and more specifically $V = 1865.87$ m/s and $T = 76855.1$ K. Also the minimum value of density (1.905062×10^{-3} kg/m³) is achieved at the torch exit when the electrical power corresponds to 13 kW.

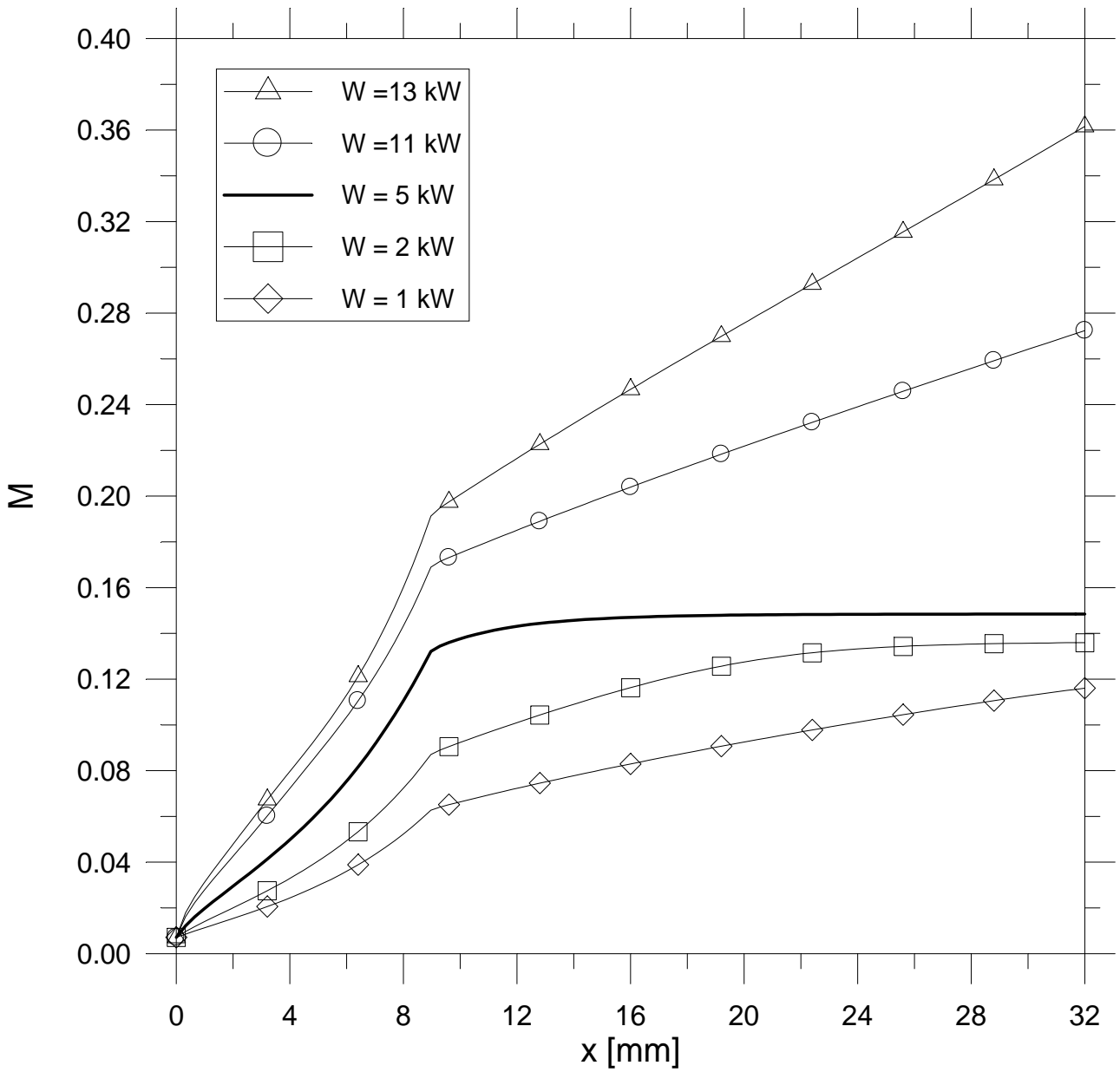


Fig. 7.3 a – Profiles of Mach number along the torch axis at different electrical power

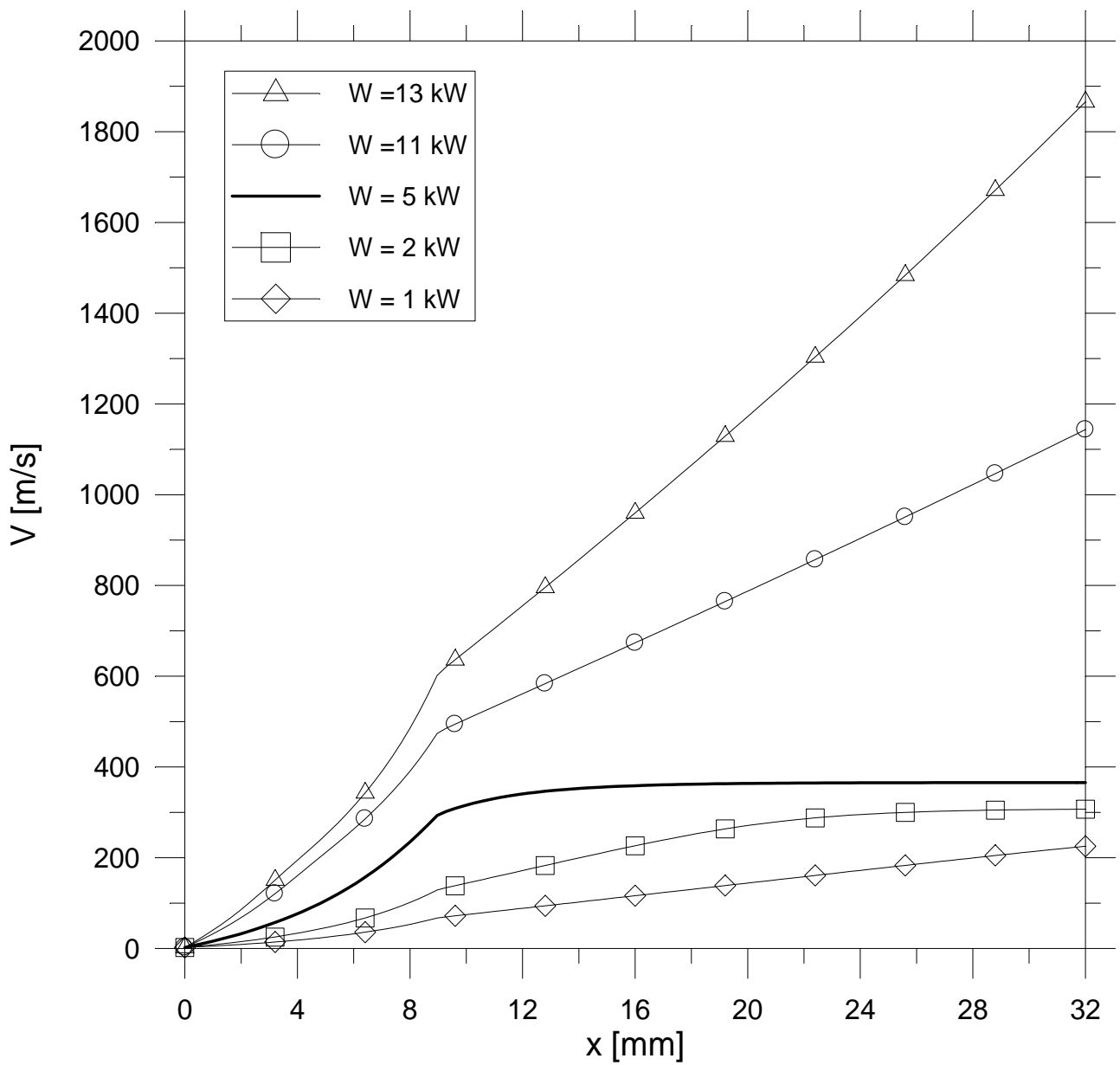


Fig. 7.3 b – Profiles of velocity along the torch axis at different electrical power

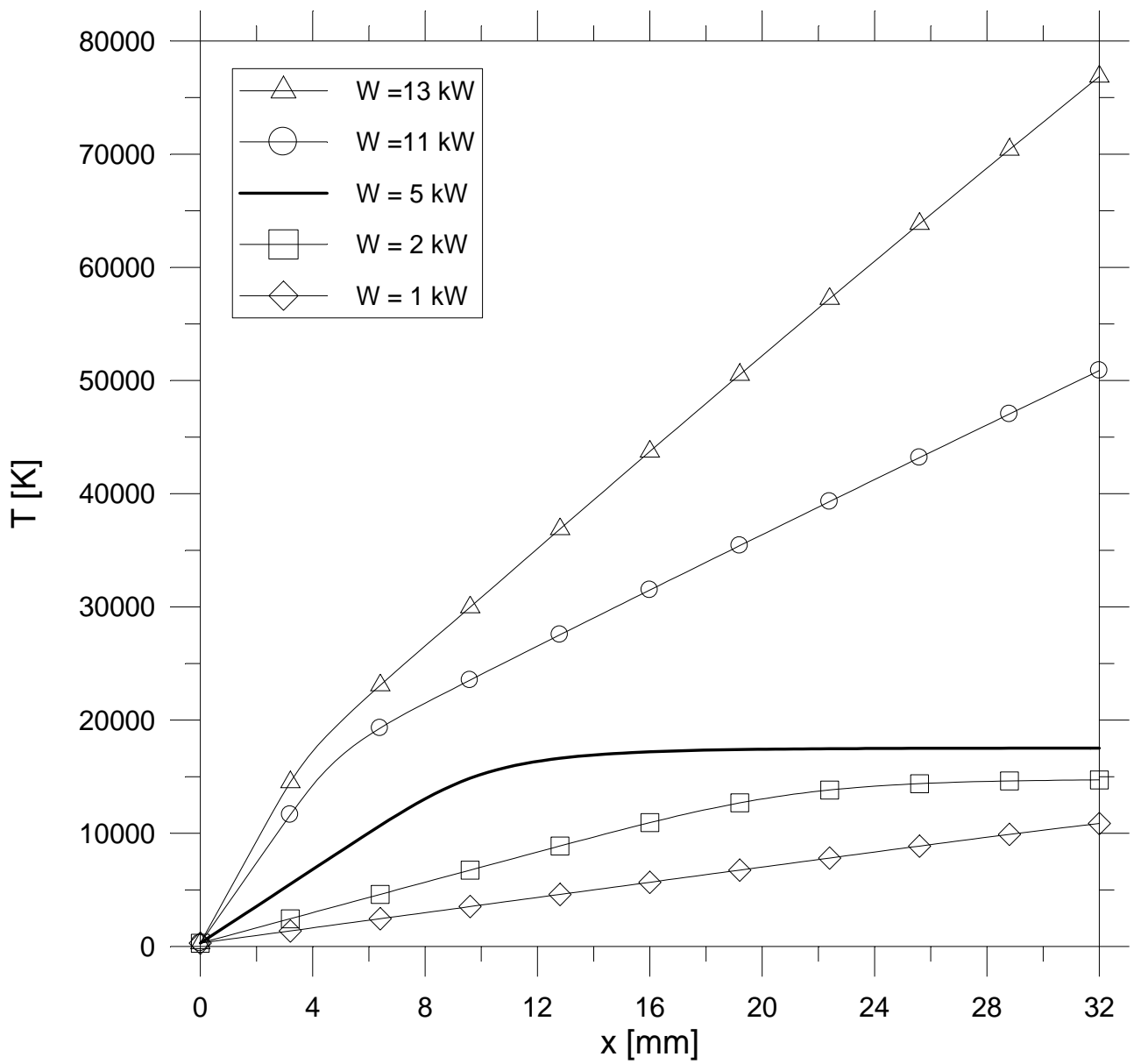


Fig. 7.3 c – Profiles of temperature along the torch axis at different electrical power

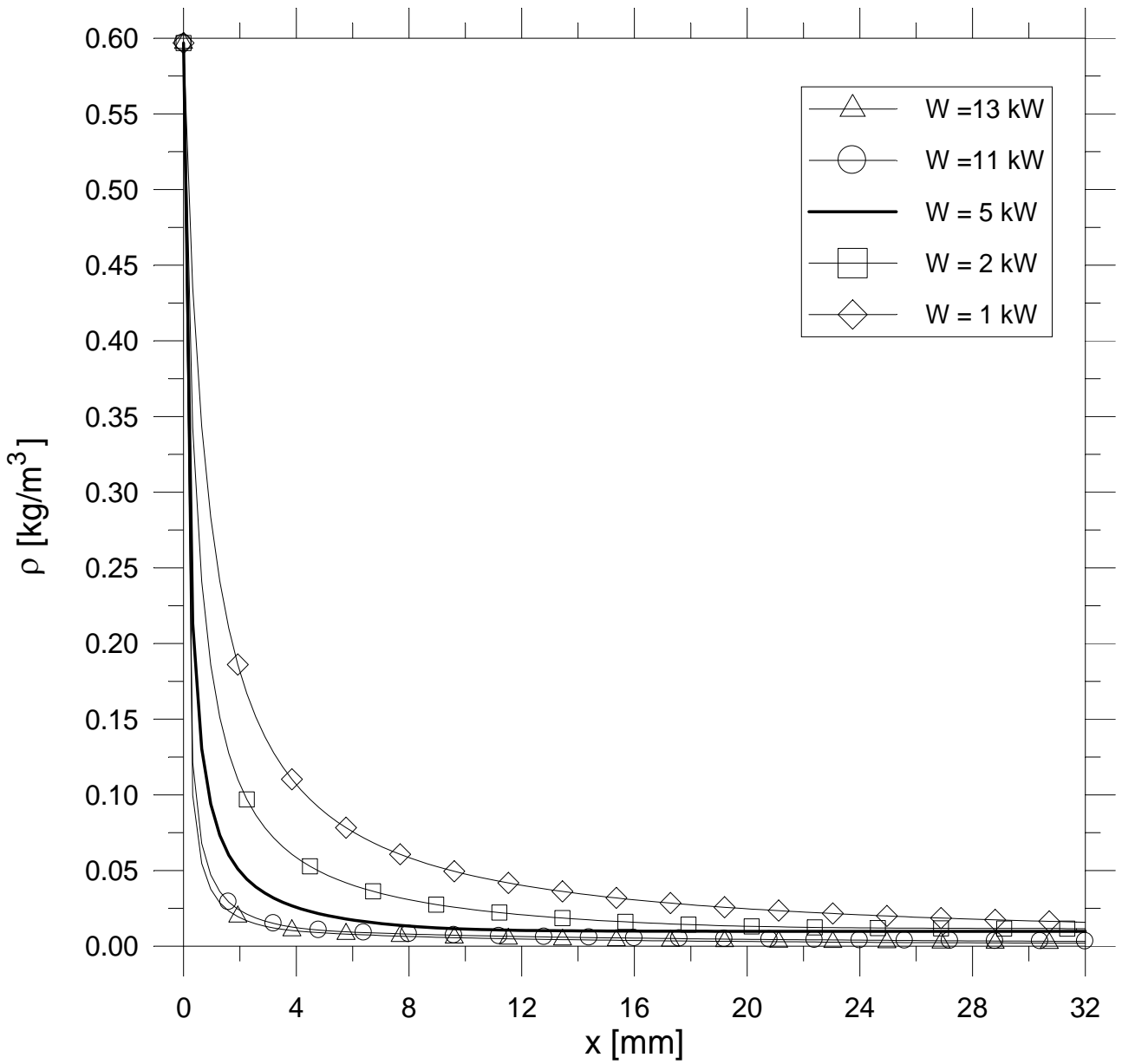


Fig. 7.3 d – Profiles of density along the torch axis at different electrical power

As typical example, figures 7.4a, 7.4b and 7.4c show the profile of Mach number, velocity and temperature along the torch axis for the test A5-5 (i.e. nozzle A, electrical power furnished to torch equal to 5 kW and C₂H₂ mass flow rate equal to 5 sccs) with and without considering the ionization effects. It is to point out that in the following each test is labeled by a letter and two numbers. The letter identifies the type of nozzle, the first number represents the electrical power furnished to torch in kW while the last number is equal to C₂H₂ mass flow rate in sccs. The flow field with ionization effects corresponds to a plasma mixture made up of Ar and Ar⁺, while in the flow field without ionization effects there are only Argon atoms. In each figure the two profiles (with and without considering the ionization effects) initially are the same and successively a difference between them increases going towards the torch exit. More specifically the plasma shows a mach number lower because the power furnished to the gas is spent to make possible the ionization. For what concern the temperature, once again the plasma presents a temperature lower. This is due to the fact that thermal energy of the flow field is consumed in order to obtain the ionization which is an endothermic process and, as well known, temperature is representative of thermal energy. At the torch exit the gas not ionized is characterized by a temperature (51122.51 K) which is about 3 times that of plasma mixture. Similarly for the velocities, the plasma shows a velocity lower because kinetic energy of the flow field is consumed in order to obtain the ionization. At the torch exit the gas not ionized is characterized by a velocity (1159.572 m/s) which is about 3.2 times that of plasma mixture.

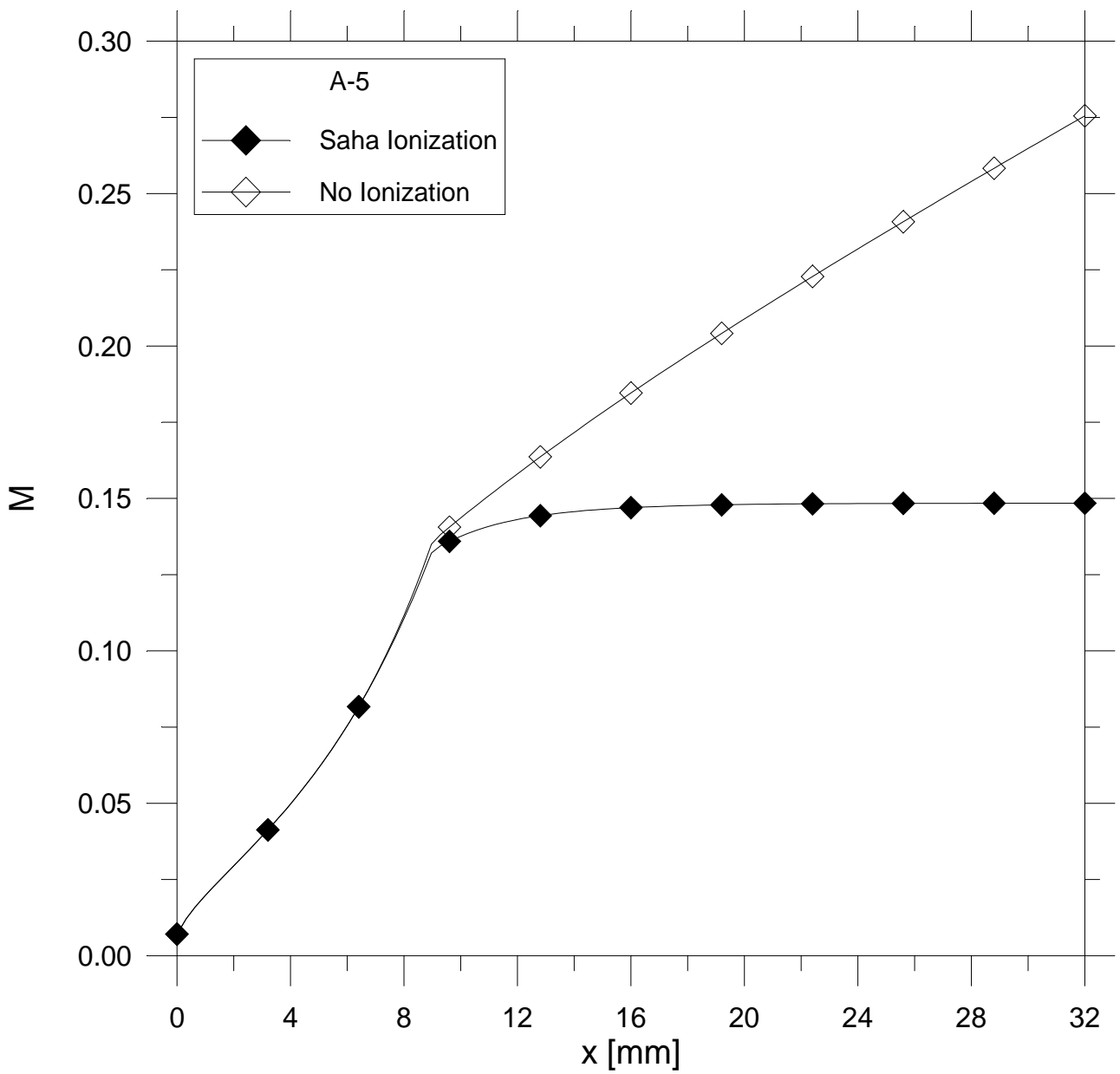


Fig. 7.4 a – Profiles of Mach number along the torch axis for test A5-5

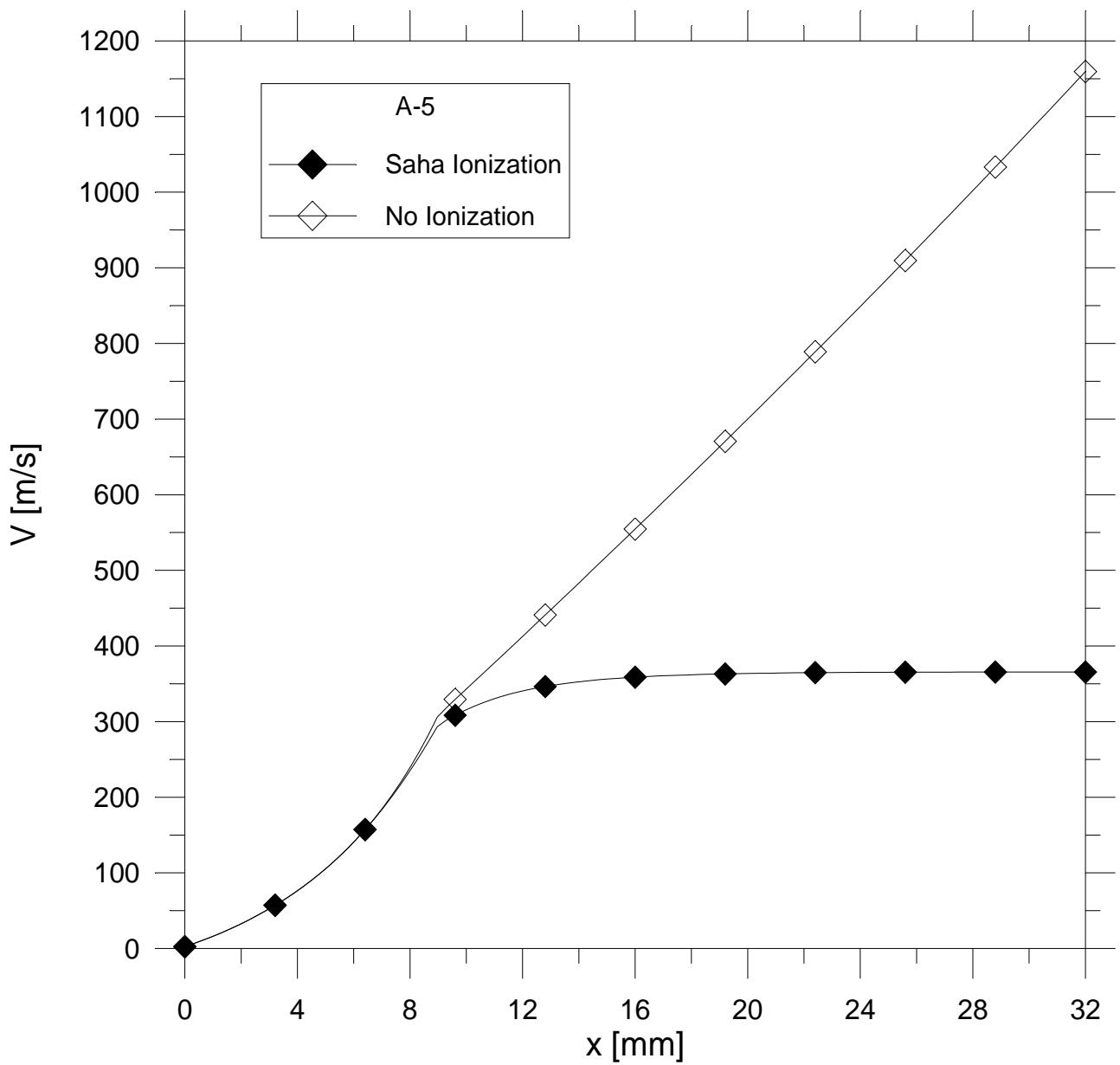


Fig. 7.4 b – Profiles of velocity along the torch axis for test A5-5

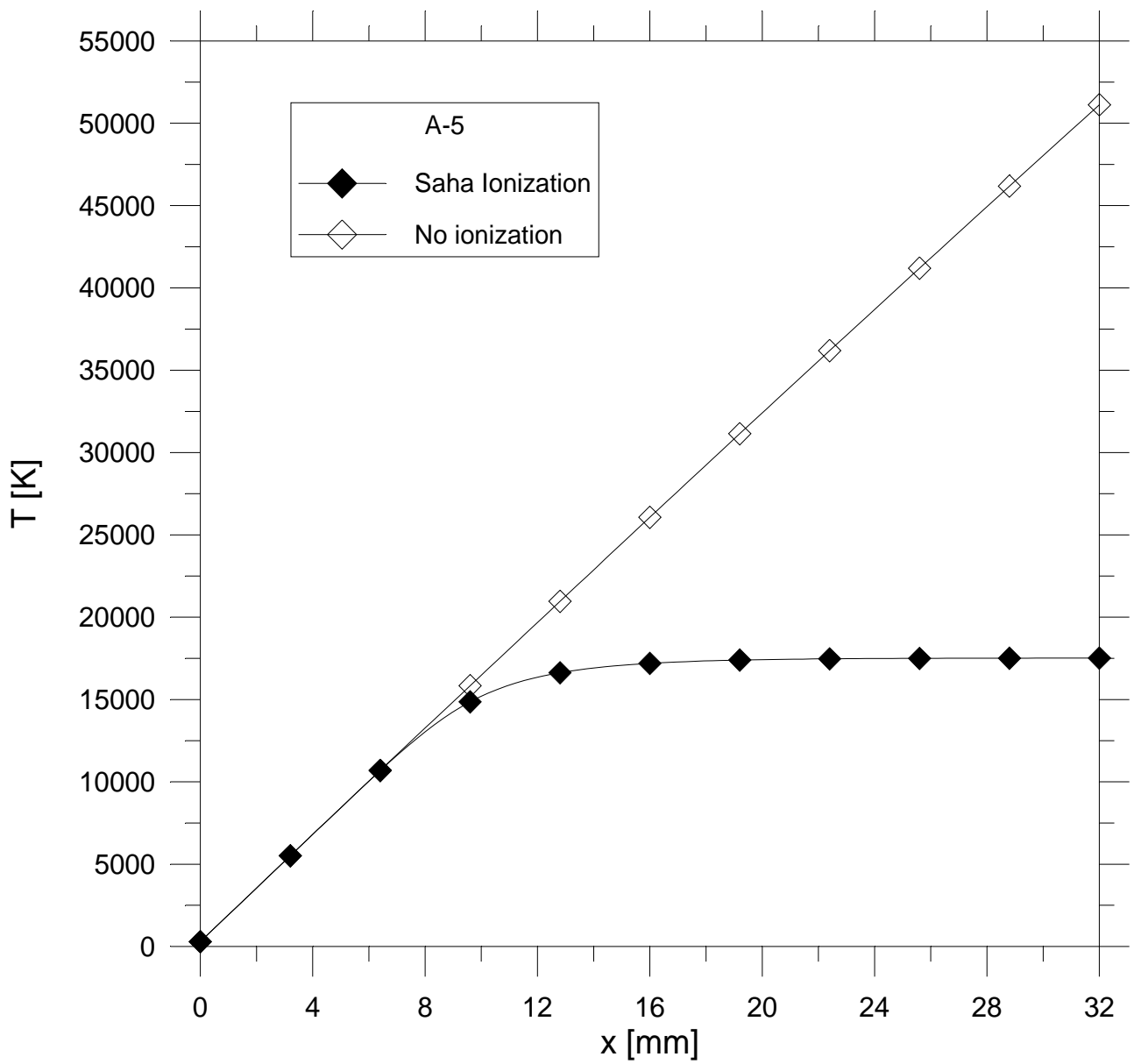


Fig. 7.4 c – Profiles of temperature along the torch axis for test A5-5

7.3 Nozzle

The nozzle is very important in the deposition apparatus because through it the plasma mixture of inert Argon, Argon ions and electrons expands becoming a supersonic flow field. At the 90% of nozzle axis the precursor Acetylene is injected and reacts chemically leading to the formation of a “new” plasma mixture made up of different 21 chemical species (15 radicals and 6 ions) and electrons. The nozzles considered are installed in the plasma wind tunnel at the University of Naples “Federico II” (see section 4.4).

Figures 7.5a, 7.5b and 7.5c show the profiles of Mach number, velocity and temperature along the chamber axis evaluated by NOZVS.BAS for nozzles A, B and C. As expected the higher is the area ratio, the higher are Mach number and velocity and the lower is temperature.

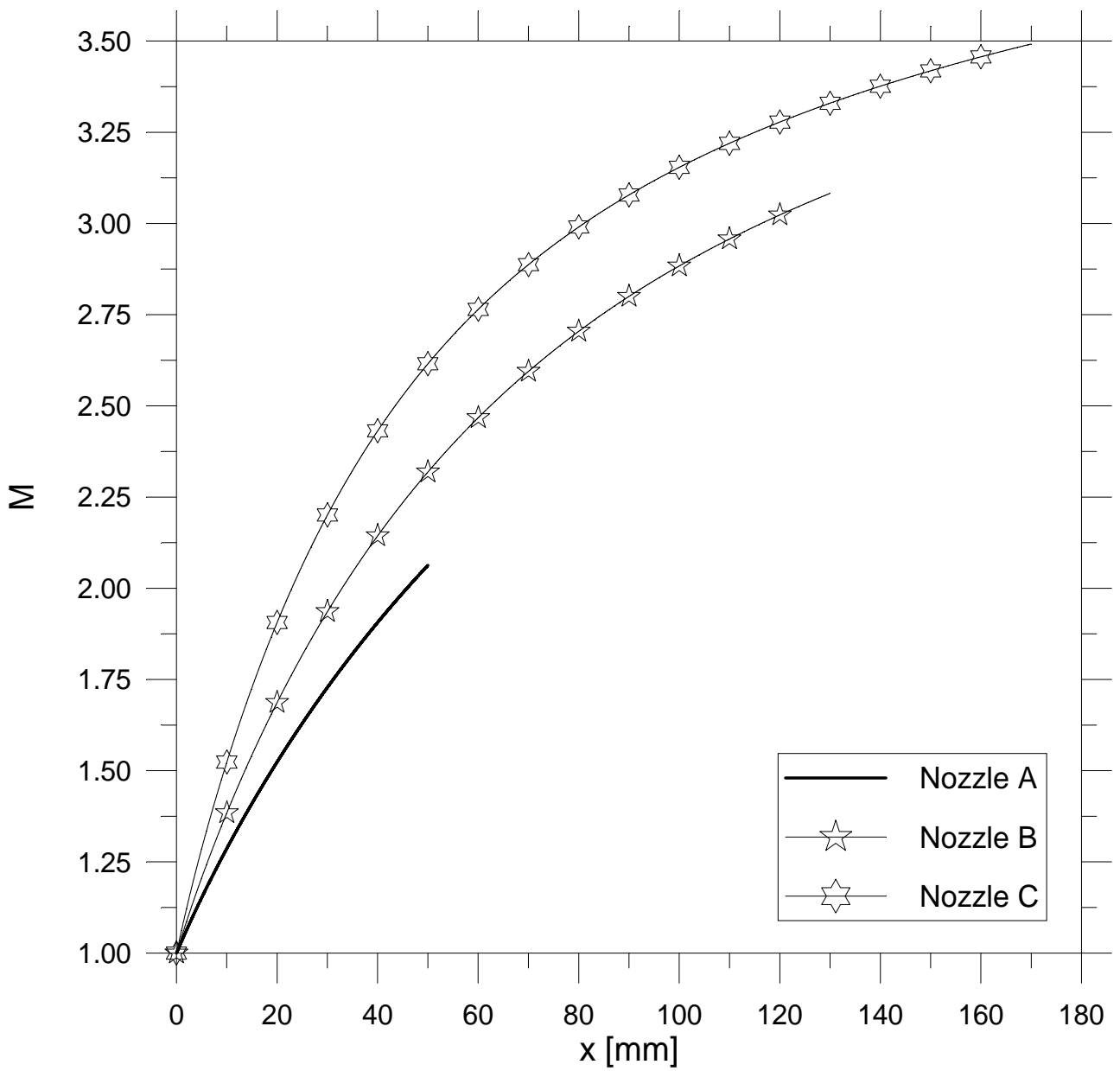


Fig. 7.5a – Profile of Mach number along the nozzle axis for different types of nozzle

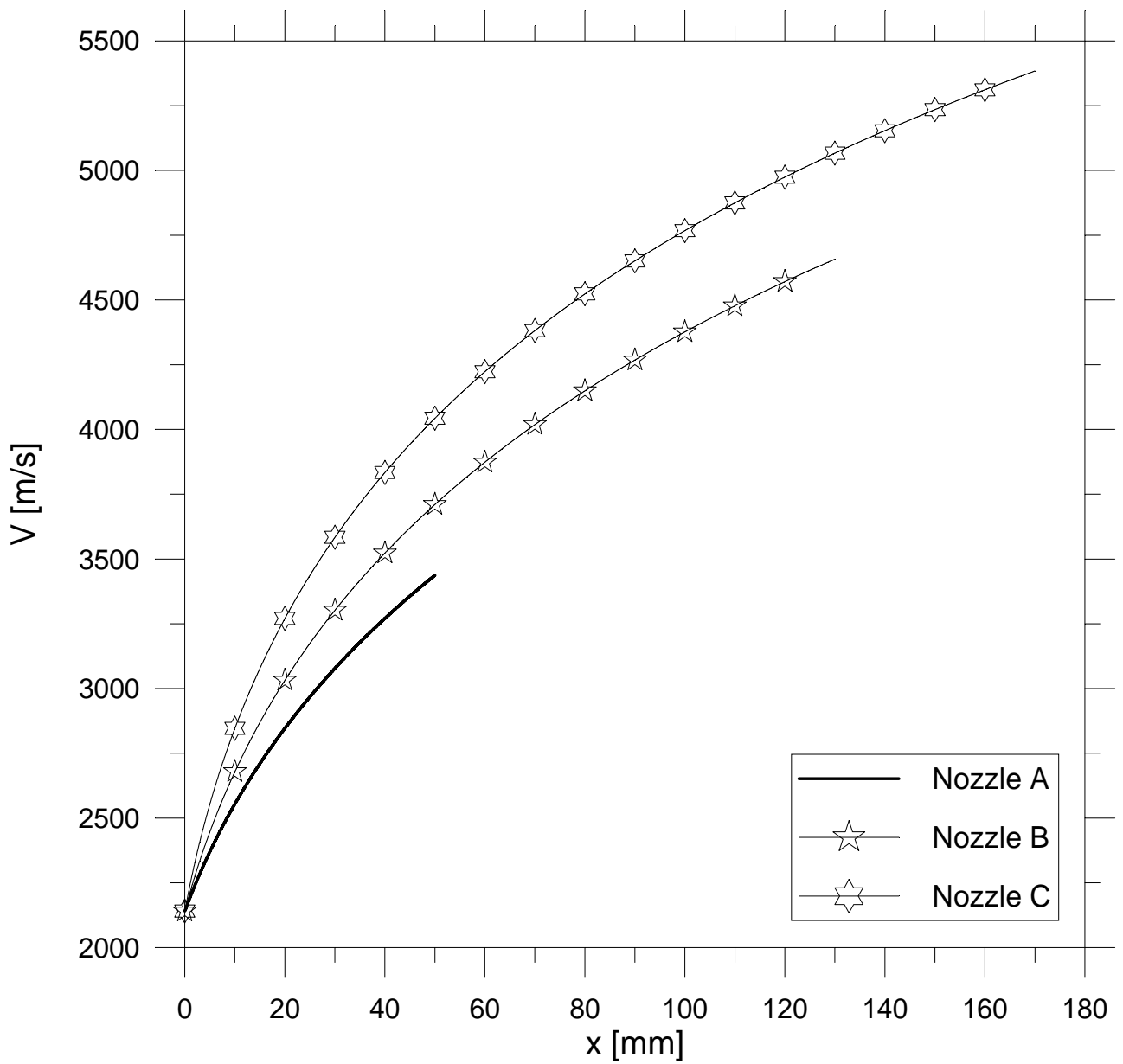


Fig. 7.5b – Profile of velocity along the nozzle axis for different types of nozzle

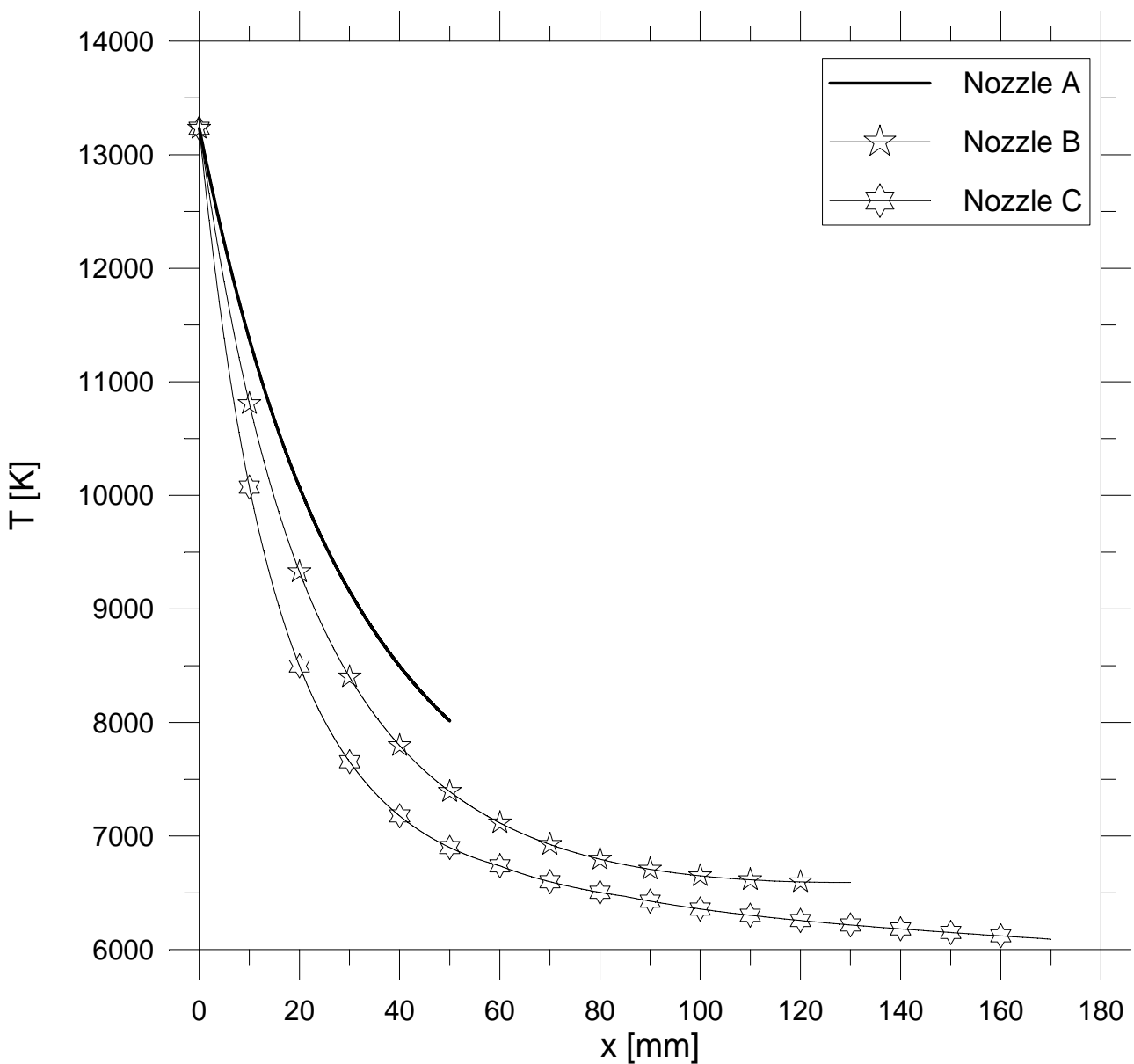


Fig. 7.5c – Profile of temperature along the nozzle axis for different types of nozzle

As said before, in the present simulation the injection of Acetylene at the 90% of nozzle axis is taken into account. The sub-code CHIBEVS.BAS evaluates 24 chemical reactions in the zone along the nozzle axis extended 10^{-5} m from the injection point of Acetylene. The Acetylene mass flow rate ranges in the interval 1÷15 sccs. The various chemical reactions lead to the generation of a “new” mixture formed by 21 chemical species (15 radicals and 6 ions), the electrons are not involved. The properties of all species considered, such as physical mass (m), molecular weight (pm) and the constant for each gas (R_{gas}) are listed in table 7.2. The specific heat at constant pressure for each species is computed as polynomial function depending on the temperature and is

different for each gas, the various terms of polynomials are taken from the literature such as the NIST web database and the Fluent code database (see section 4.4).

Table 7.2 – Chemical Species and related properties

Chemical Specie	m [kg]	pm [kg/kmol]	R _{gas} [J/kg/K]
Ar	6.644×10^{-26}	40	207.85
Ar ⁺	6.644×10^{-26}	40	207.85
C ₂ H ₂	4.324912×10^{-26}	26.038	319.3026
C ₂ H ₂ ⁺	4.324912×10^{-26}	26.038	319.3026
C ₂ H	4.1525×10^{-26}	25	332.56
H	1.661×10^{-27}	1	8314
C ₂	3.9864×10^{-26}	24	346.4167
CH	2.1593×10^{-26}	13	639.5385
C ₂ H ⁺	4.1525×10^{-26}	25	332.56
C	1.9932×10^{-26}	12	692.8333
C ₂ ⁺	3.9864×10^{-26}	24	346.4167
CH ⁺	2.1593×10^{-26}	13	639.5385
CH ₂	2.3254×10^{-26}	14	593.8571
CH ₂ ⁺	2.3254×10^{-26}	14	593.8571
H ₂	3.322×10^{-27}	2	4157
C ₃	5.9796×10^{-26}	36	230.9444
C ₃ H	6.1457×10^{-26}	37	224.7027
C ₃ H ₃	6.4779×10^{-26}	39	213.1795
C ₄ H	8.1389×10^{-26}	49	169.6735
C ₄	7.9728×10^{-26}	48	173.2083
C ₄ H ₂	8.305×10^{-26}	50	166.28

The chemical reactions implemented in the sub-code are some of those considered by Benedikt (see table 2.1).

Figure 7.6 and table 7.3 show the molar fractions of some chemical species constituting the mixture at the 90% of the nozzle axis after the simulations by CHIBEVS.BAS, as function of the electrical power considering nozzle A and acetylene mass flow rate equal to 5 sccs. It is evident that the highest values are linked to Ar^+ species while the lowest values are those of α_{C} . The molar fractions change of two order of magnitude, however the molar fractions of all species, except for Ar^+ , are close to zero.

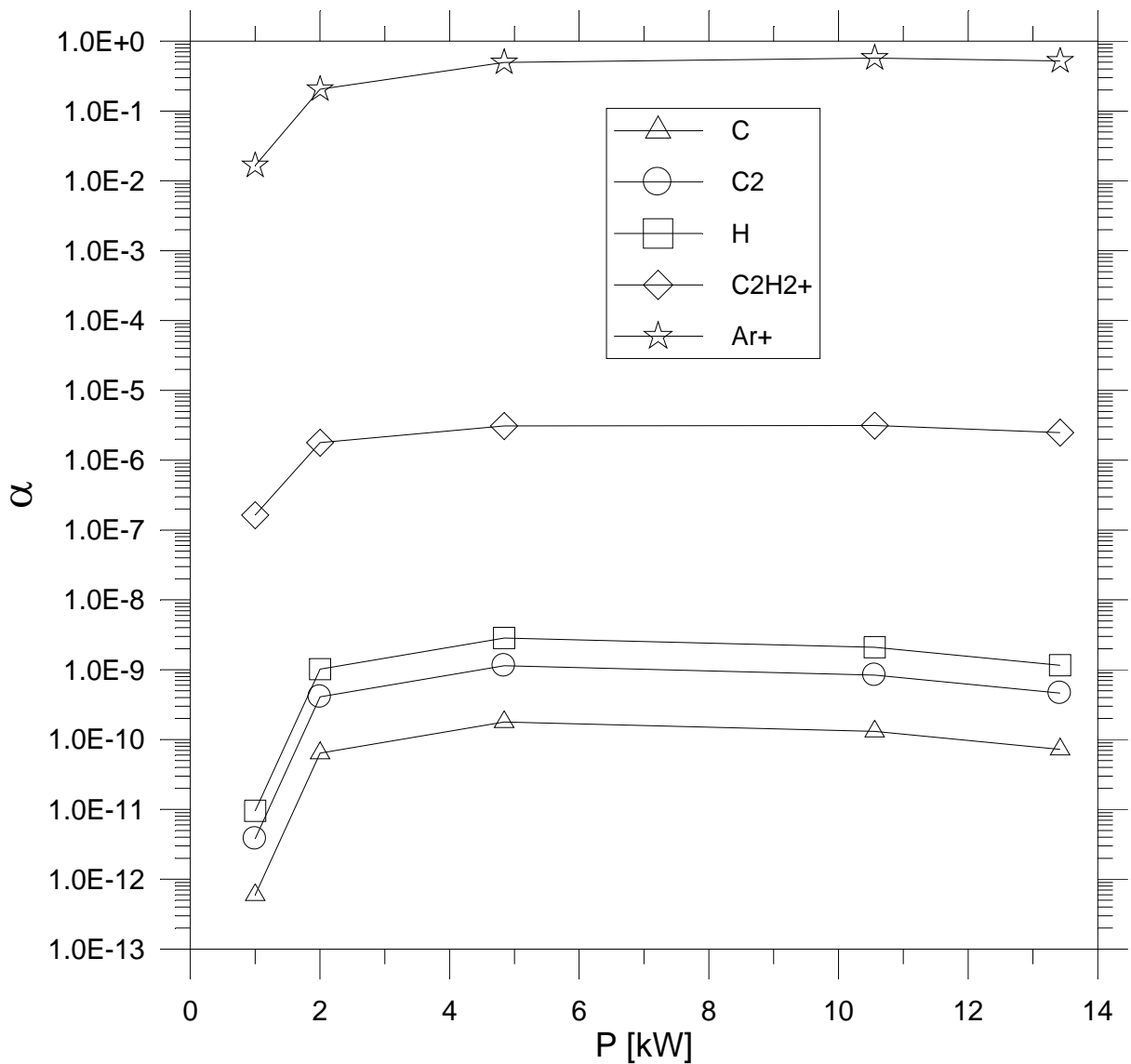


Fig. 7.6 – Molar Fractions of some species at 90% of nozzle axis as function of electrical power

Table 7.3 – Molar Fraction of some species at 90% of nozzle axis as function of electrical power

Test	α_C	α_{C_2}	α_H	$\alpha_{C_2H_2^+}$	α_{Ar^+}
A-13-5	7.23×10^{-11}	4.63×10^{-10}	1.16×10^{-9}	2.47×10^{-6}	0,521
A-11-5	1.31×10^{-10}	8.38×10^{-10}	2.09×10^{-9}	3.14×10^{-6}	0,575
A-5-5	1.78×10^{-10}	1.14×10^{-9}	2.85×10^{-9}	3.08×10^{-6}	0,497
A-2-5	6.36×10^{-11}	4.07×10^{-10}	1.02×10^{-9}	1.78×10^{-6}	0,205
A-1-5	5.95×10^{-13}	3.81×10^{-12}	9.52×10^{-12}	1.63×10^{-7}	0,017

Figure 7.7 and table 7.4 show the molar fractions of some chemical species constituting the mixture at the 90% of the nozzle axis after the simulations by CHIBEVS.BAS, as function of precursor mass flow rate at fixed electrical power of 5 kW and using nozzle A. The Ar^+ molar fraction assumes the maximum value and slightly decreases with increasing $\dot{m}_{C_2H_2}$ while the other molar fractions are close to zero and increase also of about 1 order of magnitude with increasing the precursor mass flow rate. The minimum values are obtained by C species.

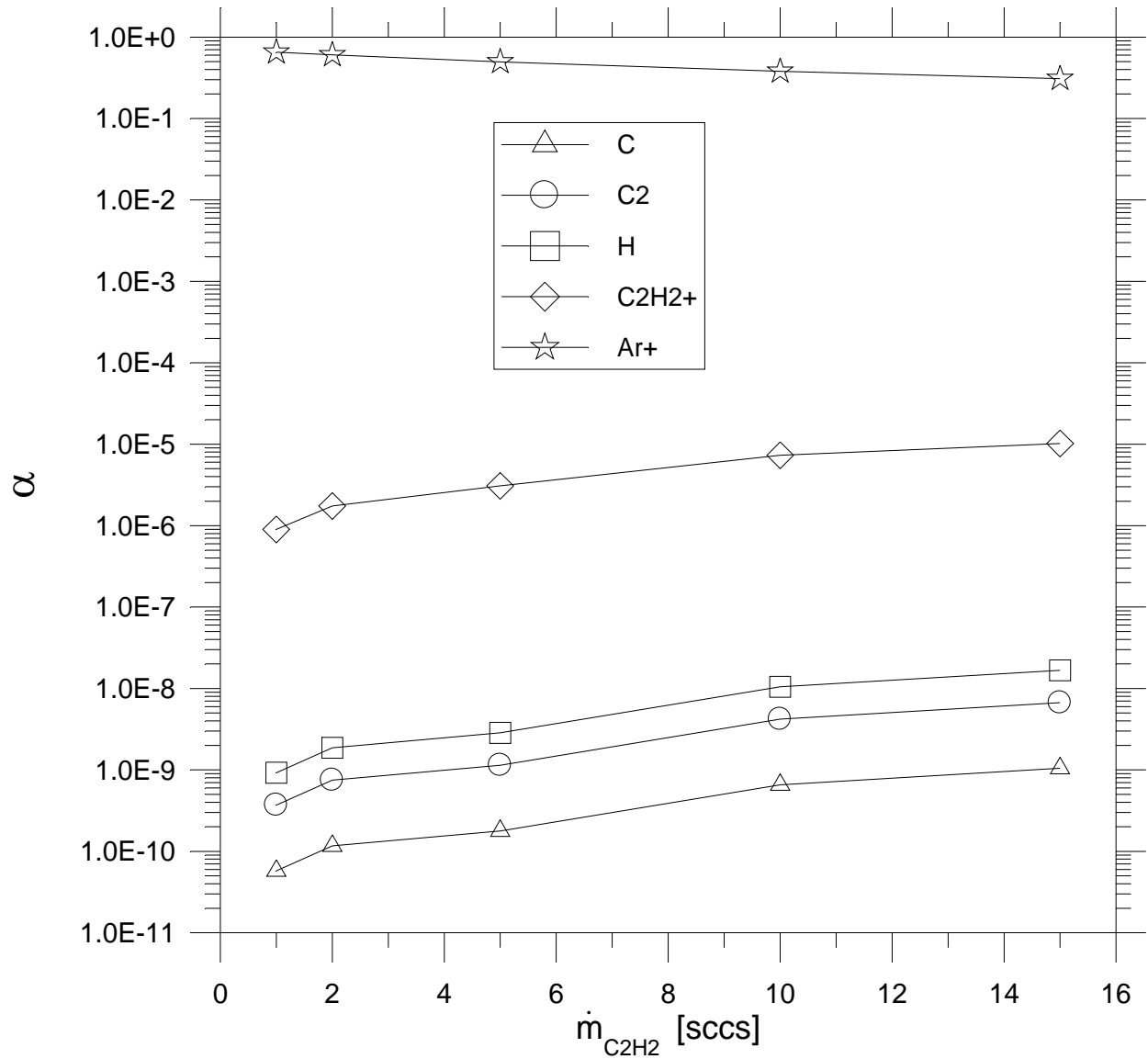


Fig. 7.7 – Molar Fractions of some species at 90% of nozzle axis as function of $\dot{m}_{C_2H_2}$

Table 7.4 – Molar Fraction of some species at 90% of nozzle axis as function of $\dot{m}_{C_2H_2}$

Test	α_C	α_{C_2}	α_H	$\alpha_{C_2H_2^+}$	α_{Ar^+}
A-5-15	1.04×10^{-9}	6.68×10^{-9}	1.67×10^{-8}	1.02×10^{-5}	0.310
A-5-10	6.54×10^{-10}	4.19×10^{-9}	1.05×10^{-8}	7.32×10^{-6}	0.382
A-5-5	1.78×10^{-10}	1.14×10^{-9}	2.85×10^{-9}	3.08×10^{-6}	0.497
A-5-2	1.17×10^{-10}	7.47×10^{-10}	1.87×10^{-9}	1.74×10^{-6}	0.606
A-5-1	5.75×10^{-11}	3.68×10^{-10}	9.20×10^{-10}	8.98×10^{-7}	0.654

Figure 7.8 and table 7.5 show the molar fractions of some chemical species at the 90% of nozzle axis after the simulations by CHIBEVS.BAS, as function of nozzle type at constant electrical power of 5 kW and constant precursor mass flow rate of 5 sccs. The highest values are linked to Ar^+ while

the lowest values are related to C. Each molar fraction decreases passing from nozzle A to nozzle C and they are close to zero (except for Ar^+).

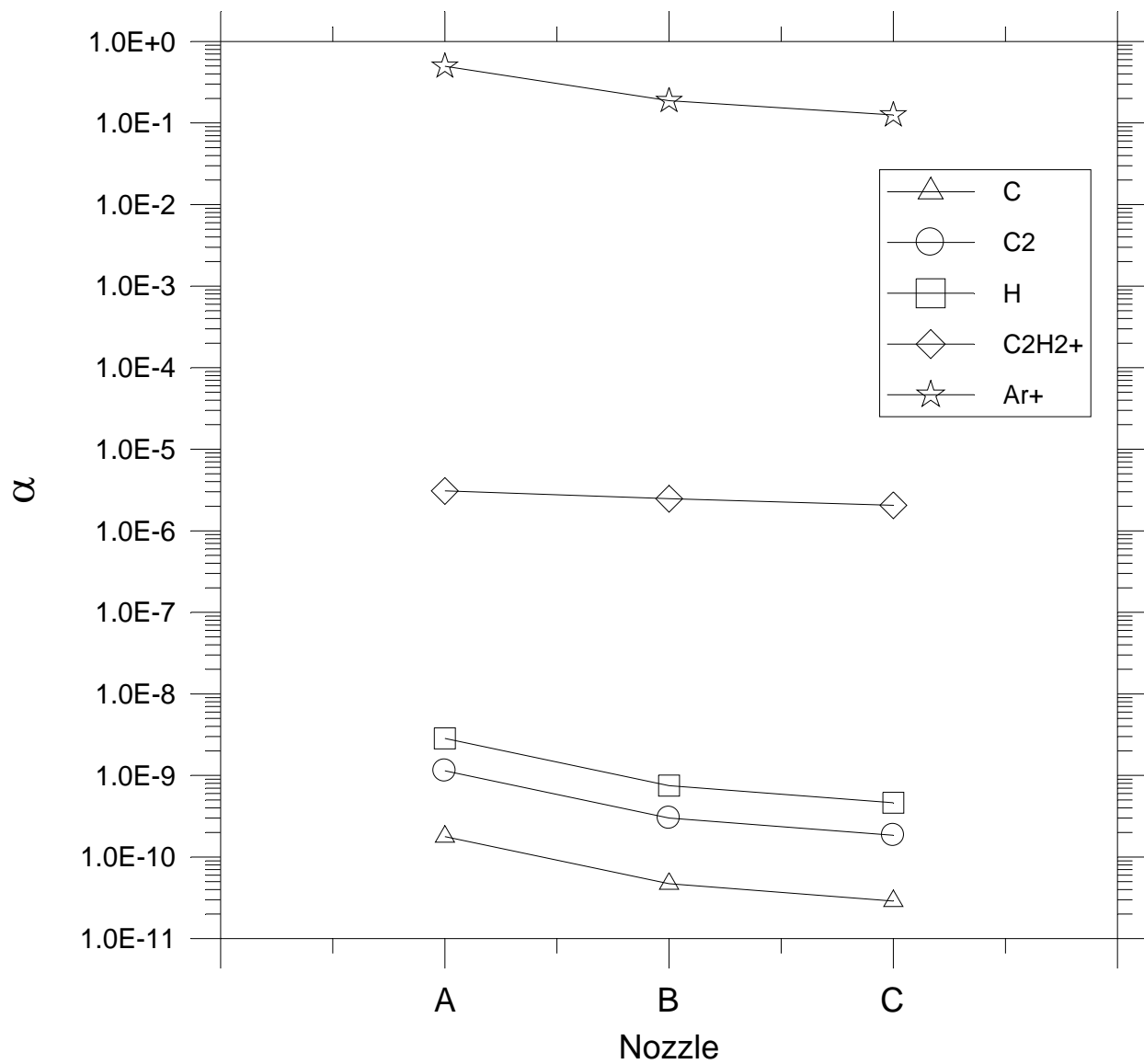


Fig. 7.8 – Molar Fractions of some species at 90% of nozzle axis as function of nozzle type

Table 7.5 – Molar Fraction of some species at 90% of nozzle axis as function of nozzle type

Test	α_C	α_{C_2}	α_H	$\alpha_{\text{C}_2\text{H}_2^+}$	α_{Ar^+}
A-5-5	1.78×10^{-10}	1.14×10^{-9}	2.85×10^{-9}	3.08×10^{-6}	0.497
B-5-5	4.69×10^{-11}	3.00×10^{-10}	7.50×10^{-10}	2.47×10^{-6}	0.188
C-5-5	2.88×10^{-11}	1.84×10^{-10}	4.61×10^{-10}	2.05×10^{-6}	0.126

7.4 Chamber

The chamber is fundamental in the deposition apparatus because from its inlet section the flow field continues to expand supersonically until a shock wave. After the shock the plasma mixture proceeds sub-sonically towards the substrate where some chemical species deposit onto it and form the thin film. The pressure in the vessel is maintained low (around 30 Pa) by the use of pumps. On the other hand the value of temperature is still unknown and it is very difficult to measure experimentally. In the deposition chamber a supersonic zone and a subsonic zone are well evident. The supersonic part assumes the form of a “leaf-blade”. Furthermore there are stagnation regions near the chamber inlet and at the chamber end after the exit slot. In the flow field during its evolution many chemical reactions occur changing continuously the chemical composition of the mixture. Surface reactions can take place on the substrate. The shock wave assumes a fundamental role because characterizes the fluidics of the entire vessel and a deepen study for this reason is necessary. In the present simulation the van de Sanden deposition chamber used at the University of Eindhoven is taken into account. The DSMC simulations start before of the chamber inlet and exactly they begin at 90% of nozzle axis length in order to improve the analysis. Output by sub-code CHIBEVS.BAS is a part of the input to DS2V. Figure 7.9 shows the scheme of apparatus studied, it is supposed that the distance between the inlet section and the substrate is constant and equal to 0.45 m. The dimension of the chamber inlet section, equal to the nozzle exit section, changes depending on the type of nozzle used, however the abscissa of the chamber inlet section is zero in all tests.

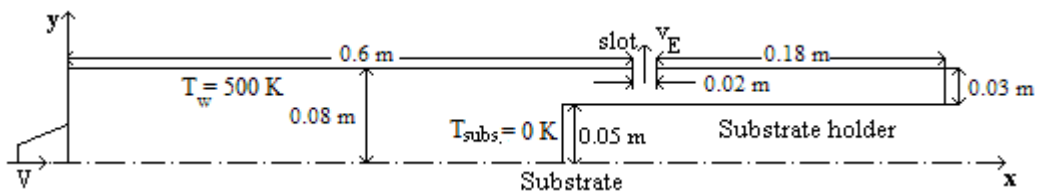


Fig. 7.9 – Scheme of the van de Sanden deposition apparatus

In the present tests the flow field is a mixture formed by the same 21 chemical species (15 radicals and 6 ions) simulated by CHIBEVS.BAS and in addition electrons are contemplated. Being DS2V a molecular code, it requires in input not only the physical mass, but also the diameter (D_{ref}) evaluated at reference temperature of 300 K and the temperature exponent (ω). All these data are

reported in table 7.6. The Variable Hard Sphere model is taken into account for each chemical species. The rotational degree of freedom is 2 for linear species (for example C₂), is equal to 3 for cyclic species (such as C₄H₂).

Table 7.6 – Chemical Species and related properties

Chemical Specie	D _{ref} [m]	ω [-]
Ar	3.804103×10 ⁻¹⁰	0.6593
Ar ⁺	3.804103×10 ⁻¹⁰	0.6593
C ₂ H ₂	5.126779×10 ⁻¹⁰	0.6759
C ₂ H ₂ ⁺	5.126779×10 ⁻¹⁰	0.6759
C ₂ H	5.12514×10 ⁻¹⁰	0.6759
H	2.36076×10 ⁻¹⁰	0.6612
C ₂	3.923725×10 ⁻¹⁰	0.6514
CH	2.909121×10 ⁻¹⁰	0.6476
C ₂ H ⁺	5.12514×10 ⁻¹⁰	0.6759
C	3.441456×10 ⁻¹⁰	0.6455
C ₂ ⁺	3.923725×10 ⁻¹⁰	0.6514
CH ⁺	2.909121×10 ⁻¹⁰	0.6476
CH ₂	4.377149×10 ⁻¹⁰	0.661
CH ₂ ⁺	4.377149×10 ⁻¹⁰	0.661
H ₂	3.171426×10 ⁻¹⁰	0.8616
C ₃	5.125682×10 ⁻¹⁰	0.6759
C ₃ H	5.12541×10 ⁻¹⁰	0.6759
C ₃ H ₃	6.975485×10 ⁻¹⁰	0.6854
C ₄ H	7.476705×10 ⁻¹⁰	0.7089
C ₄	7.47693×10 ⁻¹⁰	0.7089
C ₄ H ₂	7.476419×10 ⁻¹⁰	0.7089

The chemical reactions implemented are the same considered in CHIBEVS.BAS (see table 2.1).

DS2V code requires in input the rate constant in the Arrhenius form:

$$K(T) = AT^b \exp\left(-\frac{E_a}{kT}\right) \quad (7.4.1)$$

where A is the pre-exponential constant, b is the temperature constant, E_a is the activation energy and k is the Boltzmann constant. The conditions $A = 1$, $b = 0$ and $E_a = 0$ are strictly necessary to implement rate constants as temperature independent (in the present simulation the reactions are temperature independent).

In the vessel at starting condition the gas mixture is stationary ($V = 0$). Temperature and density both in the chamber and at the exit slot are identical to those at the 90% of nozzle axis in order to obtain a value of pressure in chamber very close to one obtained by experiments. The velocity at the chamber exit slot (V_E) has been calculated by the conservation of mass flow rate considering the exit, which in reality is a hole, as an annulus with area equal to 0.01 m^2 :

$$\dot{m} = \rho V_E A \Rightarrow V_E = \frac{\dot{m}}{\rho A} \quad (7.4.2)$$

Table 7.7 reports the input parameters necessary to DS2V where for space there are only the molar fractions of Ar^+ and of C_2H_2 and not those of all 21 chemical species. The letter V in the table denotes the velocity at the 90% of nozzle axis, T and N are the temperature and the number density at the 90% of nozzle axis (equal to the values in the chamber and at the exit slot). The molar fractions in the chamber and at the exit slot at the starting condition are equal to ones obtained at the 90% of nozzle axis by means of CHIBEVS.BAS.

Table 7.7 – Input parameters to DS2V code

Test	V [m/s]	T [K]	N [1/m ³]	V _E [m/s]	α_{Ar+} [-]	$\alpha_{C_2H_2}$ [-]
A-13-5	4737	12543	2.24×10^{21}	149	0.521	0.479
A-11-5	4118	9386	2.52×10^{21}	130	0.575	0.425
A-5-5	2772	4327	3.56×10^{21}	87	0.497	0.301
A-2-5	2587	3794	3.79×10^{21}	81	0.205	0.283
A-1-5	2287	3006	4.23×10^{21}	72	0.017	0.253
A-5-15	2050	2359	5.70×10^{21}	65	0.310	0.564
A-5-10	2346	3025	4.63×10^{21}	74	0.382	0.463
A-5-2	3131	5946	2.92×10^{21}	99	0.606	0.147
A-5-1	3276	6820	2.70×10^{21}	103	0.654	0.079
B-5-5	1714	1212	1.46×10^{21}	257	0.188	0.735
C-5-5	1380	902	1.30×10^{21}	300	0.126	0.823

The surface temperature is fixed at 500 K while the substrate temperature is equal to 10^{-3} K (practically zero) and a diffusive reflection totally accommodate is taken into account only for the four species constituting the film (C, C₂, CH and C₂H), while a specular reflection is considered for all remaining chemical species (see section 6.3). It results that the sticking probability of C, C₂, CH and C₂H are equal to one, while the sticking probability of each remaining species is zero. The sticking probability of a single species is defined as the ratio of the number of molecules of the single species which deposit to the total number of the single species which arrive to the substrate. Therefore, as said in section 6.3, in a first, preliminary and very simple analysis of film properties the molecule number fluxes of C, C₂, CH and C₂H on the substrate can be considered as a rough estimation of the film distribution. The analysis of film properties is carried out in terms of:

- 1) thickness, estimated by the arithmetic average (\bar{N}_f) of N_f . The higher is \bar{N}_f the higher is the film thickness [23],
- 2) uniformity, expressed by the standard deviation (σ) of N_f . The lower is σ the higher is the film uniformity.

In the DSMC simulations the number of megabytes used at the start of the calculations is 150 Mb. The run is stopped when the simulation time (t_s) is higher than the reference time (t_{ref}) equal to the period necessary to cross the computing domain, in this case the length of the chamber (0.8 m)

starting from the inlet chamber with velocity equal to the one obtained by the flow field at the 90% of nozzle axis. The ratio of the zone occupied by the flow to the entire computational domain is about 0.63 in all runs while the estimated ratio of final average flow field density to stream (or reference gas density) is put to 0.81 in each test. It is supposed that steady state condition is obtained at large times. The simulations include the ionization effects, the electron moves with the related ion, the whole flow field is considered electrically neutral. The radial weighting factor is taken into account and the cell adaptation is used. Table 7.8 reports the reference time (t_{ref}) and some important parameters achieved at the end of the molecular simulation such as the simulated time, the average and maximum values of mcs/mfp (the maximum and average values are those obtained in the whole flow field), the stream mean free path (i.e. the mean free path at the 90% of nozzle axis). It is evident that the results by the DSMC code can be easily considered as reliable. In fact the parameter mcs/mfp assumes proper values, its value averaged in the whole flow field is always less than 0.2 in each run except for test A1-5 ($(mcs/mfp)_{Average} = 0.252$). The maximum value obtained in the entire flow field exceeds 0.2 at tests A1-5, A5-15, A5-10, A5-2 and A5-1. The ratio of simulated time to reference time ranges from about 3.8 (test A11-5) to about 15 (A1-5) i.e. a ratio sufficient to consider the flow field as steady state. Thus the number of simulated molecules and the simulation time are proper at each test.

Table 7.8 – Reference time and some useful parameters

Test	$t_{ref} \times 10^{-4}$ [s]	$t_s \times 10^{-3}$ [s]	t_s/t_{ref} [-]	(mcs/mfp)		$\lambda \times 10^{-4}$ [m]
				Mean	Max	
A-13-5	1.689	0.6953	4.1166	0.054	0.156	9.45
A-11-5	1.943	0.7417	3.8173	0.052	0.132	8.24
A-5-5	2.886	2.125	7.3631	0.034	0.194	5.51
A-2-5	3.092	2.7357	8.8477	0.068	0.136	5.12
A-1-5	3.498	5.3089	15.177	0.252	0.475	4.49
A-5-15	3.902	2.7449	7.0346	0.143	0.291	2.68
A-5-10	3.41	3.2179	9.4367	0.127	0.524	3.63
A-5-2	2.555	2.8598	11.193	0.081	0.501	7.78
A-5-1	2.442	2.7631	11.315	0.075	0.245	8.98
B-5-5	4.667	3.1	6.6424	0.068	0.123	8.55
C-5-5	5.797	2.596	4.4782	0.034	0.053	8.70

In the following, the results obtained by the use of DS2V are carried out. The results related to test A5-5 can be considered as reference data because as reported also by Abbate [21] the geometrical characteristics of nozzle A, the electrical power of 5 kW and the precursor mass flow rate of 5 sccs are comparable with the nozzle geometry and with the experimental test conditions used at the University of Eindhoven. For this reason a thick line plots the results linked to test A5-5. Post-run rarefaction analysis verifies that the flow field is rarefied enough to consider proper the use of DS2V. As typical example figures 7.10a, 7.10b and 7.10c report the profile of P parameter of Bird, the local Knudsen number based on the local temperature gradient (Kn_T) and on the local velocity gradient (Kn_V) along the chamber axis for test A5-5. In many points both the Navier-Stokes equations applicability limit and the continuum validity limit are exceeded.

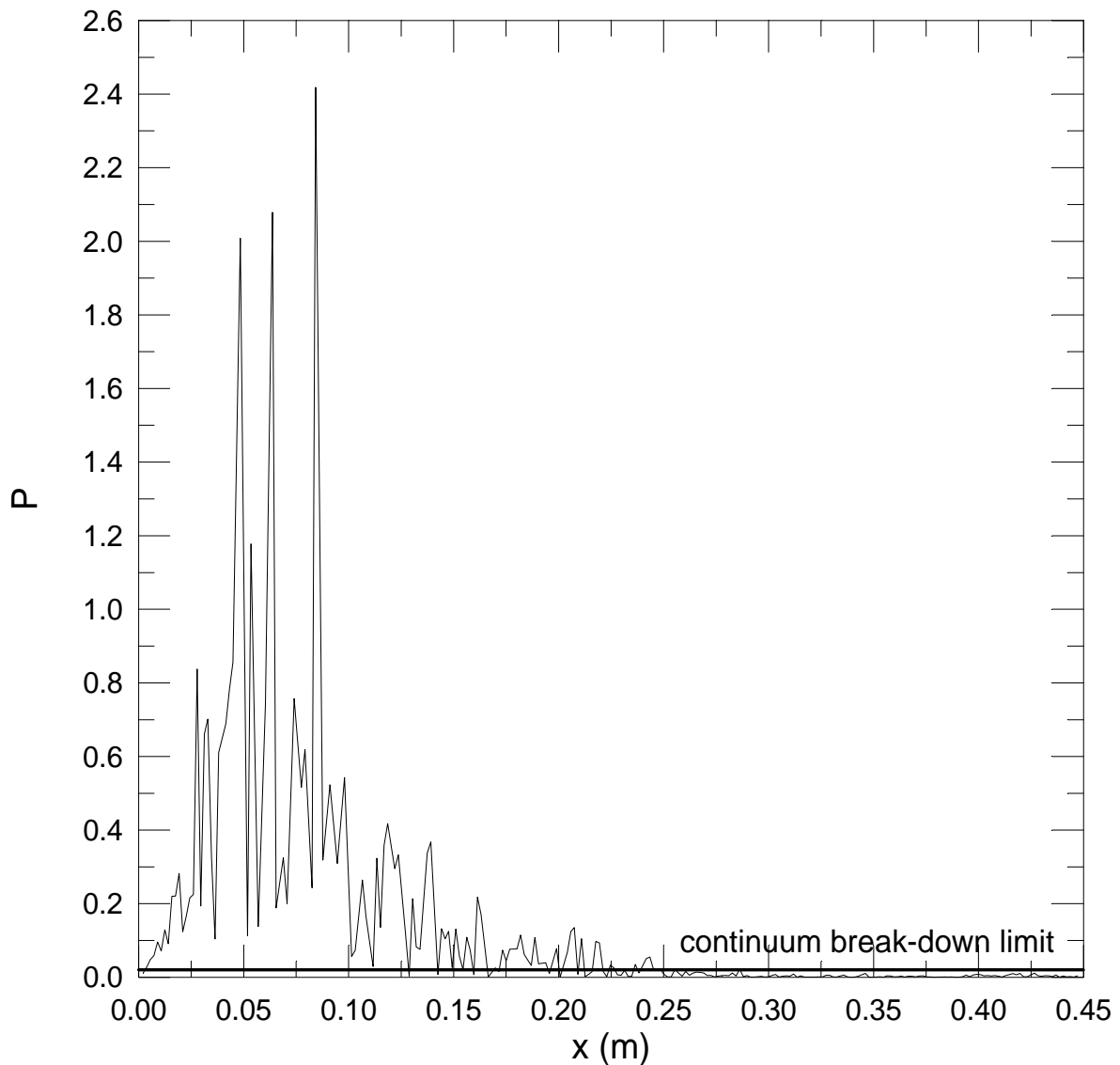


Fig. 10a – Profile of P parameter of Bird along the chamber axis for test A5-5

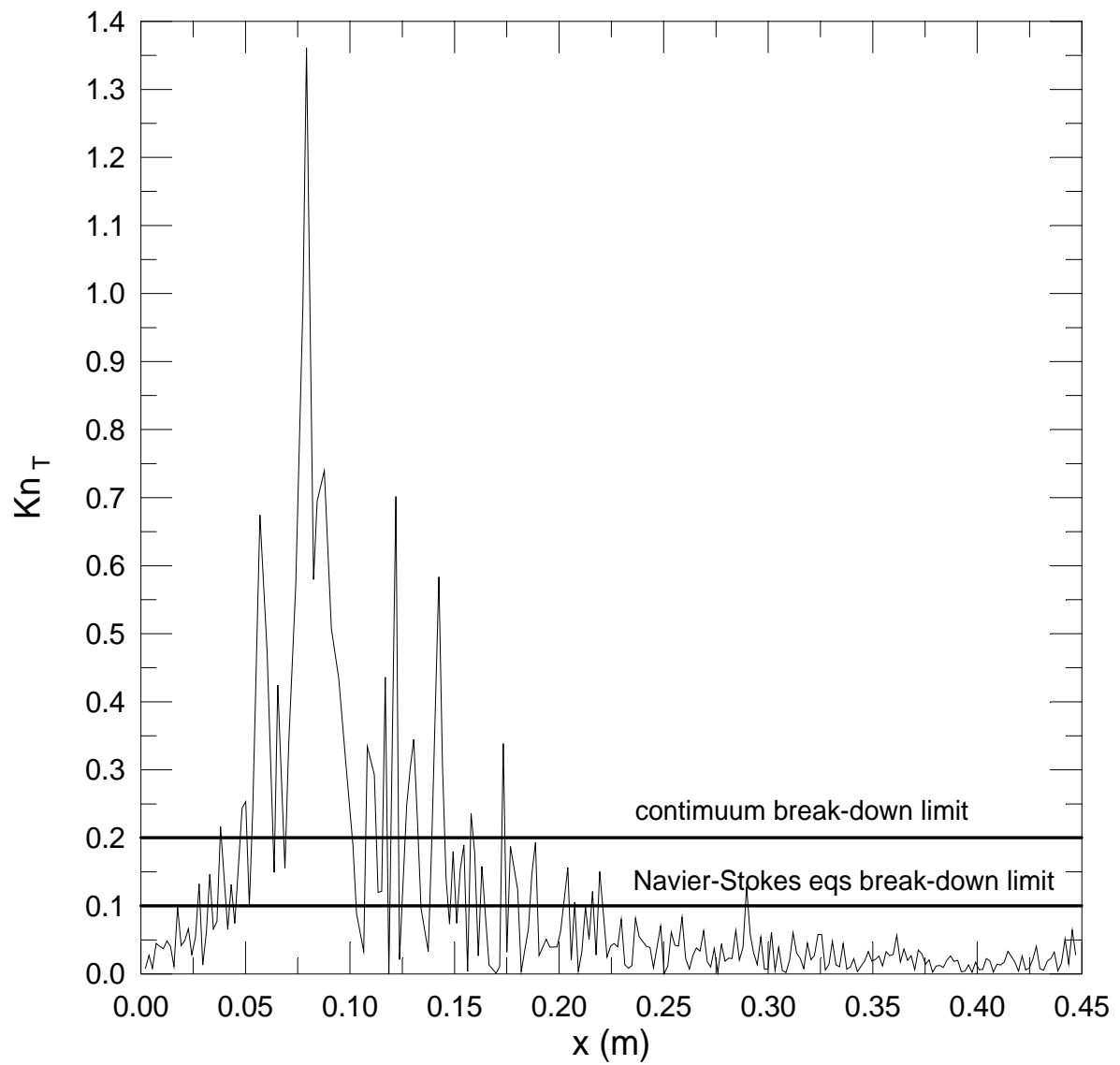


Fig. 7.10b – Profile of Kn_T along the chamber axis for test A5-5

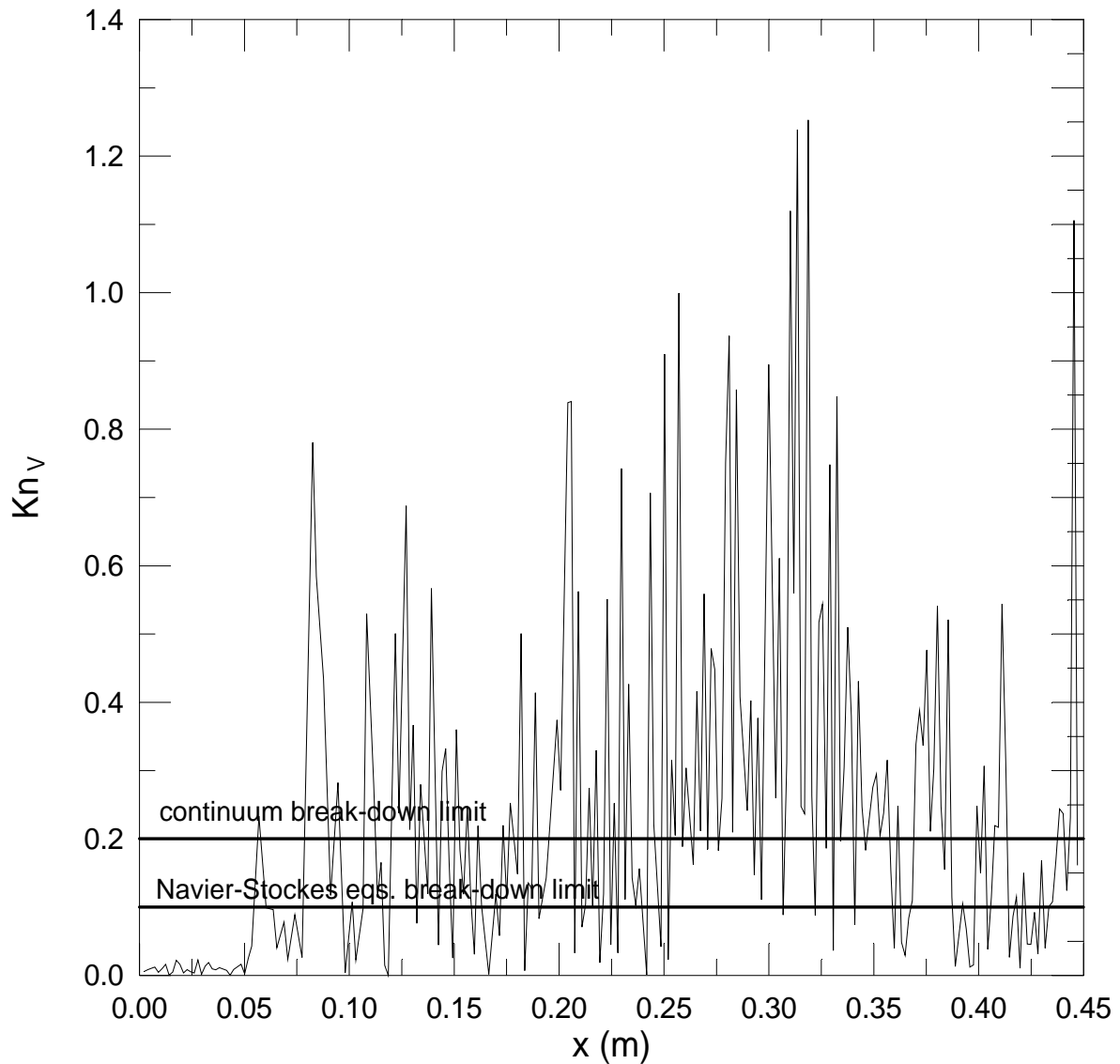


Fig. 7.10c – Profile of Kn_V along the chamber axis for test A5-5

Table 7.9 reports the average value evaluated along the chamber axis of the above mentioned different rarefaction parameters for all runs. The maximum average P value is obtained when the electrical power is greatest (A13-5), its minimum value is achieved using nozzle C (C5-5). The maximum average Kn_V value is shown when the precursor mass flow rate is lowest (A5-1), its minimum value is found using nozzle B (B5-5). The highest average Kn_T is acquired when the electrical power is maximum (A13-5), its minimum value is obtained using nozzle C (C5-5). It is to point out that Kn_V average value is higher than Kn_T mean at runs A13-5, A5-5, A2-5, A1-5, A5-2 and A5-1, is lower for test B5-5 and is comparable at the remaining simulations. Even if in some points the rarefaction parameters are so low to consider the flow field as continuum, the DS2V code can simulate accurately the flow field being, as said before, sophisticated and thus able to simulate in reliable way severe conditions from the rarefaction point of view.

Table 7.9 – Rarefaction parameters averaged along the chamber axis

Test	P	Kn _V	Kn _T
A-13-5	0.2603	0.2533	0.1738
A-11-5	0.1549	0.1197	0.0924
A-5-5	0.1249	0.2378	0.0968
A-2-5	0.1654	0.2583	0.1167
A-1-5	0.0453	0.0708	0.0333
A-5-15	0.1139	0.0610	0.0487
A-5-10	0.1039	0.0548	0.0450
A-5-2	0.1297	0.2186	0.0866
A-5-1	0.2218	0.3254	0.1525
B-5-5	0.0551	0.0224	0.0233
C-5-5	0.0455	0.0242	0.0222

The results obtained both by the pre-processor and by the DSMC code can be considered reliable, also for their good match with experimental data referenced in literature [4] and [22]. In fact for example the values of pressure averaged along the chamber axis (40.8 N/m^2) for test A5-5 are close to one measured by Benedikt. In this run the position of the shock wave (0.05 m) corresponds to the experimental result evaluated by Benedikt and also the velocity after the shock position (2640 m/s at 0.06 m) is close to one experimentally reported.

7.4.1 Shock wave

In order to study the shock wave the Mach number analysis is carried out because as said before the Mach number can provide useful information to the intensity, extension and “form” of the shock wave and thus on the type of expansion occurring in the chamber. As obtained by preliminary simulations, the supersonic zone shows the “leaf-blade” shape in each run. Figure 7.11 shows, as typical example, the 2-D map of the Mach number for the test case A5-5 where the expansion zone near the chamber inlet is visible.

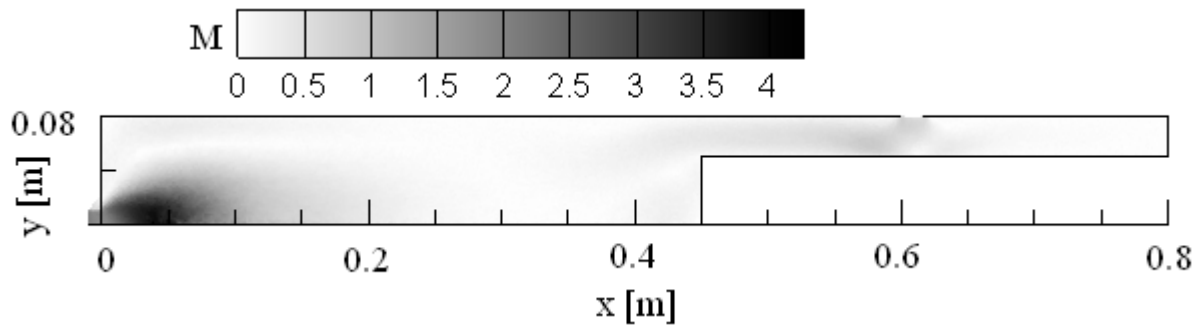


Fig. 7.11 – 2D map of Mach number for test A-5-5

Figure 7.12a shows the profile of Mach number along the chamber axis varying the type of nozzle and fixing the electrical power to 5 kW and the Acetylene mass flow rate to 5 sccs. The mix of Ar and Ar⁺ at elevated temperature (higher than 6400 K) with C₂H₂ at ambient temperature (300 K) produces particular chemical-physical mechanisms and it is evident that the highest M at the chamber inlet is obtained using nozzle A and successively by nozzle B and C although nozzle A is characterized by the lowest ratio of exit area to throat area. It results that the intensity of the shock wave is maximum by nozzle A ($M_{MAX} \cong 3.75$) and then by nozzle B ($M_{MAX} \cong 2.75$) and C ($M_{MAX} \cong 2.26$). The position of the shock wave (x_S) is almost the same, in fact it results that $x_S \cong 0.05$ m using nozzle A, $x_S \cong 0.06$ m using nozzle B and $x_S \cong 0.05$ m using nozzle C. The extension of the shock wave (Δx_S), changes consistently with the type of nozzle. In reality $\Delta x_S \cong 0.07$ m by means of nozzle A, $\Delta x_S \cong 0.24$ m using nozzle B and $\Delta x_S \cong 0.22$ m when the nozzle C is installed.

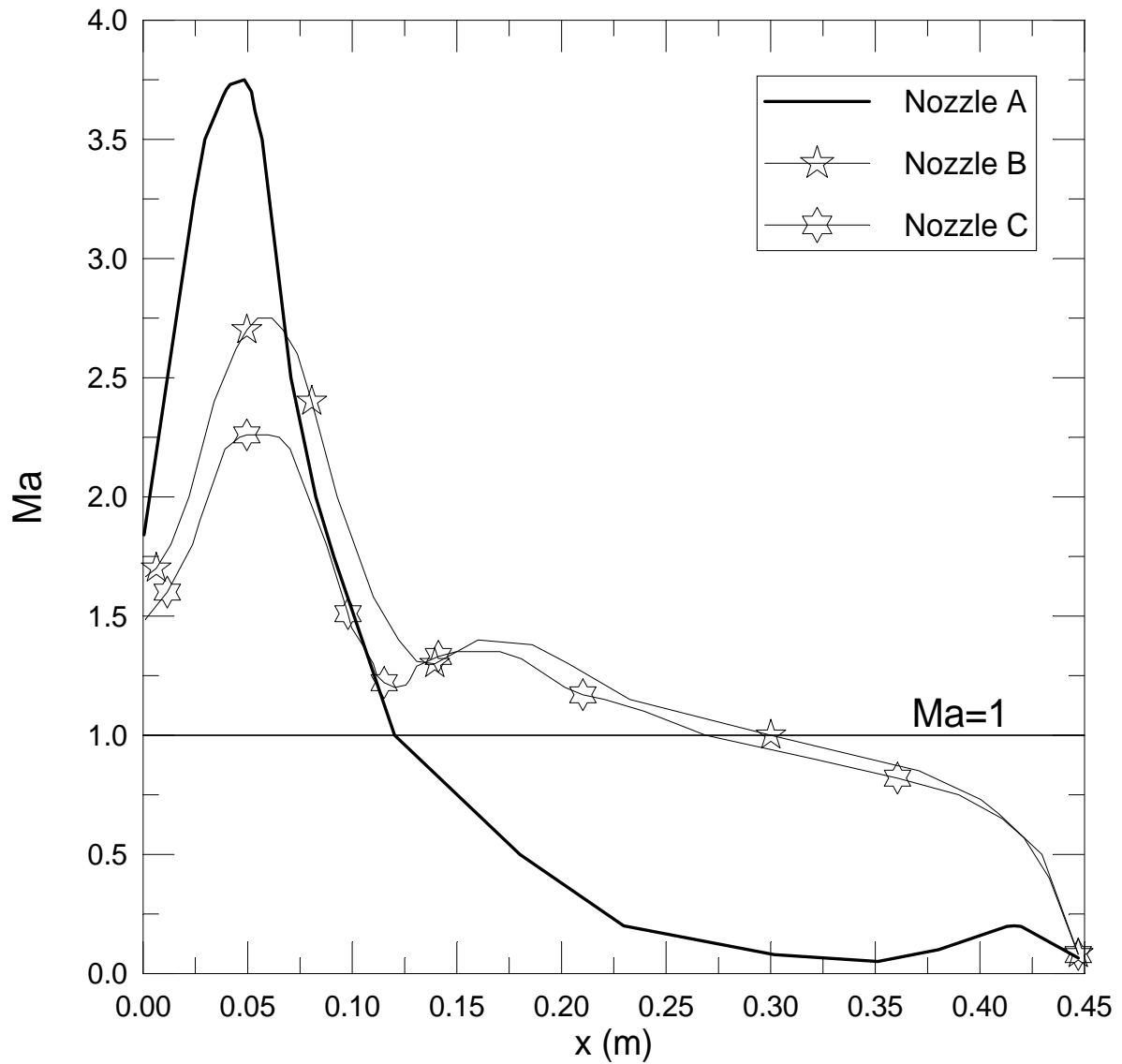


Fig. 7.12a – Profiles of Mach number along the chamber axis using different nozzles

Figure 7.12b reports the profile of Mach number along the chamber axis providing different electrical power to the torch considering nozzle A and Acetylene mass flow rate equal to 5 sccs. It results that the maximum value of Mach number is achieved when $P = 5$ kW while the minimum value at $P = 13$ kW. For what concern the position of the shock, x_s is maximum when $P = 5$ kW and minimum if $P = 13$ or 11 kW. Furthermore the extension of the shock is maximum if $P = 1$ kW while it is minimum if $P = 5$ kW.

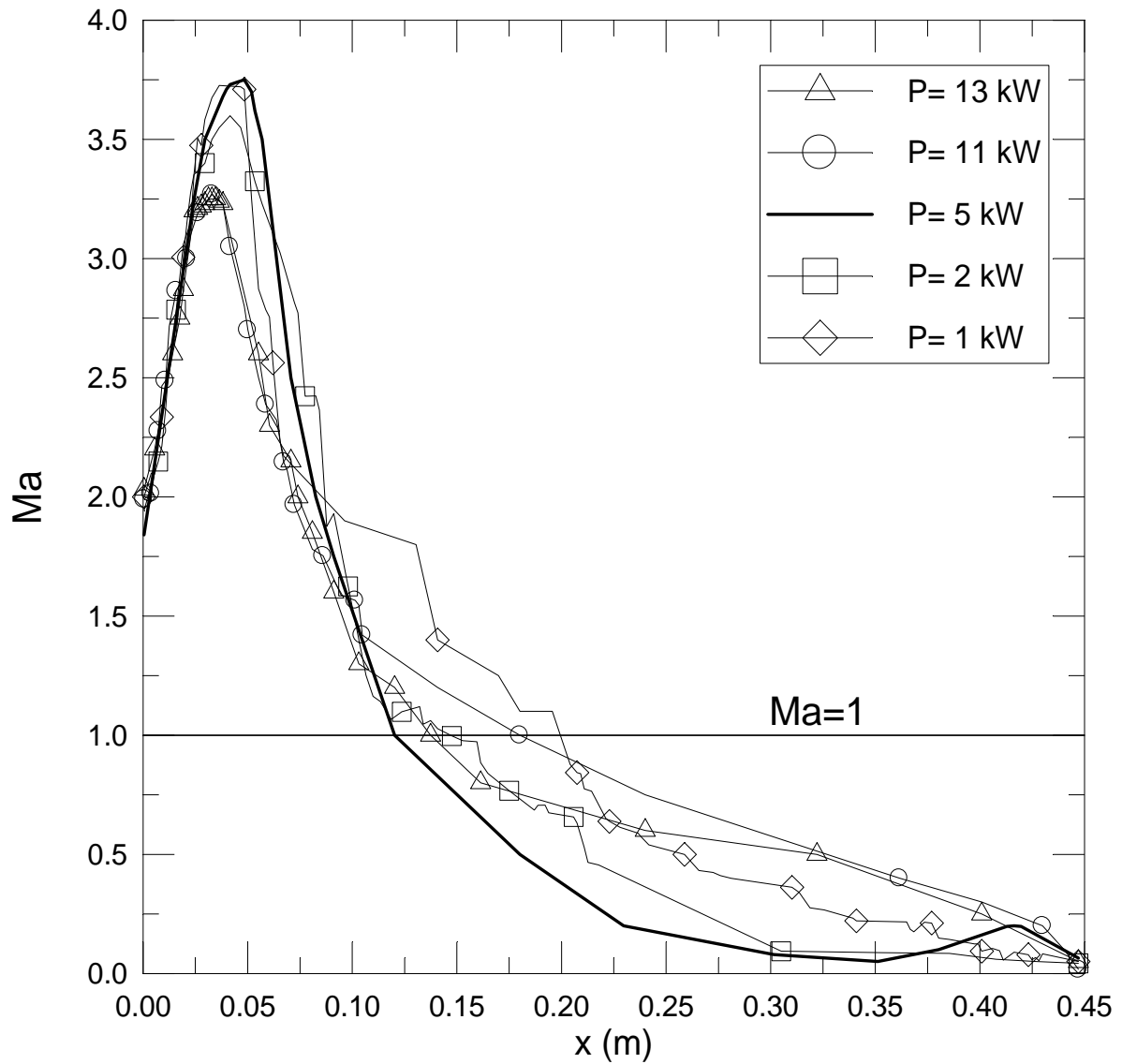


Fig. 7.12b – Profiles of Mach number along the chamber axis at different electrical power

Figure 7.12c shows the profile of Mach number along the chamber axis using different precursor mass flow rate and fixing nozzle A and electrical power to 5 kW. It results that the maximum value of Mach number is achieved when $\dot{m}_{C_2H_2} = 1$ sccs while the minimum value is at $\dot{m}_{C_2H_2} = 15$ sccs. For what concern the position of the shock, x_S is greatest when $\dot{m}_{C_2H_2} = 5$ sccs and lowest if $\dot{m}_{C_2H_2} = 1$ sccs. Furthermore the extension of the shock is highest if $\dot{m}_{C_2H_2} = 15$ sccs while is minimum if $\dot{m}_{C_2H_2} = 5$ sccs.

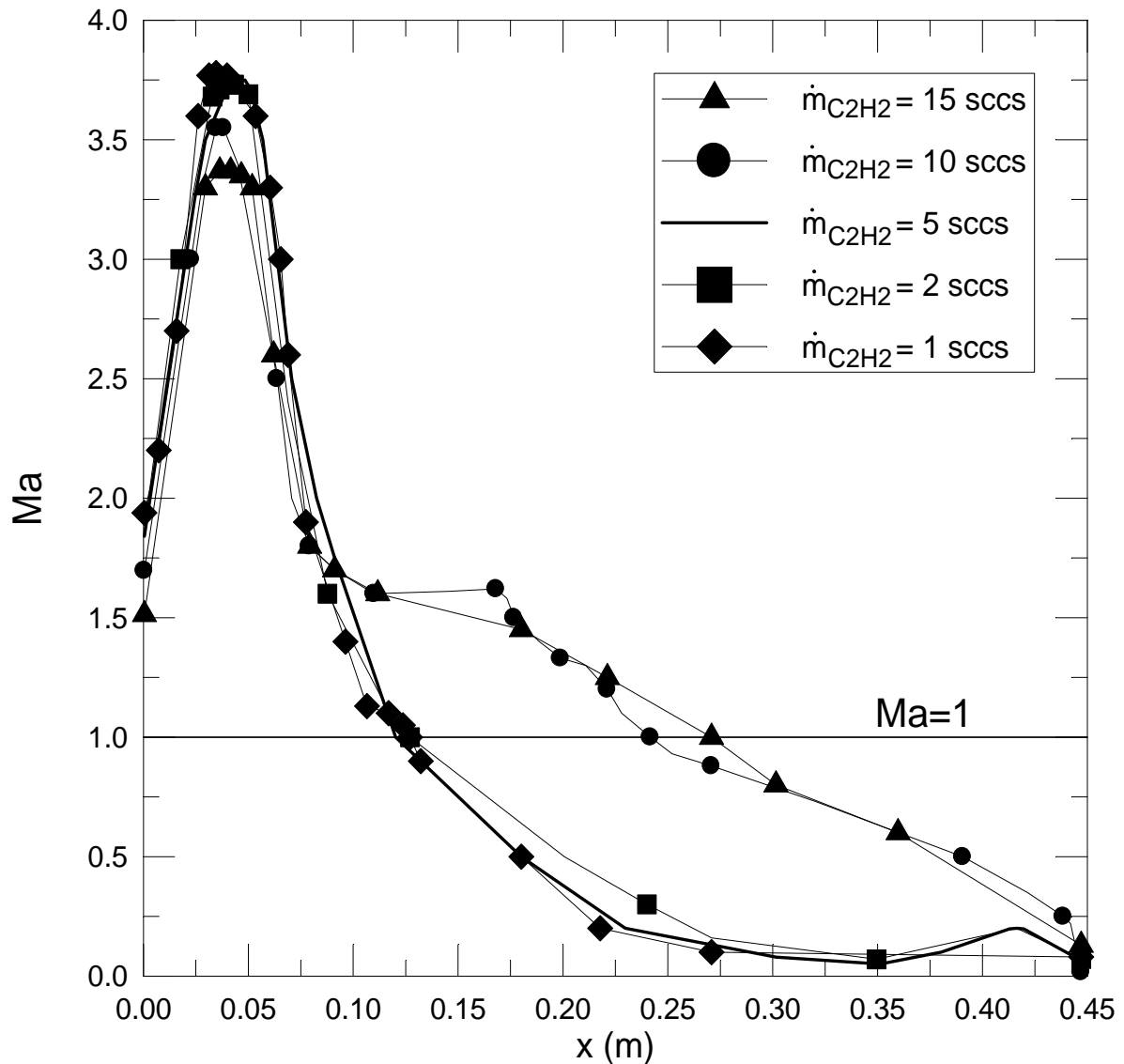


Fig. 7.12c – Profiles of Mach number along the chamber axis at different $\dot{m}_{C_2H_2}$

Table 7.10 reports the shock wave parameters and the values of Mach number at the chamber inlet at the nozzle axis (M_i) for each test. Studying all the data it is possible to say that the type of nozzle influences strongly the expansion, while the electrical power and the precursor mass flow rate do not produce very dissimilar results. In particular the maximum M_{MAX} is achieved using $\dot{m}_{C_2H_2} = 1$ sccs (test A5-1), the minimum M_{MAX} by nozzle C (C5-5). The highest x_S is by means of nozzle B (B5-5) while the lowest x_S is when $P = 13$ kW or 11 kW or $\dot{m}_{C_2H_2} = 1$ sccs (A13-5, A11-5, A5-1). The greatest extension of the shock wave is achieved by nozzle B (B5-5), the smallest one is obtained using nozzle A (A5-5).

Table 7.10 – Shock wave parameters

Test	M_i [-]	M_{MAX} [-]	x_S [m]	Δx_S [m]
A-13-5	2.03	3.25	0.03	0.11
A-11-5	2.02	3.27	0.03	0.15
A-5-5	1.84	3.75	0.05	0.07
A-2-5	1.94	3.60	0.04	0.10
A-1-5	2.12	3.73	0.04	0.16
A-5-15	1.51	3.37	0.04	0.23
A-5-10	1.70	3.56	0.04	0.20
A-5-2	1.87	3.75	0.04	0.09
A-5-1	1.94	3.78	0.03	0.10
B-5-5	1.67	2.75	0.06	0.24
C-5-5	1.49	2.26	0.05	0.22

A run without implement chemical reactions (considering nozzle A, electrical power equal to 5 kW and precursor mass flow rate equal to 5 sccs) shows that with chemistry the shock wave is stronger, farer from the chamber inlet section and with smaller thickness than the shock wave without chemistry. Obviously near the substrate surface the Mach numbers for the two profiles are close to zero because the flow field stops at the substrate surface where some chemical species deposit forming the film.

7.4.2 Fluidics

Figure 7.13a describes the profiles of temperature along the chamber radius at the station located almost at the centre of the chamber ($x = 0.2$ m) using different types of nozzle and considering electrical power equal to 5 kW and C_2H_2 mass flow rate equal to 5 sccs. The highest value of temperature is achieved by nozzle A and then by nozzle B and C. This behaviour agrees with the input data given to DS2V (see table 7.7), i.e. the higher is temperature given as input, the higher is temperature at $x = 0.2$ m. Furthermore it is to point out that the differences increase close to the axis while decrease near the surface. The maximum data are close to the chamber axis, as expected the temperature near the surface is close to the value of surface temperature (500 K).

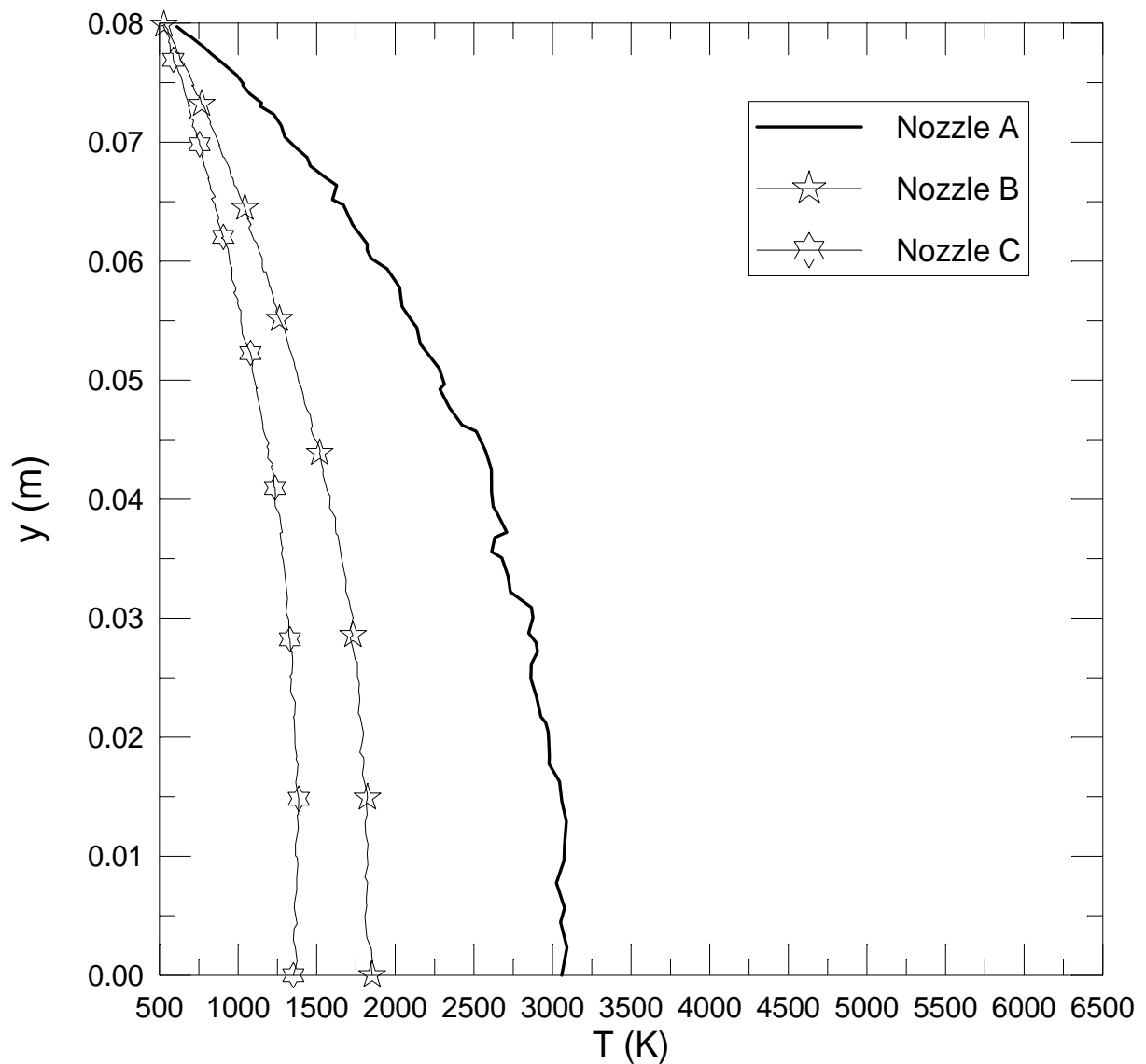


Fig. 7.13a – Profiles of temperature along the radius of the chamber at $x=0.2$ m using different nozzles

Figure 7.13b shows the profiles of temperature along the chamber radius at the station located almost at the centre of the chamber ($x = 0.2$ m) using different electrical power and fixing nozzle A and precursor mass flow rate to 5 sccs. It is easy to verify that the highest values of temperature are achieved at elevated electrical power (13 kW) while the lowest values are by 5 kW. Also in this case the maximum temperatures are close to the chamber axis while near the surface they are close to the surface temperature value.

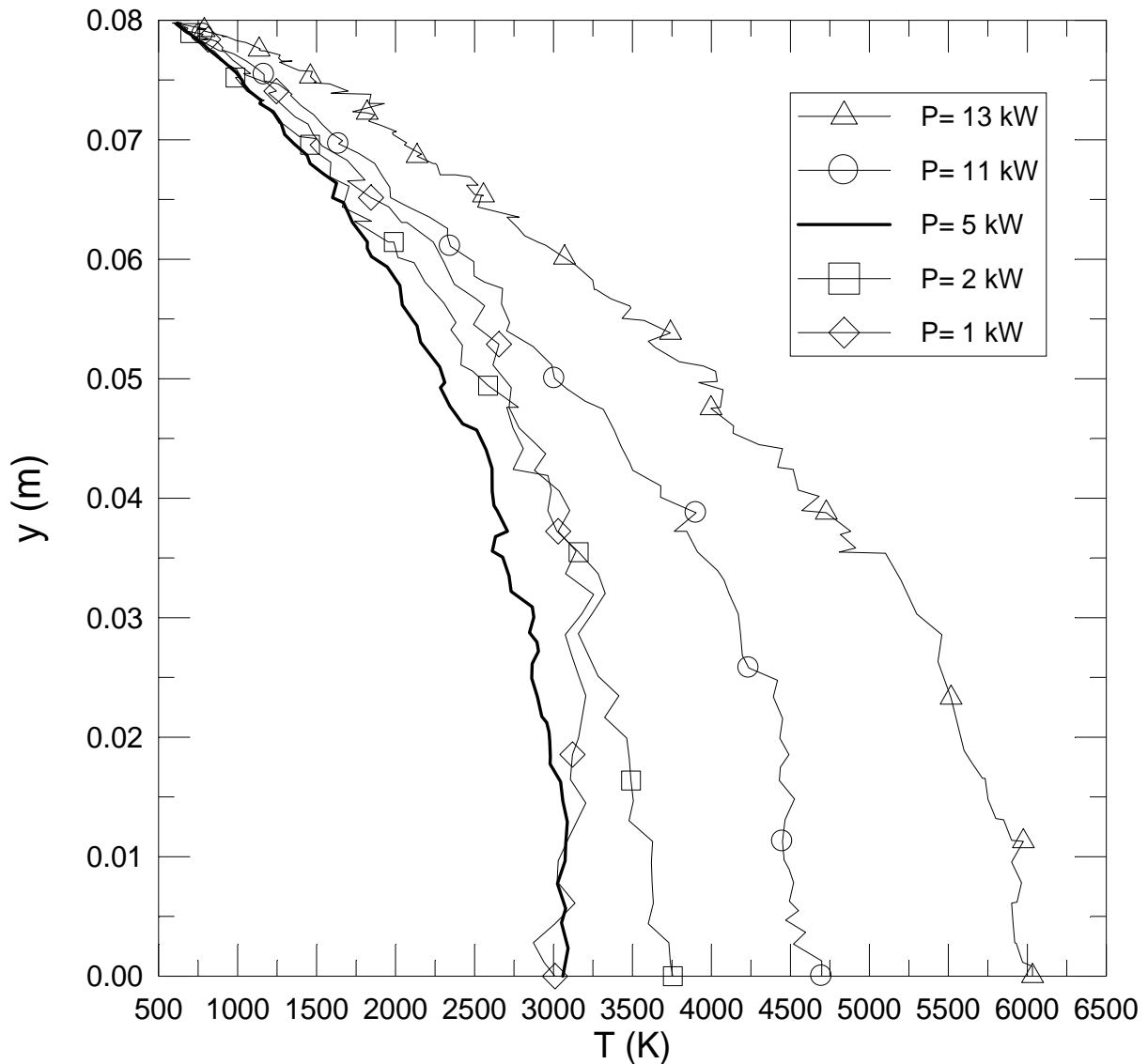


Fig. 7.13b – Profiles of temperature along the radius of the chamber at $x=0.2$ m at different electrical power

Figure 7.13c reports the profiles of temperature along the chamber radius at the station located almost at the centre of the chamber ($x = 0.2$ m) using different precursor mass flow rate and putting nozzle A and electrical power to 5 kW. The values of temperature increase with decreasing the acetylene mass flow rate. It is evident that the profile obtained by run A5-15 is close to one achieved by test A5-10 as well as the profile by run A5-2 is close to that obtained by means of test A5-1. Once again the highest temperatures are around the chamber axis while near the surface they are close to the value of surface temperature.

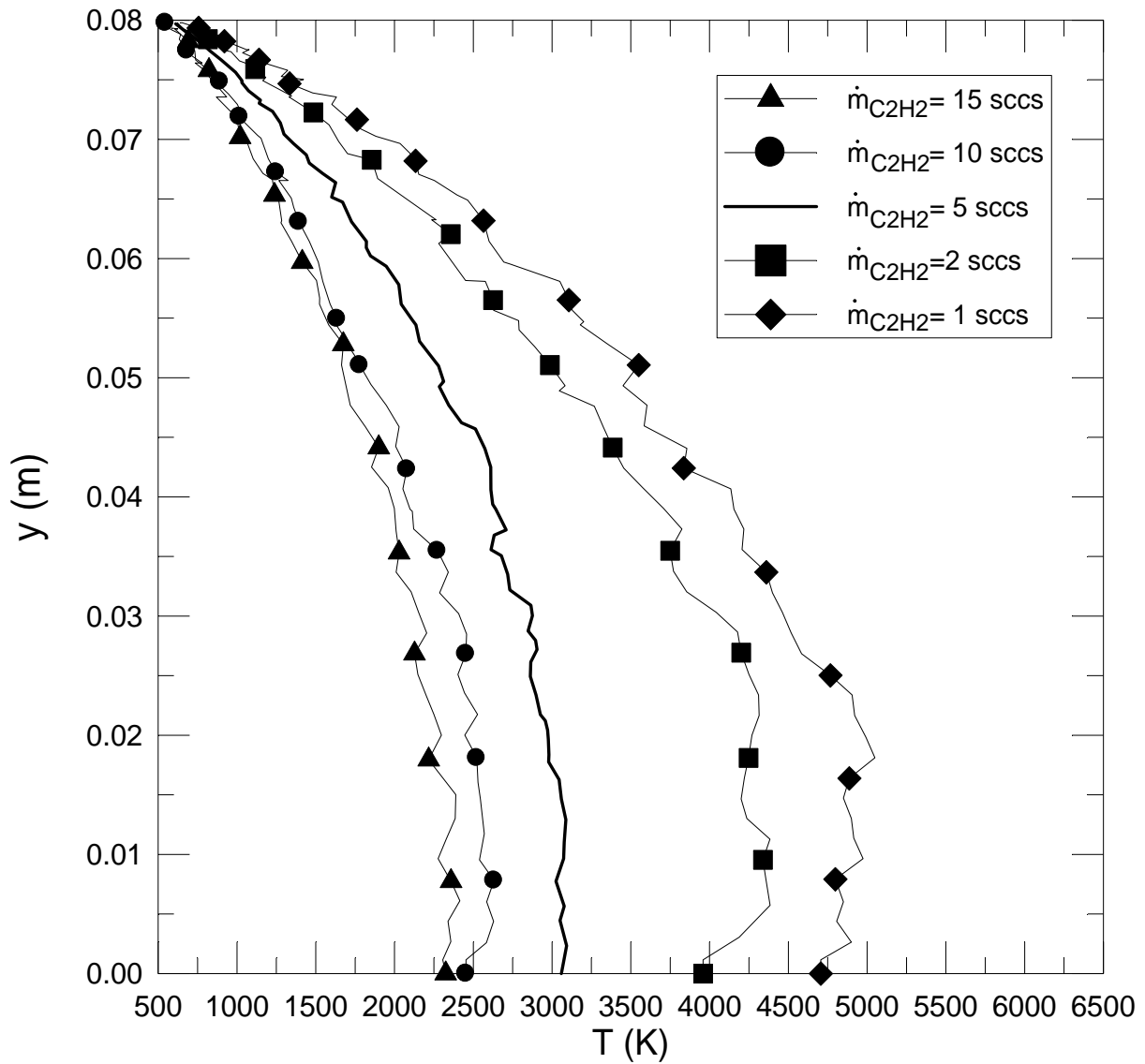


Fig. 7.13c – Profiles of temperature along the radius of the chamber at $x=0.2$ m at different $\dot{m}_{C_2H_2}$

Figure 7.14a shows the profiles of velocity along the chamber radius at the station located almost at the centre of the chamber ($x = 0.2$ m) using different types of nozzle and fixing electrical power to 5 kW and precursor mass flow rate to 5 sccs. The highest values of velocity are achieved by nozzle B while the lowest values are achieved by nozzle A. The profile obtained by nozzle B is almost similar to one achieved by nozzle C. As expected near the surface the velocity is almost zero, the difference from zero is linked to the velocity slip.

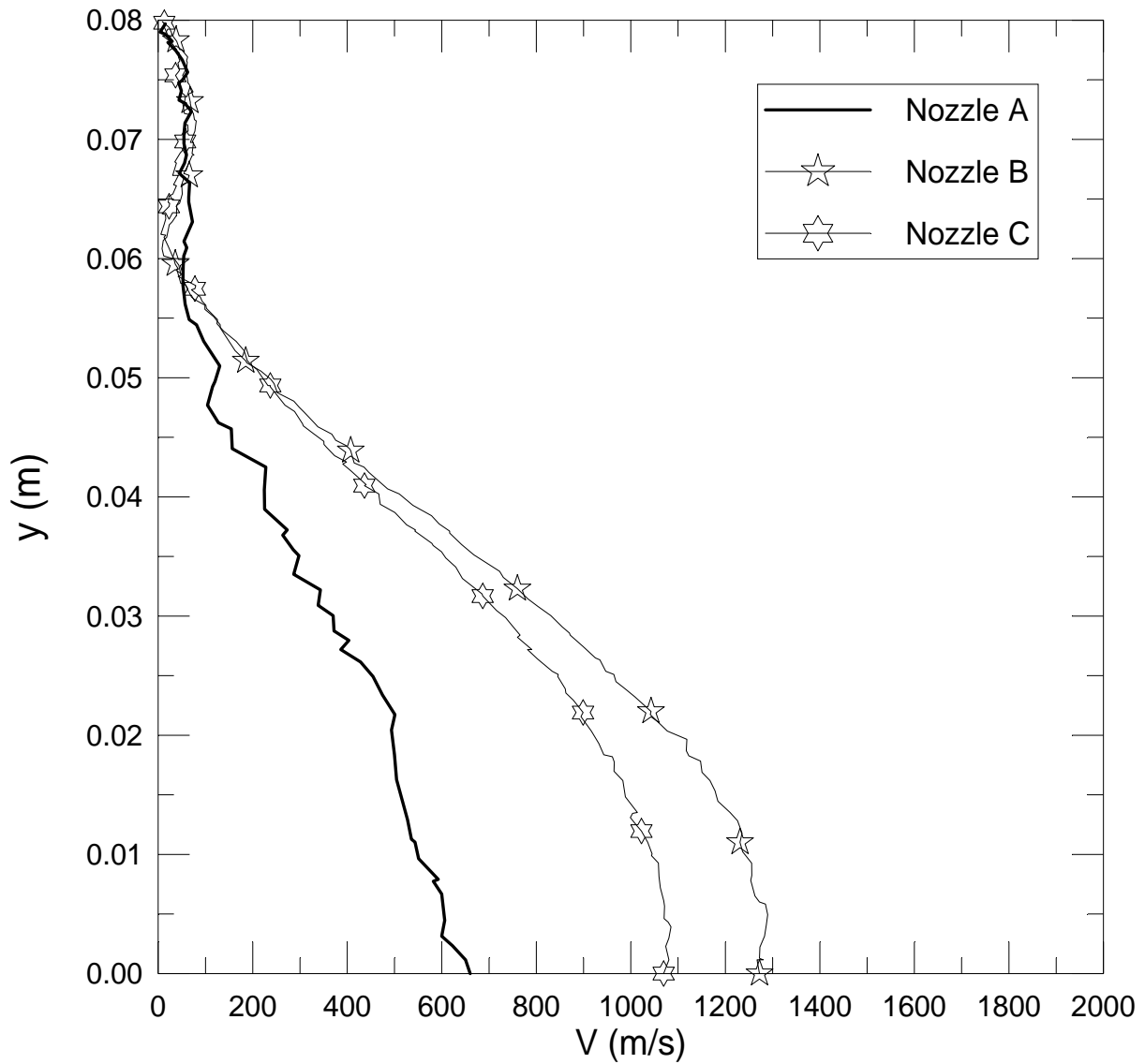


Fig. 7.14a – Profiles of velocity along the radius of the chamber at $x=0.2$ m using different type of nozzle

Figure 7.14b reports the profiles of velocity along the chamber radius at the station located almost at the centre of the chamber ($x = 0.2$ m) using different electrical power with nozzle A and Acetylene mass flow rate equal to 5 sccs. The highest values of velocity are achieved at elevated electrical power (13 and 11 kW) while the lowest values are by 5 kW. Also in these cases the velocity is almost zero near the surface. The velocity profile by 13 kW matches with one obtained by 11 kW as well as the velocity profile achieved using 2 kW is pretty close to one by means of 1 kW.

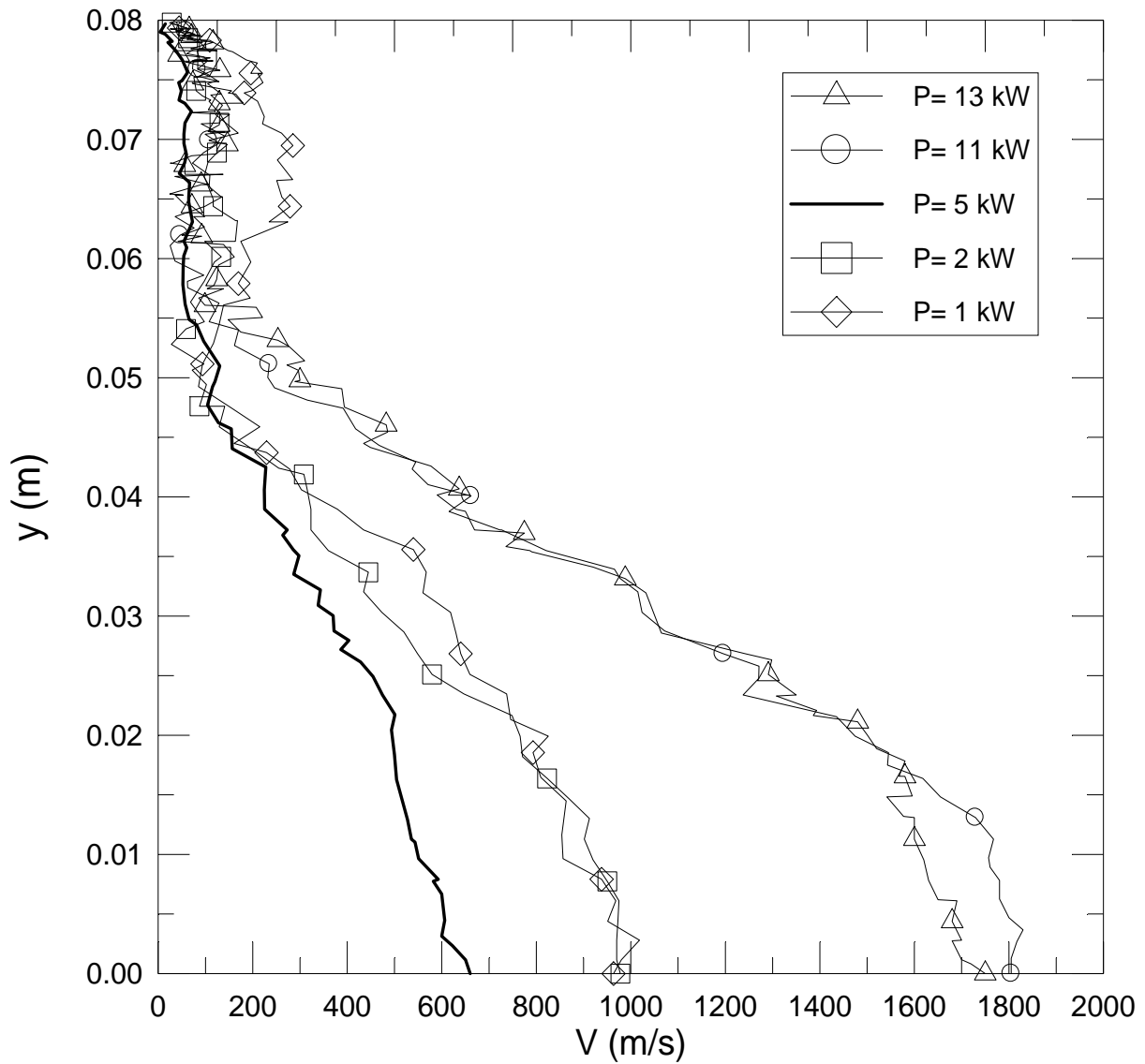


Fig. 7.14b – Profiles of velocity along the radius of the chamber at $x=0.2$ m at different electrical power

Figure 7.14c describes the profiles of velocity along the chamber radius at the station located almost at the centre of the chamber ($x = 0.2$ m) using different precursor mass flow rate and fixing nozzle A and electrical power to 5 kW. Once again near the surface the velocity is close to zero. The profiles using 10 sccs and 15 sccs are very close and assume the highest values.

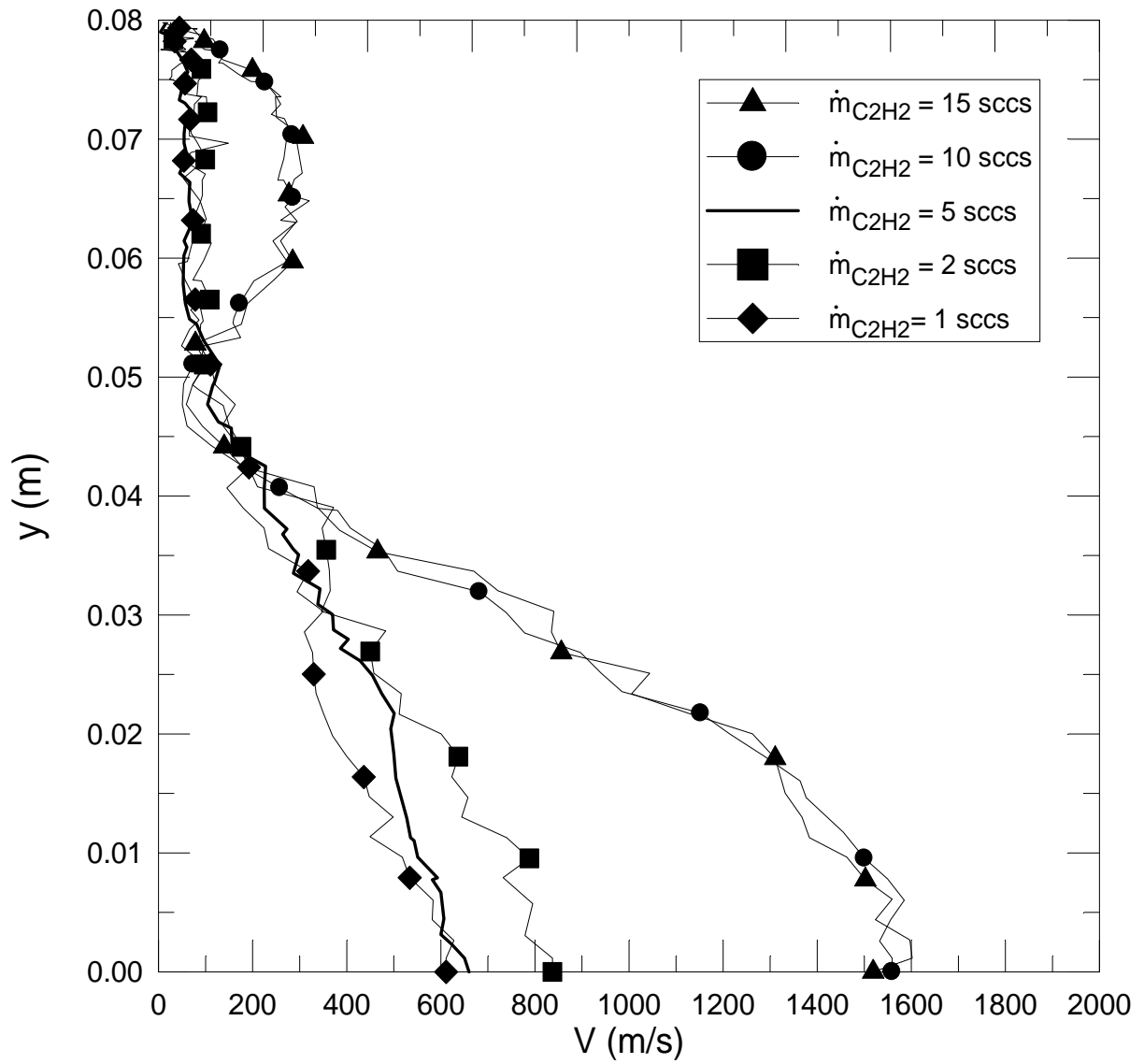


Fig. 7.14c – Profiles of velocity along the radius of the chamber at $x=0.2$ m at different $\dot{m}_{C_2H_2}$

Figure 7.15 reports, as typical example, the 2-D map of C_2 molar fraction for test A5-5 where the influence of chemistry on chemical composition is evident.

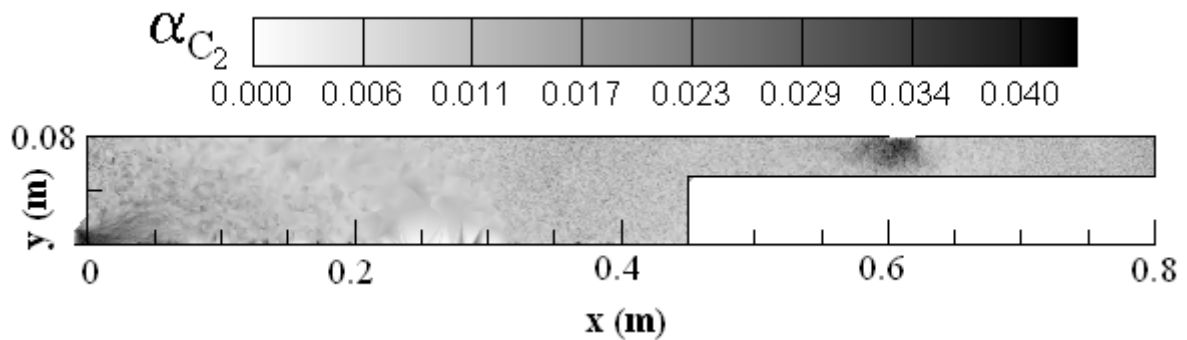


Fig. 7.15 – 2D map of the molar fractions of C_2 for test A-5-5.

7.4.3 Film

As said before the molecule number flux is the parameter used to characterize the film distribution on the substrate. Table 7.11 shows the value of \bar{N}_f and of σ for the film and the \bar{N}_f value for each species forming the film. The thickest film is shown at maximum electrical power (test A13-5) the thinnest film is when the precursor mass flow rate is minimum (A5-1). At run A1-5 the film is not produced. The most uniform film is achieved at test A11-5 while the most not uniformity is obtained using nozzle C (C5-5). As typical example figures 7.16a, 7.16b and 7.16c report the N_f profile by tests A5-5, A13-5 and A5-10 where \bar{N}_f is represented by a horizontal line.

Table 7.11 – Values of $\bar{N}_f \times 10^{22}$ and of $\sigma \times 10^{22}$ for every tests.

Test	$\bar{N}_f \times 10^{22}$ [1/s/m ²]	$\sigma \times 10^{22}$ [1/s/m ²]	$\bar{N}_{fc} \times 10^{22}$ [1/s/m ²]	$\bar{N}_{fc2} \times 10^{22}$ [1/s/m ²]	$\bar{N}_{fCH} \times 10^{22}$ [1/s/m ²]	$\bar{N}_{fc2H} \times 10^{22}$ [1/s/m ²]
A-13-5	4.18	2.17	1.05	1.06	1.05	1.03
A-11-5	1.00	0.23	1.00	0.00	0.00	0.00
A-5-5	3.34	1.69	0.83	0.84	0.83	0.85
A-2-5	1.63	1.60	0.40	0.40	0.40	0.43
A-1-5	0.00	0.00	0.00	0.00	0.00	0.00
A-5-15	0.94	4.77	0.49	0.00	0.45	0.00
A-5-10	3.79	3.00	0.95	0.96	0.96	0.93
A-5-2	0.97	0.41	0.97	0.00	0.00	0.00
A-5-1	0.51	0.24	0.51	0.00	0.00	0.00
B-5-5	0.71	2.97	0.18	0.17	0.18	0.17
C-5-5	0.64	6.18	0.14	0.18	0.18	0.14

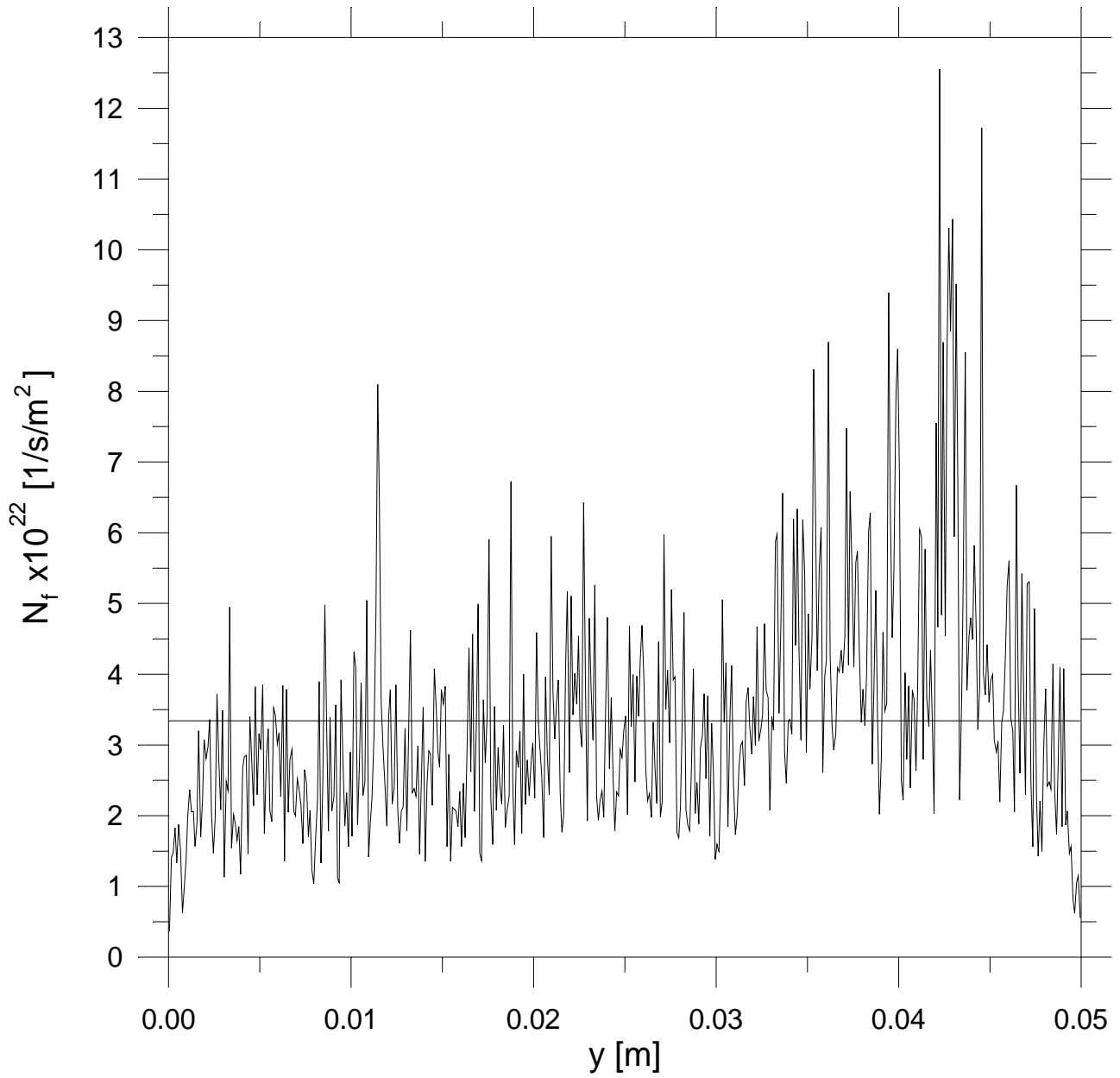


Fig. 7.16 a – Profile of N_f on the substrate surface for test A-5-5, the straight line represents \bar{N}_f

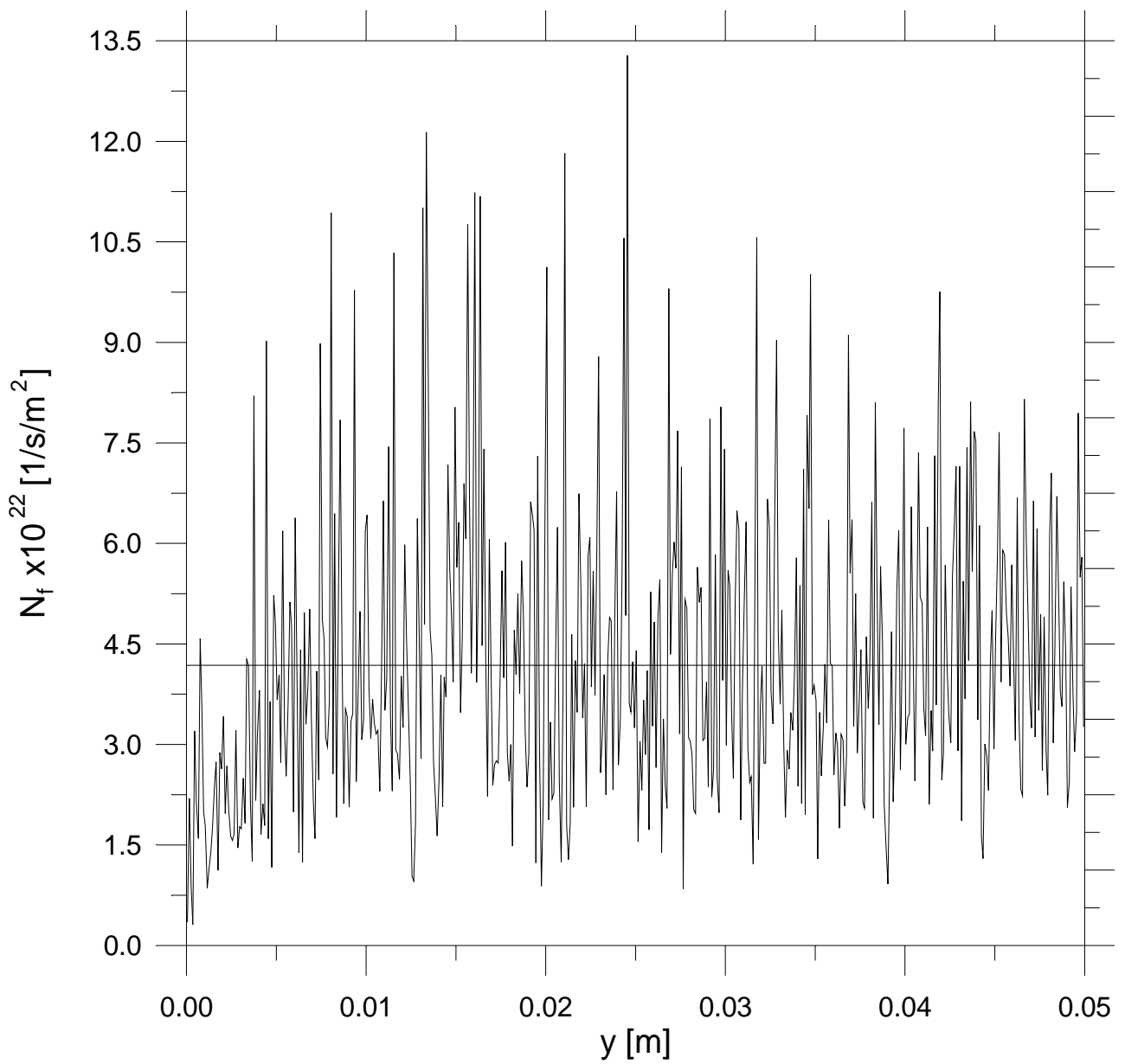


Fig. 7.16b – Profile of N_f on the substrate surface for test A-13-5, the straight line represents \bar{N}_f

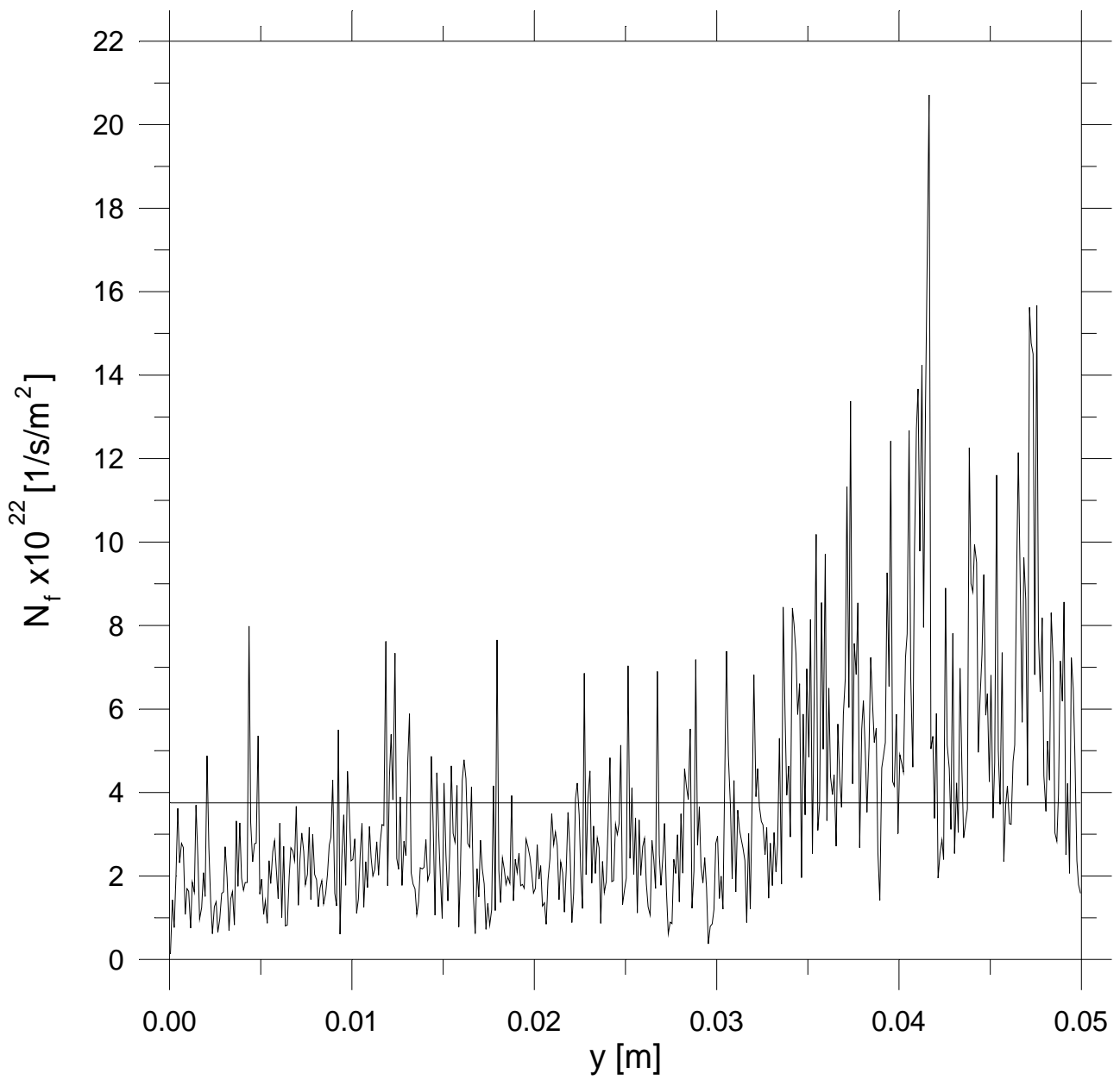


Fig. 7.16c – Profile of N_f on the substrate surface for test A-5-10, the straight line represents \bar{N}_f

Conclusion

In this Ph.D thesis the thin film deposition process is taken into account and studied in detail. This process is very significant and widely used because implied in many industrial applications, such as chemical, electronic, mechanical, optic fields and so on. In fact, thanks to its particular characteristics, thin film is widely used for the coating purposes, magnetic recording media, semiconductor quantum dots, solar cells, displays, sensors, electrodes et cetera. For this reason many researchers analyzed and analyze deeply this technique both by experiments and by numerical computations. Various categories of deposition processes have been carried out.

Among the numerous types of deposition processes, the Expanding Thermal Plasma (ETP) apparatus similar to that developed by van de Sanden and co-workers at the University of Eindhoven is simulated and analyzed profoundly. Complex and several physical-chemical phenomena take place in the ETP deposition method, in fact Argon is ionized in an electrical torch forming a thermal plasma mixture made up of Ar, Ar⁺ and electrons. This mixture expands supersonically in the nozzle where Acetylene as precursor gas is injected at the 90% of divergent part along the nozzle axis. Due to the presence of Acetylene, many complex chemical reactions take place and generate a mixture made up of several chemical species based on carbon and hydrogen. In the present simulation 24 chemical reactions (taken into account by Benedikt) lead to formation of 21 chemical species (15 radicals and 6 ions). Flow field expands supersonically from nozzle and in the chamber until a barrel shock wave, the expansion zone assumes the leaf-blade shape. After the shock the plasma mixture flows (sub-sonically) towards a substrate and some of them (C, C₂ and also partially CH and C₂H) deposit on a surface called substrate forming an amorphous a-C:H thin film.

The study evaluated in this work is carried out considering the influences in the plasma mixture evolution of the following test parameters:

- 1) Acetylene mass flow rate in the range 1-15 sccs (Argon mass flow rate is constant and equal to 100 sccs). The presence of Acetylene affects the rarefaction degree.
- 2) electrical power supplied to the torch in the range 1-13 kW. High electrical power implies high ionization of Argon, low electrical power involves low Argon ionization.

- 3) thermo-fluid-dynamic parameters at chamber inlet section using three different supersonic conical nozzles. Obviously the higher is area ratio the higher is the thermo-fluid-dynamic expansion in the nozzle.

In order to obtain this analysis a computing procedure has been developed. This procedure relies on two codes working in tandem, i.e. output from the first code is input to the second one. The first code is a pre-processor code based on continuum approach and considers flow field in the torch and in part of the nozzle, exactly from throat until to the Acetylene injection point. The output from pre-processor is the input for the DS2V (Ver. 4.5.06) code which simulates using a Direct Simulation Monte Carlo approach the flow field in the last part of the nozzle and in the whole film deposition chamber, similar in shape and dimension to the van de Sanden deposition chamber. A post-processor code is also written to examine the rarefaction level and the film distribution. In this work an exclusively molecular approach by means of DS2V, to simulate in reliable way the flow field in the remaining part of the nozzle (from the Acetylene injection point) and in the vessel, is proper. In fact the flow field in chamber is highly rarefied and even if in some points the local Knudsen number (and/or the P parameter of Bird) is not very high, the molecular code is sophisticated and thus can simulate accurately flow field characterized by a not very high rarefaction level.

A computing method to estimate the film distribution on substrate surface is developed. In particular the substrate temperature is put at 0 K and a fully accommodate gas surface interaction model is considered only for the species forming the film (C, C₂ CH, and C₂H), while a specular interaction model is simulated for the other chemical species. The hypothesis of zero temperature is a numerical artifice for a correct simulation of the sticking process. In fact, in this way the velocity of the molecules re-emitted by the diffusive model is zero. Consequently, molecules do not move from the surface and do not return to the flow, completing the sticking process simulation. In this way a value of the sticking factor equal to one is simulated in the present application. This means that all molecules of C, C₂ CH and C₂H arriving on substrate form the film. For this reason the profile of the molecule number flux (physical dimension of Length⁻²×time⁻¹) of C, C₂ CH and C₂H to the substrate, output by DS2V, provides a very preliminary measure of the film thickness and of its uniformity. The influences of mixture evolution due to the above mentioned test parameters (Acetylene mass flow rate, electrical power supplied to the torch and thermo-fluid-dynamic parameters at chamber inlet section using three different supersonic conical nozzles) on film thickness and distribution is computed.

The sensitivity analysis on fluidics, in terms of position, intensity and extension of the shock wave, demonstrates that the effects of the electrical power as well as of the mass flow rate look to

be not very strong on the shock wave intensity, while are not negligible on the shock wave thickness. For what concern the film distribution, the sensitivity analysis verifies that the higher is electrical power and the precursor mass flow rate, the thicker and less uniform is the film.

References

- [1] M.C.M. van de Sanden, R.J. Severens, J.W.A.M. Gielen, R.M.J. Paffen and D.C. Schram, "Deposition of a-Si:H and a-C:H using an expanding thermal arc plasma", *Plasma Sources Sci. Technol.*, vol. 5, pp. 268-274, 1996
- [2] M.C.M. van de Sanden, J.M. Regt and D.C. Schram, "The behaviour of heavy particles in the expanding plasma jet in argon", *Plasma Sources Sci. Technol.*, vol. 3, pp. 501-510, 1994
- [3] E. Neyts, "Mathematical simulation of the deposition of diamond-like carbon (DLC) films", Ph.D. Thesis, University of Antwerpen, 2006
- [4] J. Benedikt, D. C. Schram and M. C. M. van de Sanden, "Detailed TIMS study of Ar/C₂H₂ expanding thermal plasma: identification of a-C:H film growth precursors", *J. Phys. Chem. A*, vol. 109, 10153, 2005
- [5] Yu.A. Mankelevich, N.V. Suetin, M.N.R. Ashfold, W.E. Boxford, A.J. Orr-Ewing, J.A. Smith and J.B. Wills, "Chemical kinetics in carbon deposition d.c.-arc jet CVD reactors", *Diamond and Related Materials*, vol. 12, pp. 383-390, 2003
- [6] D.A. Ariskin, I.V. Schweighert, A.L. Alexandrov, A. Bogaert and F.M. Peeters, "Modeling of chemical processes in the low pressure capacitive radio frequency discharges in a mixture of Ar/C₂H₂", *Journal of Applied Physics*, vol. 105, 063305, 2009
- [7] K.J. Kuijlaars, "Detailed modelling of chemistry and transport phenomena in CVD reactors", Ph.D. Thesis, TUDelft, 1996
- [8] C. Shen, "Rarefied gas dynamic: fundamentals, simulations and micro flows", Berlin, Springer-Verlag, 2005
- [9] G.A. Bird, "Molecular gas dynamics and Direct Simulation Monte Carlo", Oxford, Clarendon, 1998
- [10] R. Monti, G. Zuppari, *Elementi di Aerodinamica Ipersonica*, Liguori Editori, 2002
- [11] G. Zuppari, A. Esposito, "Blowdown arc facility for low-density hypersonic wind-tunnel testing", *Journal of Spacecraft and Rockets*, vol. 38, pp. 946-948, Nov.-Dec 2001
- [12] G.P. Russo, G. Zuppari, A. Esposito, "Computed versus measured force coefficients on a cone in a small arc facility", *Journal of Aerospace Engineering*, vol. 222 Part G, pp.403-409, May 2008

- [13] J. D. Cobine, "Gaseous conductors theory and engineering applications", New York, Dover Publication, 1958
- [14] G.A. Bird, "Sophisticated versus simple DSMC", in 2006 25th International Symposium on Rarefied Gas Dynamics, Saint Petersburg, pp. 349-354
- [15] G.A. Bird, "Sophisticated DSMC", notes from a short course held at the DSMC07 Conference, Santa Fe, 2007
- [16] G.A. Bird, "The DS2V program user's guide, (Version 4.3)" (included in the program), G.A.B. Consulting Pty Ltd, Sydney, 2006
- [17] G. Zuppardi and F. Romano, *Influence of thermo-fluid-dynamic parameters on fluidics in an expanding thermal plasma deposition chamber*, ICFTE, Venice Italy, 24-26 Nov. 2010.
- [18] G. Zuppardi, F. Romano, "Direct Simulation Monte Carlo Method in Industrial Applications" in Direct Simulation Monte Carlo, Theory, Methods & Applications, (DSMC09) Workshop, Santa Fe, 2009
- [19] S.E. Selezneva, M.I. Boulos, M.C.M. van de Sanden, R. Engeln, D.C. Schram, "Stationary supersonic plasma expansion: continuum fluid mechanics versus direct simulation Monte Carlo method", J. Phys. D, vol. 35, pp. 1362-1372, 2002
- [20] G. Abbate, C.R. Kleijn, B.J. Thijssen, R. Engeln, M.C.M. van de Sanden and D.C. Schram, "Influence of rarefaction on the flow dynamics of a stationary supersonic hot-gas expansion", Physical Review E, vol. 77 036703, 2008
- [21] G. Abbate, "Multi-scale modelling of gas flows with continuum-rarefied transitions", Ph.D. Thesis, TUDelft, 2009
- [22] J. Benedikt, S. Agarwal, D. Eijkman, W. Vandamme, M. Creatore and M. C. M. van de Sanden, "Threshold ionization mass spectrometry of reactive species in remote Ar/C₂H₂ expanding thermal plasma", J. Vac. Sci. Technol. A, vol. 23, pp. 1400-1411, 2005
- [23] H. Mizuseki, K. Hongo, Y. Kawazoe, L.T. Wille, "Multiscale simulation of cluster growth and deposition processes by hybrid model based on direct simulation Monte Carlo method", Computational Materials Science, vol. 24, pp. 88-92, 2002

Publications linked to this thesis

[1] G. Zuppardi and F. Romano, *Direct Simulation Monte Carlo in Industrial Applications*, DSMC09 theory, methods and applications, Santa Fe U.S.A., 13-16 Sep. 2009.

[2] G. Zuppardi and F. Romano, *Influence of thermo-fluid-dynamic parameters on fluidics in an expanding thermal plasma deposition chamber*, ICFTE, Venice Italy, 24-26 Nov. 2010.